NASA CONTRACTOR REPORT CR-166044

SHUTTLE ENTRY AIR DATA SYSTEM (SEADS) HARDWARE DEVELOPMENT VOLUME I, SUMMARY

JANUARY 1983

PREPARED UNDER
CONTRACT NAS1-16000

PREPARED BY
D. M. WHILE
VOUGHT CORPORATION
DALLAS, TEXAS

FOR

NASA
National Aeronautics and
Space Administration
Langley Research Center
Hampton, Virginia 23665

PREFACE

VOLUME I

This report, Volume I, summarizes significant developments of the SEADS program, primarily dealing with the Vought activities. Rockwell data is included in some instances to support the presentation. Unlike Volume II, which is a historical summary, Volume I is organized by subject and treats the highlights of SEADS hardware development. More detailed information may be found in Volume II and the various reference documents.

SEADS early hardware development was conducted by Vought to establish feasibility of the SEADS concept. Rockwell and Vought jointly collaborated on final development and on production design. NASA/LaRC conceived the system and directed Vought development activities. NASA/JSC managed the Rockwell production design activity in cooperation with NASA/LaRC.

Development ultimately proved successful, leading to the fabrication of SEADS for early incorporation on Shuttle Orbiter OV-102 for flight test. The SEADS flight hardware assembly is pictured on Figures 1-1 and 1-2.

Acknowledgement is given to the following principals who had responsibility for managing their respective areas of activity:

- P. M. Siemers, III, NASA/LaRC, overall system development and Technical Manager of Vought activities.
- R. L. Cox, NASA/JSC, Technical Manager of Rockwell Activities
- R. M. Hamilton, Rockwell International
- D. M. While, Vought Corporation

TABLE OF CONTENTS

LIST OF TABLES

LIST OF FIGURES

LIST OF FIGURES

1.0 INTRODUCTION

Shuttle Entry Air Data System (SEADS), illustrated on Figure 1-3, is an innovative, flush mounted orifice, air data system, mounted in the Reinforced Carbon-Carbon (RCC) nose cap of the Shuttle Orbiter. Conceived by NASA/LaRC, it provides accurate data across the Orbiter speed range throughout the sensible atmospheric flight region. It is comprised of a cruciform array of fourteen total pressure ports located in the nose cap, that, when coupled with static pressure ports mounted on the fuselage, permits computation of angle of attack, angle of side slip, Mach number, and velocity. The large number of ports includes a degree of redundancy, such that the loss of data from some of the sensors produces only modest degradation of system accuracy.

The system is composed of the penetration assemblies, two tube arrays to transmit the pressure data through two manifolds to a series of transducers, mounted to the aft side of the nose cap support bulkhead, and a data recorder. The recorded data are analyzed after flight to provide the desired flight information. The system is capable of being expanded to provide real time data for flight profile management.

The production design penetration assembly is shown on Figure 1-3. A mockup of the system is shown by the photo on Figure 1-4 to better illustrate the two manifolds and the pressure tubes configurations. The production SEADS nose cap, on Figure 1-1, illustrates the cruciform configuration of the pressure port array.

SEADS is currently a Shuttle OEX program, approved for early introduction on Orbiter OV-102. It's initial function will be to support the data analysis of other OEX programs by providing the necessary accurate flight data.

2.0 SUMMARY

SEADS development consisted of a series of analyses and tests leading to an acceptable design for flight hardware. Significant activities and findings are summarized on Table 1. Discussions of these activities are found in other sections of this report.

The successful development of this system is exemplified by the fabrication of a production assembly for flight on Orbiter OV-102.

TABLE 1 SIGNIFICANT ACTIVITIES AND FINDINGS RELATIVE TO FINAL CONFIGURATION

ITEM	EVALUATION MEANS	FINDINGS	SECTION	REFERENCE
LOCAL EFFECT OF COUNTERSUNK HOLE IN NOSE CAP	PLASMA ARC TEST AND PHOTOMICROGRAPHIC EVALUATION	SUBSURFACE OXIDATION IN COUNTERSUNK HOLE NO DIFFERENT THAN WITHOUT-15 HOUR TEST	5.1	2
THERMAL LIFE OF COLUMBIUM COMP-ONENTS	PLASMA ARC TESTS TO COMPUTED TEMP	FIVE-HOUR EXPOSURE PRODUCED MINOR OXIDATION NOT DETRI-MENTAL TO FLIGHT SAFETY	5.1	3, 8, 16
TEMPERATURE OVER-SHOOT	PLASMA ARC TEST	2950F EXPERIENCED WITHOUT DAMAGE	5.1 9.2	16, 19
STICKING OF COLUMBIUM THREADED CONNECTIONS	FURNACE AND PLASMA ARC TESTS	SiC POWDER PROVIDES ACCEPTABLE ANTI-SEIZE COMPOUND	4.0 5.1	13, 16
PRESSURE MEASURE-MENT WITH FINGER TIGHT JOINTS	PLASMA ARC TESTS	TEST MODEL PRESSURE EQUIVALENT TO FACILITY PRESSURE ALTHOUGH RESPONSE RATE SUFFERS	5.1	2, 16
CHEMICAL COMPATIBILITY	FURNACE AND PLASMA ARC TESTS	RCC, COLUMBIUM AND IRIDIUM ARE MUTUALLY COMPATIBLE TO DESIGN TEMP	5.1	1, 2
THERMAL STRESS RESISTANCE OF PRESSURE TUBES	RADIANT TEST	MINIMUM LIFE WAS FACTOR OF TWO GREATER THAN REQUIRED EVEN IN EXCESSIVELY SEVERE ENVIRONMENT	8.1	8, 20

TABLE 1 SIGNIFICANT ACTIVITIES AND FINDINGS RELATIVE TO FINAL CONFIGURATION (CONTINUED)

ITEM	EVALUATION MEANS	FINDINGS	SECTION	REFERENCE
STRUCTURAL INTEGRITY IN DYNAMIC LOAD ENVIRONMENT	ANALYSIS AND VIBRATION TEST	ANALYSIS, PURPOSELY CONSERVATIVE, ADEQUATELY CORRELATED WITH TEST RESULTS. TESTING FOR EQUIVALENT 30 MISSIONS PRODUCED NO FAILURES	8.2	22, 24
EFFECT OF HOLES ON THE STABILITY OF THE NOSE CAP	ANALYSIS	NO REDUCTION OF STABILITY MARGIN FOR 6-PLY RING STIFFENED DESIGN	6.2	6
EFFECT OF FLAT SIDED HOLE ON LOCAL NOSE CAP STRESSES	ANALYSIS	MARGINS ARE ADEQUATE AND EXCEED THE MINIMUM MARGIN OF SAFETY	6.3	7
STRENGTH DETERMIN-INATION OF PENE-TRATION	ANALYSIS AND TEST	PRESSURE TUBE IS WEAK LINK	5.4	11, 12
FREEDOM FROM SIGNIFICANT THERMAL STRESS OR DIFFERENCES FROM BASELINE NOSE CAP	ANALYSIS	THERMAL GRADIENTS IN PENE-TRATION ASSY AND THERMAL STRESS CHANGE IN NOSE CAP ARE INSIGNIFICANT	6.1	9, 10
INTERFACE WEAR BETWEEN FAYING SURFACES	VIBRATION TEST	NO RUBBING WEAR NOTED FLARED END OF PRESS-URIZE TUBE SUBJECT TO MECHANICAL/THERMAL DAMAGE	8.2	24

3.0 DEVELOPMENT HISTORY SUMMARY

Development of the mechanical components of SEADS began in October, 1975 with the initial goal of conceiving approaches for incorporating pressure ports into the Orbiter nose cap and evaluating the local effect of the resultant holes. The design requirement was 2520F maximum surface temperature on the nose cap. A number of approaches were conceived and evaluated with promising candidates selected for test in a plasma arc. These were found to lack sufficient mission life, requiring both material and configuration changes. However, it was established in 15 hours of plasma arc exposure, that the presence of a countersunk hole to accept the pressure port assembly, was not locally detrimental to the nose cap RCC material. This, coupled with limited pressure port success in test, was sufficiently encouraging to proceed with development.

Utilizing the best features from the initially tested concepts, the pressure port assembly was redesigned to correct deficiencies. Three models were tested in the plasma arc of one geometric configuration, but with material variations. Two survived the planned 5-hour test, one with a coated columbium port and one with a silicon carbide coated graphite port.

A systems concept evaluation was also conducted, consisting of thermal analysis of the penetration assembly and dynamic analysis of both the small diameter pressure tubes and the support posts (manifolds) that collected seven each pressure tubes. Concept feasibility was established at the analytic level.

With this impetus more sophisticated analyses were conducted consisting of buckling analysis of the nose cap with SEADS holes, a detailed stress analysis for the region around a non-circular hole in the nose cap, a more refined thermal analysis of windward and leeward penetration assemblies, and a thermal analysis of the nose cap to assess heat blockage from the two support posts. Each of these analyses proved the SEADS design to be feasible.

An entry trajectory change was introduced that raised maximum design temperature to 2660F, prompting another modification to the selection of materials and produced the final configuration. This resulted in the use of all coated columbium components, including the pressure tubes, although coated graphite ports were retained as a backup in the event sufficient mission life could not be extracted from the coated columbium ports. Two additional models were tested in the plasma arc in an effort to establish satisfactory performance at the increased temperature. The models differed only in the above noted port material, and each survived the planned 5-hour exposure. However, it could not be proven that the desired test temperature was actually achieved. It was therefore necessary to build another model for test in another plasma arc facility to conclusively demonstrate survivability at the design temperature. Only the columbium pressure port model was tested. Not only was it shown that the penetration assembly would meet the design temperature requirements, but an inadvertent overshoot to 2950F was experienced without detrimental effects. The penetration assembly was thus deemed qualified.

Two other component tests were conducted to demonstrate, primarily, the acceptability of the pressure tubes to survive the design environments and to validate dynamic analysis. The first of these was a vibration test of the

left hand set of pressure ports and consisted of seven pressure port assemblies, seven pressure tubes, and the associated manifold and its insulation system. This unique test involved two simultaneously operating, independently controlled shakers, one introducing the vibration environment from nose cap acoustic response, and one simulating the nose cap support bulkhead vibration environment, applied to the base of the manifold. The input levels for this test were derived from response data measured during the Orbiter nose cap assembly qualification test, conducted at NASA/JSC. A thorough pre and post test analysis of pressure tubes response was conducted by Rockwell to support this test. Test results and supporting analysis demonstrated the acceptable performance of the SEADS system in a vibro-acoustic environment.

The second major test was one conceived to evaluate the low cycle thermal fatigue life of selected pressure tubes in the presence of thermal cycling. The concern was the stresses induced from constrained thermal expansion, as well as possible creep at high temperature, leading to induced strain in the tubes, when returned to room temperature. Although it was intended to impose a low pressure oxidizing atmosphere, representing the entry environment, the bare graphite heating elements oxidized sufficiently to create a reducing, rather than an oxidizing atmosphere. Instead of producing a more benign environment, the reducing atmosphere actually caused embrittling of the coated columbium pressure tubes and resulted in premature failure. It was encouraging that the embrittled tubes survived for a minimum of 68 mission cycles, lending confidence that the tubes, operating in the correct environment, would produce a safe failure margin far in excess of the 25-30 mission life projected for the penetration assembly.

Design evolution of the nose cap penetration assembly and pressure tube routing concept with support post (manifold) approach are shown on Figures 1-5, and 1-6, respectively. Evolution of pressure tubes configuration is illustrated by the early mockup of the tubes on Figure 1-7 as compared with the final, more orderly arrangement shown on Figure 1-4.

The successful accomplishment of the foregoing component tests resulted in acceptance of SEADS as a viable system, and a production assembly was fabricated for early incorporation on vehicle OV-102 for flight test.

The remainder of this report expands upon these highlights, providing rationale for approaches, results of analyses/tests, and identifies lessons learned.

4.0 MATERIALS SELECTION

The initial maximum temperature requirement for the SEADS penetration assembly was 2520F, but this was ultimately raised to 2660F, when design entry trajectory 14414.1C was imposed. Thus some early marginal candidate materials were completely eliminated from consideration when the higher temperature requirements were introduced.

Material requirements included the ability to withstand high temperature oxidation, chemical compatibility with the RCC nose cap and other components in the assembly, fabricability in the shapes and tolerances required without excessive cost for the limited quantities envisioned. It was also required that the port material possess a high emittance to avoid over heating the adjacent RCC.

Inital investigations focused on the 2520F surface temperature, but recognized lower temperatures would prevail when progressing inward from the surface. Candidate port materials included ceramics, silicon carbide coated graphite, and silicide coated refractory metals. Added for consideration were platinum, iridium, oxide dispersion strengthened (ODS) alloys, nickel and cobalt alloys for internal components.

Ceramics such as silicon carbide and silicon nitride bodies were quickly eliminated from consideration because of schedule and cost to achieve the necessary dimensional control for the few test components needed.

Initial chemical compatibility tests indicated (incorrectly) that platinum would survive in contact with siliconized RCC. In fact platinum proved highly incompatible in plasma arc testing. The error was attributed to the manner in which the test was conducted. It is believed that intimate contact of the platinum and RCC during the test was prevented because of seepage of bonding material between the two tested materials. Other results showed that cobalt based alloys were incompatible with RCC, but nickel based alloys and pure iridium were acceptable.

A subsequent, more thorough, chemical compatibility test was conducted and expanded to include refractory alloys. Testing was conducted at 2400F, 2450F and 2500F in 1 atm air. Specimens were either 0.75 in. diameter buttons, wire, or tube configurations, weighted to assure intimate contact. All specimens, except the RCC, were preoxidized to minimize self bonding tendencies. Testing was conducted for periods ranging between two and five hours. specimens were examined visually for chemical compatibility and hand tested for self-bonding tendencies. A typical platten of specimens is pictured on Figure 4-1.

Acceptable combinations are summarized on Table 2, while unacceptable combinations are listed on Table 3. The final selection of materials for production design was coated columbium for the penetration assembly and pressure tubes, with pure iridium for lock wire.

It was discovered in these tests, as well as in plasma arc tests that the coated columbium had a tendency to self bond at elevated temperature, making disassembly of the penetration assembly impossible without damage after a period of time. This not only would destroy the components but would add risk of damage to the nose cap, when replacing components. An investigation was, therefore, undertaken to develop a scheme for eliminating self bonding for the projected life of the components.

TABLE 2 SUMMARY OF FINDINGS
CHEMICALLY COMPATIBLE COMBINATIONS

Material	Chemically Compatible with	Up to "X" °F test temperature
RCC impregnated with TEOS (See Note 1)	Molybdenum	2500
	Columbium	2500
	CVD Coated Graphite	2500
RCC without TEOS	Iridium	2500
	Inconel 702	2450
	YDNiCrAl	2450
Molybdenum TZM Alloy With 518 Coating	Molybdenum	2500
	RCC with TEOS	2500
	Iridium	2500
	YDNiCrAl	2450
	Inconel 702	2450
Columbium C-103 Alloy With R512E Coating	Columbium	2500
	RCC with TEOS	2500
	Iridium	2500
	YDNiCrAl	2450
YDNiCrAl	YDNiCrAl	2450
	Molybdenum	2450
	Columbium	2450
	Inconel 702	2450
	Iridium	2450
	CVD Coated Graphite	2450
	RCC without TEOS	2450
	Platinum Rhodium	2400
Inconel 702	YDNiCrAl	2450
	Molybdenum	2450
	Platinum & Platinum Rhodium	2450
	Iridium	2450
	RCC without TEOS	2450
CVD Coated Stackpole 2020 Graphite	RCC with TEOS	2500
	Iridium	2500
	YDNiCrAl	2450
Iridium	Platinum	2500
	Molybdenum	2500
	Columbium	2500
	RCC with TEOS (Preoxidized)	2500
	CVD Coated Graphite	2500
	YDNiCrAl	2450
	Inconel 702	2450
Platinum	Iridium	2500
	Inconel 702	2450
	YDNiCrAl	2450

NOTES: (1)

Only the RCC in this test combination was not pre-oxidized so as to represent the nose cap at first flight. All other combinations assume pre-oxidized components.

TABLE 3 SUMMARY OF FINDINGS
CHEMICALLY INCOMPATIBLE COMBINATIONS

Material	Chemically Incompatible with:	
Platinum & Platinum Rhodium	Columbium Molybdenum RCC with or without TEOS CVD Coated Graphite	

Anti-seize tests were conducted, using both 0.75 in. diameter silicide coated columbium buttons and union/nut assemblies. An evaluation of several commercial anti-seize compounds, as well as, powders of MgO, SiC, Mo_5Si_3, HfO_2 and ZrO_2 was made. Specimens were exposed at 2500F in one hour increments to a maximum of seven hours. Torque required to separate the parts after exposure was the criteria for selecting an acceptable anti-seize system.

Results showed that SiC powder was the most effective material for this application. A slurry of methocel and SiC powder is brushed onto the faying surfaces and baked before joining the parts. Disassembly was found to be aided by squirting iso-propyl alcohol (IPA) into the joint. An additional aid was discovered by igniting the IPA. The flame temperature is not detrimental to the penetration assembly materials employed. This formulation was employed in later plasma arc tests and proved effective.

5.0 PENETRATION ASSEMBLY DESIGN DEVELOPMENT

5.1 Design Evolution and Plasma Arc Tests - In developing concepts for attaching small diameter tubes to the nose cap it was judged that there would be no reliable method of directly anchoring a thin walled pressure tube to the nose cap without some intermediate support structure. This led to concepts involving a plug with countersunk or counterbored head condiguration, inserted into the nose cap, and restrained on the back side by some nut configuration. The pressure tube was then conceived as attaching to the port by mechanical means.

While some initial concepts assumed the application of a high temperature ceramic bond for attaching or locking the various elements together, this approach was quickly abandoned, because of expected low reliability, and difficulty of disassembly with attendant potential damage to the nose cap. Thus, all concepts, given serious consideration, employed mechanical anchoring schemes.

From a total of fourteen concepts three were selected for fabrication and plasma arc testing. These employed coated graphite plugs (or ports) countersunk into a 2.8 in. diameter RCC disc, representing the nose cap. On the basis of initial chemical compatibility tests, other components of the penetration assembly consisted of coated graphite, platinum, or YDNiCrAl (an ODS alloy) with tubes of either platinum or Inconel-702. These configurations are pictured on Figure 5-1. A plain RCC disc calibrator model was also constructed to establish test conditions and to provide a point of comparison for subsurface oxidation of the test model discs. Target test conditions were 2500F surface temperature at 0.04 atm.

Only one model, Concept 1A with graphite nut, survived the 15 hours planned exposure, although not without damage. The calibrator was also exposed for 15 hours. Photomicrographic analysis of cross sectioned RCC discs from the long duration model and the calibrator revealed no differences in subsurface attack. Thus, it was concluded that the presence of a countersunk hole in the RCC (nose cap) has no local detrimental effect upon the RCC.

Model concept 1A suffered oxidation in the small diameter center hole of the plug, as well as, a chemical reaction and melting of the platinum pressure tube where it contacted the silicon carbide coating on the graphite.

The other two concepts, Nos. 6 and 13, survived for periods of 2.0 and 3.6 hrs., respectively, their early demise resulting from chemical incompatibility between the platinum elements and the coated graphite.

Concept 13 was rebuilt with nickel alloy parts replacing their platinum counterparts and was redesignated Concept 13B. The model was exposed for 4.0 hours, when the end of the pressure tube melted and fell out, presumably due to exceedance of the melt temperature of the Inconel 702. The YDNiCrAl nickel nut showed no evidence of damage and was removed from the coated graphite plug with ease. The plug was fractured during the first attempt at disassembly, however, and is attributed to excessive torqueing in the wrong direction. The nickel nut employed left hand threads to provide a mutual locking feature with the right hand threaded graphite nut, when the two were lockwired together.

The results of these tests demonstrated that platinum cannot exist in contact with the siliconized coating on graphite, which was counter to the initial chemical compatibility tests. Further, temperature of the pressure

tube exceeded the melt temperature of Inconel 702 for this model configuration but suggested that it may be applicable if attached more remote from the nose cap surface in a cooler region. The YDNiCrAl nut suffered no degradation and, because it did not bond to the coated graphite, was considered a viable candidate within its temperature limit.

Evaluation of the three configurations tested resulted in the selection of concept 6 as the one having greatest potential with appropriately selected materials. This configuraton was modeled using finite element methods to determine temperature distributions for the various components. A model of the plasma arc geometry was first constructed to compare analysis with thermocouple data secured during plasma arc testing. Once the model was checked out, it was extended to the nose cap installation and exercised with various material combinations to obtain design temperatures for the various components.

These temperature predictions, coupled with the more extensive chemical compatibility tests, summarized in Section 4.0, resulted in configuring three new models for plasma arc testing. The configuration is illustrated on Figure 5-2; the models differed only in materials selection. At this time the design trajectory was one producing a maximum surface temperature of only 2520F. (This was later increased to 2660F when entry trajectory 14414.1C was imposed.) The composition of the three models and test times experienced are summarized on Table 4. At the computed temperatures, it still appeared that, though marginal, nickel alloys might have application, which accounted for this selection for the union on two of the models. The third model provided higher temperature capability through the use of a coated columbium union.

The plasma arc test condition was targeted for 2500F at 0,.05 atm with the intent of testing for 5 hr. in 10 min. increments.

The -9 model was tested first, but after 30 min. exposure the plug fell out due to melting of the YDNiCrAl. This was unexpected, since thermocouple data indicated the temperature of the nickel to be only 2450 F or about 50-60F lower than melt temperature.

The -10 model with columbium union was exposed for 4.9 hours, but suffered severe oxidation of the head of the plug, during the last three cycles. Initial pitting was evident after 3-hr. testing (Figure 5-3), which progressed to the condition shown in Figure 5-4 at the conclusion of test. Pitting was also experienced on the -9 model columbium plug. No melting was in evidence for the Inconel 702 tube nor for the YDNiCrAl nut.

Disassembly of this model was readily accomplished after 2 and 3 hours of testing, but could not be performed after 4 hours, even with strenuous urging with wrenches. This was not entirely unexpected and pointed out the necessity for an anti-sieze compound. The development of an anti-sieze material is discussed in Section 4.0.

Because of the melting of the nickel union on the -9 model, the test temperature of the -11 model was purposely lowered about 50-60F to avoid a similar circumstance. As a result, this model was tested for the full 5 hours planned. Upon inspection it was discovered that the nickel union had apparently just reached its melt temperature, because a "blob" of nickel was found at the high temperature end of the union and the union was tenaciously attached to the graphite plug, rendering disassembly impossible. As a

TABLE 4 – MODELS TESTED

COMPONENT	MODEL		
	-9	-10	-11
DISC	RCC (TEOS)	RCC(TEOS)	RCC (TEOS)
PLUG	CB (C-103) R 512E COAT.	CB (C-103) R 512E COAT.	STACKPOLE 2020 (VOUGHT COATING)
SPACER	RCC	RCC	RCC
LOCKWASHER	YDN; CRAL	CB (C-103)	YDN; CRAL
THERMOCOUPLE MOUNT	YDN; CRAL	IRIDIUM	YDN; CRAL
UNION	YDN; CRAL	CB (C-103)	YDN; CRAL
NUT	YDN; CRAL	YDN. CRAL	YDN; CRAL
PRESSURE TUBE	INCONEL 702	INCONEL 702	INCONEL 702
LOCKWIRE	PLATINUM	IRIDIUM	PLATINUM
THERMOCOUPLES (FLIGHT) (DIAGNOSTIC)	PT/PT13RH W5RE/W26RE	PT/PT13RH W5RE/W26RE	PT/PT13RH W5RE/W26RE
EXPOSURE CYCLES	3	30	34
EXPOSURE HOURS	0.5	4.9	5.0

(1) FOR 2520F MAXIMUM NOSE CAP TEMPERATURE.

consequence, the port had to be fractured to separate the two components. The hot end of the union was found to be porous, indicating that some portion of the material makeup melted, while another portion remained stable.

In conclusion it was found from these tests that coated columbium appeared to be a viable candidate for the plug and union, but required increased corner radius on the head of the plug to reduce the tendency for pitting. it was also clear that the YDNiCrAl could not be used for the union because of excessive temperature, although the nickel nuts at the cooler end survived admirably. The Inconel 702 tubing survived all tests without tubing melting, but in all cases the electron beam welded washer, used for tube retention, broke loose. A flared tube end, as used in the final design, solved this problem.

The graphite plug on the -11 model was fractured intentionally for disassembly as noted above. Examination of the fractured surfaces revealed no evidence of subsurface oxidation. This added confidence that coated graphite could remain a viable option in the event coated columbium could not be used reliably.

It should be pointed out that in these tests the pressure tubes were active. Recorded pressure compared favorably with that measured by the tunnel probe before each test. Full pressure built up within 10 seconds. Therefore, even with finger tight, unsealed faying surfaces, satisfactory pressues can be measured, although response suffers.

Following these tests the design entry trajectory was changed to 14414.1C, which produces a design surface temperature of 2660F. This temperature level negated the use of nickel alloy for any component. Thus, material choices were reduced to coated columbium or graphite for the plug; coated columbium or platinum (with iridium chemical barrier) for the pressure tubes; and coated columbium for all other components. (Throughout this period, thermocouples were included for temperature measurement of the penetration assembly. A nickel alloy or iridium, ring shaped, thermocouple mount, depending upon temperature requirements, was used for anchoring the thermocouples. This requirement was subsequently deleted for the final design).

While the program, at this point, was not devoid of problems, the successes and projected problem solutions were sufficient to involve Rockwell as systems manager for experiments earmarked for orbiter installation. Rockwell's stance on pressure tube material was that coated columbium was preferred over designing chemical barriers for platinum, and, therefore, future designs employed columbium pressure tubes. Further, a flared pressure tube end was introduced for retention.

Since columbium can't be flared after coating, a scheme, using split ferrules, was conceived by Rockwell to permit insertion of a flared tube through the retention nut. The installation of the split ferrules then prevented the tube from pulling back through the nut. This design is illustrated by Figure 5-5 while the ferrules can be seen on Figure 5-7. This scheme worked well in trials of aluminum components, but, when applied to coated columbium on test assemblies, it was found that the ferrules invariably splayed out, where they protruded through the nut. This condition was attributed to the inability to control tolerances tightly enough on the coated parts. Although this configuration was employed on plasma arc models, an alternate approach was taken for the final design.

The alternate technique eliminated the split ferrules by leaving the cool end of the pressure tube uncoated (where it attaches to the aluminum support post or manifold). The uncoated portion was then flared on assembly after the retention nut for the penetration end was slipped onto the tube. This ultimately proved successful.

Another series of plasma arc testing was performed on revised designs to incorporate the higher temperature columbium components for the updated temperature requirement. Individual part configurations were revised to improve coatability and reduce the tendency for oxidation pitting. Specific changes included increased edge radii and increased thickness on flanges. The revised configuration is shown on Figure 5-5.

Previous columbium parts employed the R512E coating, applied by HiTemco, but with the higher temperature requirement the coating was changed to the more refractory VacHyd VH109 system. This was done at the recommendation of Rockwell, who selected VH109 for the pressure tubes.

A limited plasma arc test program was conducted on 0.75 in. diameter discs to gain confidence that the VH109 would meet the temperature requirements, and to obtain a comparison with the previously used R512E coating system. Total exposure times above 2660F were 4 and 5 hrs. for the R512E and VH109 coating systems, respectively. Neither system suffered damage, indicating either one would perform satisfactory.

Two new plasma arc test models of the penetration assembly and a calibrator model were constructed, using the updated design configuration. The models differed only in port material, where stackpole 2020 graphite was still retained as a backup to the columbium port. These models employed 5/32 in. diameter pressure tubes and the split ferrule retention device.

Target test condition was set at 2660F and 0.05 atm., the plasma arc facility test condition being established by the use of the calibrator. Pyrometer data indicated the condition was met, but thermocouples on the backside of the calibrator disc indicated by extrapolation that the temperature was 100-150F low. The disparity between thermocouple and pyrometer indicated temperature became controversial, so investigations were conducted in an attempt to resolve the issue, Section 9.1. These tended to support Vought's position that the thermocouples were reading more correctly.

The plasma arc facility (NASA-LaRC Facility B) was incapable of producing higher temperature, while maintaining sufficient exposure duration to reach, essentially, steady state temperature conditions. Since no other facility was available, it was decided to test at what was believed to be a temperature of only 2500-2550F to gain valuable performance data on the redesigned components, including the adequacy of the anti-seize compound for threaded connections.

Each model was tested in 10-minute exposures for a total duration of 5-hours. Disassembly and inspection was conducted at 1-hour intervals, at which times the anti-seize compound was reapplied.

Inspection of the model with columbium port showed evidence of local oxidation of the edges of columbium parts initiating at various times during exposure. The most serious of these was the flared end of the pressure tube, which showed early evidence of breached coating. Oxidation continued through test to produce a scalloped end at the conclusion as shown on Figure 5-6. Never-the-less, the pressure tube remained well anchored to the end. None of the oxidation sites were judged to pose a threat to the structural integrity of the assembly. Condition of parts at the conclusion of test is pictured on Figures 5-7 and 5-8.

Pressure measurements were made on this model throughout the test sequence and compared with the tunnel pressure probe used before each exposure. In a sample of six exposures, tunnel pressure was in the range 35.6 to 39.6 mm Hg, while the corresponding model pressure varied between 37.6 and 38.4 mm HG after 60 seconds and 38.3 to 42.2 mm HG after 600 seconds of exposure. This reconfirmed previous data that were used to conclude that the finger tight joints would still permit adequate pressure measurement.

The model with the graphite port was tested and inspected in the same manner as the other. Disassembly was readily accomplished. While oxidation of columbium parts was less, oxidation sites did develop at edges. The end of the flared columbium pressure tubes experienced the same type of oxidation as on the first model but to a substantially less degree. This is shown on Figure 5-9. The graphite port was discovered to have chips on three threads, presumably due to some degree of subsurface attack, which pointed out the desirability of using a post coating seal treatment like that used on RCC. Again, it was judged that structural integrity of the penetration assembly was retained throughout the test. Post test condition of components is shown on Figure 5-10

For both of these models oxidation sites noted after the first hour of exposure progressed so slowly that flight safety was not compromised, even though damage occurred. This benefit was in part due to the relative massiveness of the penetration assembly components, adding strength in excess of requirements. This was brought about by designing for possible substitution of the lower strength graphite port, the desire to design parts for ease of manufacture and coating, and the lack of emphasis on achieving minimum weight.

The effectiveness of the anti-seize compound was demonstrated, since parts were readily disassembled, although in some cases plastic faced wrenches had to be employed, where finger pressure was insufficient. This is in contrast to the previous test series, where columbium disassembly could not be accomplished even with wrenches.

Because it was not assured that the 2660F temperature requirement was met, due to the pyrometer/thermocouple discrepancy, another model was constructed for test in a NASA-ARC plasma arc facility. This model employed the columbium port and incorporated a thermocouple adjacent to the aft face of the front coating on the RCC disc, as well as others (Figure 5-11). The calibrator model also incorporated front and aft face thermocouples. The objective of the test was to demonstrate survivability at 2660F for a reasonable period of time, which was set at two hours.

The calibrator was used to establish plasma arc operating conditions in the usual manner with thermocouple response dictating the temperature level. However, when the test model was injected into the stream, the temperature rose much more quickly than expected and the peak temperature reached 2950F before power was reduced. The run was aborted after 6 1/2 minutes with the temperature remaining at 2920F. It was discovered that the graphite holder lost most of the coating on the front face, a contributor to the high temperature. Post test analysis, Secton 9.2, revealed that the columbium port was probably partially catalytic, becoming a major contributor to the temperature overshoot. This had not been encountered in NASA-LaRC tests, because of the low enthalpy of the plasma stream in that facility, where catalytic effects are not pronounced. The NASA-ARC facility operated at an enthalpy about two to three times greater than the NASA-LaRC plasma arc.

Even with the extreme over shoot, the model appeared undamaged, and was transferred to another holder for continued testing. All thermocouples were preserved in the transfer. Plasma arc power was reduced but the second exposure still reached 2830F before further power reductions were made, resulting in most of the remaining exposures being conducted at about 50F above target. The model was exposed for a total of 11 cycles, accumulating 1 hour and 57 minutes.

After 1-hour of test the model was inspected for evidence of coating breakdown. None was observed. However, the columbium parts could not be disassembled with the plastic coated wrenches available. Testing was continued without disassembly. At the conclusion of test the only observable damage was to an apex on the hexagonal flange of the union. This was believed due to the attempted disassembly after the first hour.

In anticipation of having great difficulty in unscrewing the columbium components WD-40 was squirted into the nut to union threads. Employing a better gripping technique, the nut unscrewed from the union at an estimated 10-15 ft. lb of torque. Without the aid of WD-40, but with better gripping, the union was separated from the port at the same estimated 10-15 ft. lb torque. No observable damage was inflicted to the columbium coatings during this operation. The significance of this is that, even with the temperature extreme experienced, the components can be disassembled at torque levels that should not cause damage to the coatings nor to the nose cap. Further, it was clear that properly designed and fabricated wrenches were required to affect disassembly without damage.

Inspection of disassembled components (Figures 5-12 through 5-16) produced no observable oxidation damage to parts except a shiney spot on a union thread (without the accompanying oxidation "flowering") and the expected oxidation scalloping of the flared end of the pressure tube, Figure 5-14. It was discovered, however, that the iridium thermocouple mount and coated columbium lockwasher reacted, producing damage to both parts, Figure 5-16. This was not encountered in previous tests, nor was it encountered on the iridium lockwire for this test model. This reaction is somewhat academic, however, due to both the temperature overshoot and the exclusion of a thermocouple mount from the production design penetration assembly.

The most significant result from this test is that the coated columbium components will tolerate almost 300F overshoot without failure and yet can be disassembled within reasonable torque levels.

The sum total of all of the plasma tests conducted showed the following:

(1) The presence of a countersunk hole in the RCC would not be detrimental to the local integrity of the nose cap.

(2) Coated columbium is viable for penetration assembly components with an estimated life of 25-30 missions.

(3) Oxidation damage to coated columbium progresses at a sufficiently slow rate at the test temperatures that safety of flight is not jeopardized.

(4) Significant temperature overshoot capability exists with the coated columbium components, where nearly 300F was demonstrated.

(5) Iridium lockwire is compatible with coated columbium at the temperatures of interest.

(6) The SiC powder anti-seize compound is effective.

The results of the plasma tests, coupled with other requirements, such as (1) deletion of thermocouple requirements and hence thermocouple mount; and (2) increased diameter of the pressure tubes to 1/4 in. to provide a safeguard against catastrophic damage from lightning strike, resulted in the final (production type) configuration shown on Figure 5-17. This configuration was that used for the vibration test and thermal expansion tests, Section 8.0.

5.2 Anti-Rotation - Concern was expressed that the penetration assembly, as a unit, may loosen in the RCC, vibrate or oscillate and cause excessive wear on either the RCC or columbium coatings. Eight concepts were proposed and evaluated. The two best candidates are shown on Figure 5-18, where one employs a ball lock, while the other uses a flat sided port in a flat sided hole in the nose cap. The ball for the first approach is a synthetic ruby or sapphire with a temperature capability in excess of operational requirements. The ability to withstand thermal shock was demonstrated by NASA on one of the 3/16 in. diameter rubies, procured for test. The ball lock device was installed on the thermal deflection test of the pressure tubes, Section 8.1, while both the ball lock and the flat sided hole concept were evaluated as part of the vibration test, Section 8.2.

By concensus the flat sided hole technique was selected for production design, although each should function equally well. The nose cap was structurally analyzed in detail for this hole configuration, Section 6.3.

5.3 Thermal Analysis - A finite element thermal analysis was conducted for one of the initial plasma arc test models (Concept 6) to compare the modeling technique against thermocouple test data. This model was then expanded to define temperature distributions for the penetration assembly installed in the nose cap. The latter provided early guidance for materials selection, when the design temperature was only 2520F. A final, more sophisticated analysis was conducted for the 14414.1C entry trajectory and involved cross radiation exchange between upper, sides, and lower quadrants of the nose cap. Both the stagnation region to define maximum temperatures, and the leeward region to determine maximum circumferential gradients were analyzed. Cross sections of the 48-node circular model with maximum

temperatures or gradients indicated are shown on Figures 5-19 and 5-20 for the stagnation (Port No. 7) and leeward (Port No. 1) penetration assemblies, respectively. It is seen on Figure 21 that the nose cap reaches a temperature of 2700F, which is 40F higher than computed for a full nose cap model. This disparity is attributed to modeling differences, since the penetration assembly model was confined to 11.0 in. diameter and key time-temperature histories for participating cross radiation quadrants were conservatively selected. Maximum columbium port temperature was computed to be 2650F, while the major portion of the pressure tube is 2573F, although the end must connect to the union/nut combination which peaks at 2580F. These temperatures were used for design and test guidance.

Maximum circumferential gradients, shown on Figure 5-20, were found to be inconsequential for producing thermal stress, being only 29F maximum for metal parts and only 36F for the RCC spacer.

5.4 Structural Analysis and Test - As pointed out previously, the penetration assembly was designed for purposes other than minimum weight, and, as such, possessed strength capability far in excess of that, which could reasonably be introduced from the serpentine pressure tubes. Never-the-less, a requirement was established to ensure that the weak link of the penetration assembly would be the pressure tube, the purpose of which was to assure that if failure occurred, only a small opening would be exposed for admission of hot boundary layer air into the nose cap cavity. It is apparent that with the columbium port, union, and nut that this combination far exceeds the strength capability of the pressure tube. However, the graphite port, which remained a backup, could feasibly become the weak link, and, hence, was used to evaluate strength.

The penetration assembly was analyzed for axial strength but was tested for bending capability. The original analysis was conducted, when the pressure tube was 5/32 in. diameter with 0.015 in. wall. Axial failing load of this tube was computed to be 170 lb. For the 1/4 in. diameter 0.015 in wall tube, used in the final design, the failing load increases to 313 lb. The graphite port was computed to fail in net tension at 400 lb., while thread failure should conservatively range between 132 lb. and 484 lb., depending upon whether the thread strength is dominated by graphite or SiC properties. Based upon bending tests it was judged that thread strength would be closer to the higher value. However, even if the lower value was used, it is virtually impossible to introduce a large tension load into the penetration assembly through a bent tube, so this failure mode is highly unlikely.

Two series of bending tests were conducted for the penetration assembly with graphite port. The first employed the 5/32 in. diameter columbium pressure tube and resulted in tube failing bending moments of 13.3 and 14.2 in. lb. where the tube enters the retention nut. Substitution of a 5/32 in. diameter solid steel rod resulted in a bending moment of 109.6 in. lb. before excessing yielding of the rod forced termination of the test. There was no apparent damage inflicted on the graphite port.

In order to force failure of the port the second test series was conducted using a 1/4 in. diameter solid steel, 120 KSI heat treat, rod. In addition three of the four graphite ports were subjected to oxidation at 2500F for periods ranging to 7-hours (18.4% weight loss.) No post coating oxidation protection treatment was applied to the graphite ports. Results of these tests are shown on Figure 5-21, where it is seen that the maximum moment

achieved to cause failure of the graphite port was 122 in. lb., relative to the location where the rod enters the retention nut. Two failure modes were evident. The first produced complete failure of the port in the hollowed out region where the threads terminate. The second mode, which occurred on one port, resulted in thread shear and fracture of the edge of the port. In this case the union remained trapped and could not be extracted without disassembly.

The estimated failing load for the 1/4 in. diameter, 0.015 in. wall columbium pressure tube was 35 in. lb. and is shown on Figure 23 for comparison. It is evident that there is some oxidation weight loss of a graphite port that will cause it to become the weak link in the system. If a graphite port were to be considered for the SEADS application a correlation between mission cycling and weight loss would have to be established. Further, a post coating sealer should be used like that for RCC to extend mission life.

6.0 NOSE CAP RELATED ANALYSES

6.1 Thermal - The local temperatures and gradients in the nose cap, as influenced by the presence of a SEADS penetration assembly, were computed as part of the penetration assembly thermal analysis, Section 5.3. Another thermal analysis performed was that to assess the effect of cross radiaion blockage from the two 8-in. diameter insulated manifolds (support posts) to which the pressure tubes attach. The purpose of this was to determine if significant temperature changes or gradients are introduced into the nose cap from heat blockage, as compared to the production nose cap.

Due to the assymetry of the insulated manifolds, a full nose cap cross radiation analysis was performed. The analytical technique used on the production nose cap could not be used, since view factors with blockage could not be handled. It was, therefore, necessary to employ another analytical technique and confirm that without blockage results were identical to productioin design analysis. Results showed only 2F difference at the maximum temperature location and 18F maximum difference between any two corresponding nodes, thus validating the analytical technique.

The thermal blockage model geometry included nose cap shell and insulation nodes identical to those used in the production nose cap analysis. Each insulated manifold was divided into four longitudinal segments plus an end cap. For each division an external surface node and an insulation node were used. The small diameter pressure tubes were not modeled, since their contribution to heat blockage was considered insignificant in comparison with the two 8-in. dia. insulated manifolds. Entry trajectory 14414.1C was analyzed.

Changes in peak nose cap temperature are shown on Figure 6-1. The largest increase is near the forward end of the port side manifold on the inner surface and is 56F. The corresponding external surface node incrase is 34F. The blockage raises the peak nose cap temperature to 2693F compared to 2684F without blockage. This was considered to be insignificant in terms of mission life prediction. The maximum thermal gradient increase was found to be only 1F per inch.

The hottest manifold is on the port side where the end cap reached 2585F. The starboard manifold peaked at 2476F on the cyclindrical surface.

The nose cap temperature changes were assessed for impact on thermal stress. It was conservatively estimated that the increased temperatures would produce no more than 2% increase in thermal stress in the dome. Since thermal stresses are considerably lower than those produced by airloads, the effect of heat blockage was considered inconsequential.

6.2 Structural Analysis - Concern over the stability of the nose cap with fourteen pressure port holes prompted an extensive analysis of the nose cap. It had been intended to incorporate tapered, circular pads around each penetration to build up the local thickness to 25-plies (6-ply doubler) as compared to the basic 19-ply dome. This was intended to restore local strength as well as to provide sufficient thickness for receipt of the countersink configuration of the port. In addition to analysis of the intended design, it was required to analyze other possible configurations, including 32-ply local beefup around each hole (13-ply doubler) a uniform 21-ply dome, and a 19-ply dome without local stiffening. These were compared to the baseline production nose cap without holes.

A NASTRAN differential stiffness analysis approach was used like that employed on the production nose cap. It is an iterative technique and is in effect a large deflection analysis. Buckling was assessed by tracking slope changes to individual elements as load level was increased. A "snap through" buckling mode is characterized by a slope reversal, while a "collapse" mode results, when the slope continues to increase, the limiting value being determined by the asymptote to the slope change curve. The lowest buckling levels were found to be of the snap through type. The finite element model is pictured on Figure 6-2. Because of load and geometry symmetry, only half the nose cap was modeled. This was analyzed for the production design and was found to produce identical results as a full model.

The nose cap was analyzed for vehicle 5.3 loads, in particular a boost load condition designated BP482. This condition was found to dominate for the nose cap dome, which was the region of interest.

The stability analysis results are illustrated on Figure 6-3, where snap through buckling tracking is illustrated. The critical area of the nose cap for this buckling mode is shown on Figure 6-2. The analysis produced some peculiar results in that 6-ply ring stiffening around each hole produced a modest increase in stability, while further stiffening by using a 13-ply doubler or 2 additional plies over the entire nose cap actually resulted in decreased stability. The latter effect was unexpected and resulted in intense evaluation to determine the reasons for this phenomenon.

That this effect is not the result of holes in the nose cap is demonstrated by the 21-ply dome analysis (Figure 6-3), where the buckling level with or without holes is reduced substantially from the 19-ply nose cap. It was found from the evaluation that the phenomenon was produced by the flatened regions of the nose cap and the redistribution of internal loads that results from stiffness changes, particular the ratio of dome to flange stiffness. The 21-ply dome (and the 13-ply ring stiffened dome to a lesser extent) cause more load to be carried in the critical flattened regions, where the added bending stiffness is insufficient to overcome the load increase.

The results of the buckling analysis showed that the 6-ply ring stiffened dome, as originally conceived, is near optimum and provides a stability margin slightly greater than the production nose cap.

Actually, the buckling analysis is somewhat of an academic issue, since the structural integrity of the nose cap is dominated by flange strength. This is shown on Table 5, where it is shown that for all of the SEADS type configurations analyzed, the flange region margin of safety at ultimate is 0.40, whereas stability margins are greater than 4.91, and for the 6-ply ring stiffened design it is 8.46.

Stability and local hole stresses were also examined for the application of bending moments from the pressure tubes. For this analysis it was assumed that each of the tubes applied a limit bending moment of 25 in-lb (35 in-lb ult.) in a direction that would lower the stability margin. Only the unstiffened SEADS nose cap was analyzed for stability, where it was determined that for the critical buckling region of the nose cap the change in stability was only 0.27%. This was considered to be insignificant, particularly in view of the fact that the nose cap flange limits the load capability.

The effect of tube bending moment upon local hole stresses was determined for each of the SEADS configurations in combination with the applied airloads. It was found that hole No. 1 at the top centerline produced the lowest margin. Results of this analysis are summarized on Table 5. It is seen that the 6-ply ring stiffened design has a margin of safety of 7.11 at ultimate, far in excess of the flange margin. With the decision to use the flat sided hole in the nose cap for anti-rotation of the penetration assembly, the hole region was analyzed in detail to more accurately define margins. This analysis is described next.

6.3 Flat Sided Hole Stress Analysis - A finite element NASTRAN analysis of hole No. 1 was conducted for the flat sided hole configuration. This hole was determined to produce the lowest margin from the previous analysis, when a 25 in-lb limit bending moment was applied in conjunction with airloads.

The non-circular hole configuration is depicted in Figure 6-4. The approach taken was to obtain a unit solution for 20 in-lb tube moments applied in two mutually orthogonal directions and then couple the solutions to determine the tube moment to cause hole failure. The bending moments were introduced as running loads around the hole. Boundary conditions (loads and enforced displacements) were obtained from the nose cap stability model. These were checked out using the hexagonal hole configuration to assure comparable results between the full model and the localized detail model. The overall math model is illustrated on Figure 6-5, while a view of the solid elements describing the details around the hole is shown on Figure 6-6.

It was found that a moment vector parallel to the flat sides of the hole produced maximum stresses, and the allowable or maximum moment at ultimate was computed to be 109 in-lb. Since the maximum moment capability of a 1/4 in. dia. x 0.015 in. wall columbium tube is only about 35 in-lb, a margin of safety greater than 2 exists. The flange region with a margin of safety of 0.40 (Section 6.2) thus remains the critical element of the nose cap.

TABLE 5

SEADS NOSE CAP FAILURE SUMMARY

Failing Load Level (Margin of Safety at Ultimate)

$$M.S. = \frac{\text{Failing Load Level}}{1.4} - 1$$

NOSE CAP CONFIGURATION	STRENGTH FAILURE				STABILITY FAILURE
	DOUBLER FLANGE	FLANGE LUG	ORIFICE HOLE WITHOUT TUBE BENDING	ORIFICE HOLE WITH TUBE BENDING	
LESS PRODUCTION	4.24(2.03)	1.91(0.37)	N.A.	N.A.	12.74(8.10)
SEADS, UNSTIFFENED	4.29(2.06)	1.96(0.40)	14.11(9.08)	7.45(4.32)	11.70(7.36)
SEADS, 6-PLY RING STIFFENED	4.28(2.06)	1.96(0.40)	15.79(10.28)	11.35(7.11)	13.25(8.46)
SEADS, 13-PLY RING STIFFENED	4.28(2.06)	1.96(0.40)	18.41(12.15)	13.82(8.87)	11.60(7.29)
SEADS, 2-PLY DOME STIFFENED	4.06(1.90)	1.96(0.40)	15.19(9.85)	8.03(5.31)	8.28(4.91)

Failing Load = (Failing Load Level) x (Applied Limit Load)

7.0 PRESSURE TUBE ROUTING AND SUPPORT

During the early stages of the program, Vought was responsible for developing the scheme for routing the fourteen pressure tubes from the penetration assemblies to the nose cap bulkhead. Subsequently, Rockwell undertook this aspect of design but employed the basic concept devised by Vought.

Several routing schemes were considered, such as (1) individual routing of tubes, (2) ganging several tubes together for mutual support and (3) utilizing two stiff support posts, cantilevered off the bulkhead with each collecting seven pressure tubes. The latter scheme was selected on the basis of stiffness in a dynamic environment, ease of insulation and relative ease of installation. The schemes are illustrated on Figure 1-6.

Examination of the nose cap bulkhead revealed a location on either side that would accommodate mounting of the support posts and enable pass-through or pickup of individual pressure ports. The concept is illustrated on Figures 1-6 and 6-1. Each support post, Figure 7-1, was conceived as a thin (10-12 mil) walled nickel alloy tube (rolled and welded) to support 3/8 in. diameter individual internally mounted pressure tubes. The small 5/32 in. diameter pressure tubes, running from the penetration assembly, would attach to the 3/8 in. diameter tubes at the end of the support post. This concept was analyzed both thermally and dynamically to determine feasibility.

Thermal analysis showed that there would be no problem in protecting the aluminum nose cap support bulkhead to its 350F temperature limit with 2.5 in. thickness of 12 PCF Dynaflex or 9PCF HRSI insulation attached to the 2.75 in. diameter support tube. Details of this analysis are not included in this volume because the final design configuration selected by Rockwell was a solid aluminum post (manifold), gun drilled at each of the pressure tube locations. See Figure 1-4. The aluminum manifold was insulated with Dynaflex to limit the aluminum to 350F maximum. The analysis was conducted by Rockwell.

Dynamic analyses were performed by Vought on the support post and the small diameter tube array to determine if this system was feasible. At the time of analysis 5/32 in. diameter Inconel 702 tubes were under consideration, since the higher temperature requirements of entry trajectory 14414.1C had not yet been imposed. Further, the vibration environment analyzed was quite high, producing 29.5 GRMS with a peak power spectral density of 2.0 G^2/Hz in the 50-250 Hz band. This vibration level was applied in all three axes at both the nose cap and bulkhead, simultaneously. Ultimately, as noted in Section 8.2, the level was reduced such that the largest test level was .55 G^2/Hz in the 30-50 Hz range on the nose cap.

Several tube configurations were investigated in an effort to find those that could survive in the dynamic environment. It should be noted that all tubes required bends or loops to avoid excessive loads as the tubes expand during imposition of the thermal entry environment, and as the nose cap and bulkhead deflect under airloads. Tube configurations were found that appeared to be able to meet the requirements. However, since the design environments were reduced significantly and Rockwell developed the final design configuration and performed the final analysis, the Vought analyses are not described in this document. Rockwell results are summarized in Section 8.2.

In summary it was concluded that a design employing two support posts, cantilevered off the nose cap support bulkhead, and collecting seven, small diameter pressure tubes each, was feasible and offered the most desireable arrangement.

8.0 COMPONENT TESTS

Two major component tests were conceived to demonstrate, primarily, structural integrity of the pressure tube routing design. The first of these was a thermal exposure of two selected tube configurations to determine resistance to repeated temperature cycles with the tubes constrained. The second was a dynamic test of the left hand tube array and support manifold with simultaneously applied, independently controlled nose cap and bulkhead vibration spectra. Each of these are described in this secion.

8.1 Thermal Deflection Test of Pressure Tubes - Each pressure tube is anchored at a penetration assembly at one end and the manifold at the other. During entry, the thermal environment in the nose cap produces a computed temperature level of 2573F on each of the tubes, causing them to expand, while essentially fully constrained at each end. While bends in the tubes relieve axial strain, a significant bending strain may be induced by constrained expansion, causing material creep strain. Returning to room temperature would then result in a built-in strain, opposite in sign to the creep strain. Repeated cycling could then feasibly cause low cycle fatigue failure.

In addition to the thermally induced strain a deflection induced strain is introduced into the pressure tubes which is maximum at room temperature. The condition occurs when airloads on the nose cap cause the support bulkhead to dish, which in turn rotates the mounting base of the manifold and swings the tube attach end. This angluar movement pulls the manifold end of each tube relative to the penetration end. Early analyses indicated this movement could be as much as 0.25-0.30 in. depending upon the tube. However, revised airloads (downward) and shorter manifolds ultimately reduced this forced deflection to an insignificant 0.04 in. The tube test rig was designed to accommodate a forced deflection test requirement, but, because of the small deflection computed, it was not applied.

The thermal strain and forced deflection scenarios prompted the need for a test to evaluate the integrity of the tubes under these conditions. The test was conceived as one in which a graphite fixture would hold a single tube for test with the nose cap tube end attached to a penetration assembly and RCC disc. The manifold end of the tube was anchored to the graphite fixture. The scheme is illustrated on Figure 8-1.

Although graphite was used for the test fixtures it was found that it had to be insulated to restrict its' temperature rise to 500F to avoid excessive thermal expansion and relief of pressure tube thermal strain. Each pressure tube was built with an additional length to simulate the thermal expansion of the aluminum manifold, which, although insulated, would have some temperature rise and extension when the tubes were at maximum temperature. The added length also offset thermal expansion of the graphite test fixture.

Rockwell determined that tubes No. 5 and No. 8 would be the most critical for thermally ionduced strain. These were 1/4 in. diameter x 0.015 in. wall coated columbium. Three tubes of the No. 8 configuration and one of the No. 5 configuration were supplied by Rockwell for test. In addition a tube for calibration and checkout was provided. The calibrator tube with thermocouples attached was used to establish test facility power settings, cycle times, and prove the uniformity of heating.

The facility in which the test was conducted is pictured on Figure 8-2. It included a bare graphite heater bar array and a water cooled radiator. Two pressure tube assemblies were tested simultaneously. They were shuttled back and forth between the heater and radiator to alternately heat and cool the tubes to represent to a degree the design temperature history imposed on the tubes and to reduce the overall test time. The profile is shown on Figure 8-3. No attempt was made to actually duplicate the temperature history. The atmosphere was air set at 0.4 mm Hg.

The low pressure, coupled with the bare graphite heater bars, almost proved the undoing of the test. The graphite heater bars oxidized, but, apparently, oxidation was incomplete, producing CO, rather than CO_2. As Rockwell diagnosed the problem, the smaller CO molecule was able to penetrate the coating on the columbium, creating an embrittled substrate. With the embrittled tubes it is somewhat remarkable that they survived for the number of cycles that they did. The cycling history for the four test tubes is as follows:

SPECIMEN	TUBE CONFIGURATION	CYCLES COMPLETED	FAILURE
1	8	74-87	YES
2	5	140	NO
3	8	68	YES
4	8	136	YES

The specific cycles of failure on specimen No. 1 is unknown, since initially the tubes were to be inspected after a block of cycles. Subsequently, the tubes were observed through a view port in the vacuum chamber to determine the precise cycle for failure. Note that all failed tubes are of the No. 8 configuration.

As a means of gaining some insight into possible creep strain, the movement of the "manifold end" of each tube was measured after "x" cycles, when freed from the graphite fixture. The movement was invariably a shortening of the tube as expected, the values being as follows:

SPECIMEN	TUBE CONFIGURATION	MEASUREMENT CYCLE	"SET", IN.
1	8	50	0.19
2	5	50	0.25
3	8	36	0.10
4	8	49	0.15
5	8	100	0.14

Following these measurements the tubes were pulled to their original position and reclamped for continuance of cyclic testing.

Post test evaluation of the tubes showed the embrittled nature as well as crystal growth. In addition flaking on the external surface of the tubes was observed during the test. This is apparently normal and was encountered during chemical compatibility tests, as well. It was also observed that a deposite of material tended to form inside the tubes to close off the bore just down stream of the flare. No such deposits were found in the union, port, or anywhere else along the tube. This material was analyzed by Rockwell and was found to be silica, believed to have outgassed from the silicide coating. The outgassed material migrated to the open end of the tube (the manifold end was sealed off with a plug of insulation), where it condensed at the cooler region near the penetration assembly. This phenomenon is not expected to be a flight problem because (1) the penetration assembly is hot, preventing condensation and (2) localized flow and turbulence at the port hole from leakage should discourage buildup. Penetration assemblies, employing the ball lock anti-rotation device, were used in these tests. Post test inspection showed no damage or anomalous behavior of these assemblies. Disassembly was conducted with ease.

In summary, the test atmosphere created an environment that was excessively severe to the test tubes, promoting embrittling and early tube failure. Even so, the tubes survived for periods in excess of the estimated 25-30 mission life of the SEADS components. Judging from the measured set data, a degree of creep strain exists, but is not severe enough to cause concern. None of the penetration assemblies suffered oxidation during test nor did threaded connections tend to lockup.

8.2 Vibration Test - Random vibration testing was conducted on the left hand tube array. The test article consisted of the manifold, its insulation assembly, the seven pressure tubes and their penetration assemblies mounted in RCC. In an effort to reduce cost, while still maintaining a test program with good fidelity, a method of testing was conceived wherein two simultaneous, independently controlled shakers provided input spectra to both the bulkhead and nose cap end. The nose cap was simulated by a multifaceted aluminum casting with each facet receiving a penetration assembly with RCC disc, located as it would be on the nose cap. The concept is illustrated on Figure 8-4. This approach was considered less expensive that an "all up" test, complete with RCC nose cap and tested in an acoustic environment.

The primary reasons for conducting the test were to:

(1) Validate the Rockwell dynamic anmalysis, since analysis was the method by which SEADS was to be certified for flight for the dynamic environment.

(2) Demonstrate the structural dynamic integrity of the system.

The input vibration test levels (and design values) were based upon measured nose cap and bulkhead vibration response of the production design qualification nose cap assembly to the acoustic environment. The accumulated vibration data was analyzed by Rockwell to establish enveloped design spectra in each of three mutually perpendicular axes for the nose cap and bulkhead.

Rockwell analyzed the SEADS system, both left and right hand arrays, using a finite element technique. Each tube was modeled as 26 nodes and 24 elements. Inputs were simultaneously applied to determine mode shapes, frequencies, responses, deflections, stresses, and bending moments.

The analysis technique was also employed to determine static stresses for launch accelerations and entry loads. Analyses results showed that the tubes would not be overstressed and fatigue life was adequate. However, as noted in the purposes above the analysis would be accepted only if vibration test data and analysis were comparable.

From the above analysis optimum setups were determined for the vibration test, recognizing that for each shaker only one axis could be input for a given setup, whereas the design analysis included simultaneous application of vibration levels in three axes. By analyzing nine possible test configurations (three axes for each of two shakers) it was determined that two setups as follows would produce maximum stress levels for all tubes without significantly overstressing any one tube:

(1) Bulkhead Y-axis with Nose Cap Y-axis

(2) Buldhead X-Axis with Nose Cap Z-axis

Because a single axis design level input would not produce stresses as high as when three axes were input simultaneously, the single axis levels were increased to produce stress levels as high as design levels. The resultant test spectra are shown on Table 6.

The test setup is pictured on Figures 8-5 and 8-6. It should be noted that, due to a drawing error, the mirror image of the left hand system was actually tested. Since all components were mirror images, response and results were identical to that which would have resulted from testing the left hand system.

Each pressure tube was instrumented at each end with three axial strain gages spaced 120° apart such that bending and axial strain components could be separated if desired. In addition, four traixial accelerometers and four axial accelerometers were installed on the "nose cap" fixture, one triaxial accelerometer was mounted to the "bulkhead" fixture and two triaxial accelerometers were installed on the manifold, one at the base and one at the free end. The four axial accelerometers were located adjacent to selected penetration assemblies to detect any loosening, should it occur. Since the number of desired data channels exceeded recording capacity, data sampling from one minute bursts were accumulated over the first three minutes of test to gather data on all channels. Results were reviewed and the channels showing highest stress levels were selected for record during the remainder of the 21- minutes for each test. The duration was equivalent to 30 missions with scatter factor of four.

As noted previously, there were seven penetration assemblies attached to the simulated nose cap casting. However, these were not all identical. In an effort to evaluate two alternate anti-rotation schemes and to assess the behavior of graphite as a possible port material the seven locations were divided as follows:

TABLE 6

SEADS RANDOM VIBRATION TEST CRITERIA

BULKHEAD

X-Axis

20-25 Hz:	+15dB/OCT
25-30 Hz:	$0.117g^2/Hz$
30-40 Hz:	-15dB/OCT
40-120 Hz:	$0.025g^2/Hz$
120-300 Hz:	-3dB/OCT
300-2000 Hz:	$0.010g^2/Hz$

Y-Axis

20-50 Hz:	+6dB/OCT
50-100 Hz:	$0.018g^2/Hz$
100-2000 Hz:	-6dB/OCT

NOSE CAP

Y-Axis

20-30 Hz:	+6dB/OCT
30-50 Hz:	$0.55g^2/Hz$
50-120 Hz:	-10dB/OCT
120-600 Hz:	$0.028g^2/Hz$
600-700 Hz:	+24dB/OCT
700-900 Hz:	$0.11g^2/Hz$
900-2000 Hz:	-10dB/OCT

Z-Axis

20-30 Hz:	+6dB/OCT
30-50 Hz:	$0.44g^2/Hz$
50-120 Hz:	-10dB/OCT
120-600 Hz:	$0.022g^2/Hz$
600-700 Hz:	+24dB/OCT
700-900 Hz:	$0.088g^2/Hz$
900-2000 Hz:	-10dB/OCT

DURATION

42 seconds/mission/axis in each axis of vibration
(70 minutes/axis/100 missions)

PORT LOCATION IDENT. NO.	PORT MATERIAL	ANTI-ROTATION FEATURE
5	Columbium	None
6	Columbium	Flat Sided Hole
7	Graphite	Ball Lock
8	Columbium	None
9	Columbium	Flat Sided Hole
10	Columbium	Ball Lock
11	Columbium	None

Thus, graphite ports were represented at two locations and no anti-rotation device was used at three. As noted above, accelerometers were installed near four of these locatons (No. 5, 6, 7, and 11) in an effort to detect loosening. None were detected and by post test, hand feel, none occurred.

A fabrication problem on the columbium pressure tubes was exposed during final configuration adjustment by Rockwell after coating. A tube snapped at the coating to bare section juncture at the manifold end of the tube, revealing a highly brittle structure. (The uncoated portion is to enable final cutting and flaring on assembly). The problem was traced to insufficient thermal protection of the uncoated section of the tube during routine thermal oxidation acceptance testing of the coating. The temperature of the uncoated end apparently exceeded 800F, enabling oxidation embrittlement to occur. This was solved by Rockwell with a water cooled collar to limit the temperature of the uncoated section to an acceptable level. Remade tubes using this approach functioned well and flared easily.

It was discovered, during installation of the pressure tubes, that three out of seven MS type 90° elbows at the end of the manifold exceeded angular tolerance. This prevented strain free tube installation. The out of tolerance condition was deduced when "good" elbows were substituted for "bad" elbows and the previously errant pressure tubes fell into place. The out-of-tolerance condition was subsequently confirmed by direct measurement. Replacement units solved the problem.

Because the test setup represented installation in the nose cap, advantage was taken of this opportunity to check out installation and fitup of the manifold insulation system. The insulation design was that proposed for production, deviating only on the segments adjacent to the base of the manifold. The elements are pictured in Figure 8-7, while the installed system is shown on Figure 8-8. Installation proved somewhat difficult and resulted in some damage to one of the collars by the manifold elbows. Further, some degree of gapping occurred lending fear to possible excessive radiation heating of the aluminum manifold. This experience subsequently resulted in a revised design. Therefore, installation details are not provided in this volume.

The two vibration tests wre conducted without incident. Transformation from the Y-Y axis configuration to the X-Z axis configuration, which involved relocating the shakers, was aided by a spacer tube connected between the "bulkhead" and "nose cap" shakers, thus preserving accurate geometric relationship between components. The accuracy was evident, when all pressure tubes were reinstalled at the penetration assemblies without having to forcible move them into place.

Predicted versus measured stresses for each of the tubes are summarized on Table 7 In general, Rockwell predicted stresses were higher than measured, due to a purposely conservative analysis. Only Tube No. 8 displayed a significant reversal to this trend. It produced the highest strain levels for both test configurations and, typical of all tubes, was highest at the manifold end. This tube was the straightest of all, having two 90° bends but no complete reversals, so it would be expected to experience highest strains. Typical power spectral density (PSD) strain plots for Tube No. 8 response are shown on Figures 8-9 and 8-10. The low frequency response was typical of all the tubes and was believed to be due to forced deflection rather than response. This was confirmed, when control accelerometers were analyzed for displacement. A typical PSD plot of displacement is shown on Figure 8-11. It displays the characteristic shape of the PSD strain plots, providing evidence that the high strains are not resonance induced.

Rockwell re-analyzed this low frequency region for Tubes No. 5 and No. 8. These represented a typical and highest strain tubes. Strain spectral density (SSD) plots were generated which compared favorably (though conservatively) with the test results. Typical results for Tube No. 8 are shown on Figure 8-12. The general agreement between analytical predictions and test results validated the analysis approach, which was used to confirm flight worthiness of both left hand and right hand pressure tube arrays.

Post test inspection showed all hardware survived without failure. None of the penetration assemblies loosened, even those without an anti-rotation feature. Nut to union removal torques varied between 5 and 30 in-lb and compares with an assembly torque of 20 in-lb.

In the process of disassembling the No. 9 penetration assembly, the graphite port was fractured. It isn't clear if this was the result of vibration damage or improper removal technique. However, it does point out the need for caution if graphite was to be used, and a requirement to gather more peformance data on graphite ports.

The ends of the flare on the pressure tubes appeared to have coating damage. This is shown by Figure 8-13 which shows the best and worst of the tubes. This region is fragile and vulnerable to chipping, where it is sandwiched between the union and nut. The vulnerability was evident in each of the plasma tests, so it is not confined to the vibration environment. Exposure of the tubes to 2000F for 15 minutes confirmed coating damage at the flare, but no other coating damage along the length of the tube was evident. Rockwell proposed that the damage tolerance could be enhanced by dressing the coating buildup at the end of the flare to avoid installation crushing damage.

In conclusion the dynamic analysis was validated by being able to conservatively predict tube response and stresses. The test demonstrated system dynamic loads surviveability for at least 30 missions, which is the life limit expected, based upon plasma arc tests. The vulnerability of the flared end of the tubes was again evidenced, although this should be alleviated somewhat by dressing the coating to eliminate local thickness buildup. Rotational oscillation of the penetration assemblies did not surface as a problem, but it was decided to employ the flat sided hole anti-rotation scheme for final design as a precautionary measure.

TABLE 7

COMPARISON OF PRESSURE TUBE STRESSES

TUBE NO.	TUBE END	3σ PEAK TUBE STRESS, PSI Y-Y AXES* TEST	Y-Y AXES* ANALYSIS	X-Z AXES* TEST	X-Z AXES* ANALYSIS
5	Blkhd.	5640	7548	5264	8312
	Nose Cap	3399	11179	2578	6737
6	Blkhd.	4984	7311	4480	6970
	Nose Cap	2669	9412	2298	7430
7	Blkhd.	5144	8706	4429	6813
	Nose Cap	3441	7837	3246	6679
8	Blkhd.	14836	12730	10872	8458
	Nose Cap	4801	7344	1665	3459
9	Blkhd.	3172	8478	7416	10712
	Nose Cap	2048	4427	3770	3877
10	Blkhd.	3600	7858	8244	9380
	Nose Cap	2519	3957	3708	6650
11	Blkhd.	4638	7099	6552	8338
	Nose Cap	5838	5618	4086	5550

*Y-Y Axes = Shaker Y-Axis Bulkhead and Y-Axis Nose Cap.
X-Z Axes = Shaker X-Axis Bulkhead and Z-Axis Nose Cap.

9.0 MISCELLANEOUS ACTIVITIES

In the conduct of the foregoing tasks two incidents arose on which further investigation was conducted in an effort to resolve discrepant behavior. One of these was the disparity between pyrometer and thermocouple data noted during plasma arc testing in the NASA-LaRC test facility. The second was the unexpected high temperature excursion encountered during plasma arc testing in the NASA-ARC test facility. The investigations and resultant conclusions are addressed in this secton.

9.1 Pyrometer/Thermocouple Disparity - As noted in Section 5.1 for the last plasma arc test series, conducted in NASA-LaRC Facility B, a discrepancy arose between pyrometer measured surface temperature and that indicated by thermocouples installed on the model. Pyrometer temperatures were approximately 300F higher, when corrected for spectral emittance of coated RCC. Attempts to determine if the difference was associated with arc reflection by tracking temperature response after the arc was extinguished proved unfruitful, presumably due to data system time lag.

Two other approaches were, therefore, pursued in an attempt to determine the validity of the thermocouple measurements. It should be noted that thermocouples were mounted on the aft side of the RCC disc as well as on other internal components. It was therefore necessary to extrapolate backside temperatures to the front face, based upon previous thermal analyses of the penetration assembly. However, because of differences in model geometry and environmental conditions, it was felt necessary to thermally analyze the test model to validate the gradient across the RCC disc and determine the ability to predict temperature measured on other parts of the model.

In addition, concern was expressed about the mounting technique of the thermocouples, including possible poisening of the bead from the attachment cement, error due to conduction losses, or electrical losses through the insulator. A thermocouple test program was conducted to evaluate these effects.

9.1.1 Model Thermal Analysis - A finite differencing analysis was performed on the model with columbium pressure port. Model geometry is shown on Figure 9-1. Two analyses were conducted: one in which the imposed heat flux on the front face was adjusted to produce backface temperature response corresponding to backface thermocouple data; and one where the imposed heat flux was adjusted to match pyrometer indicated frontface temperature.

A comparison between calculated and measured response, during the heating phase, are shown on Figures 9-2 and 9-3, respectively for controlling to thermocouple response and controlling to pyrometer response. It is evident that the first technique corresponds more closely to all thermocouple data and results in a maximum gradient through the RCC disc of 119F at the end of test. If the pyrometer data is to be believed then all of the thermocouples would have to be substantially in error. This would have to include platinum rhodium thermocouples, used in a previous test series which agreed well with tungsten rhenium thermocouples.

A similar analysis was conducted for the cooldown phase after the arc was extinguished. These results are illustrated on Figures 9-4 and 9-5. While the thermocouple controlled model indicates some inaccuracies of prediction remote from the heat source, the pyrometer controlled model is even more so.

These results by themselves do not conclusively prove that the thermocouples were providing the more correct temperature indications, but if they weren't, then even the platinum rhodium thermocouples, from previous tests, which were not affected by bonding material or electrical loss across the insulator, would have to be in error. This could only occur from heat conduction losses. This effect was investigated in the test program discussed next.

9.1.2 Thermocouple Measurement Accuracy - A test program was conducted to assess thermocouple measurement variations, when attached to RCC in the manner used on the plasma arc models. Alternate installation configurations and alternate thermocouple types were examined for comparison. Three types of pyrometers were also involved for interest. The heater for this test was a resistance heated, air, tube furnace that had been routinely used for the Shuttle Leading Edge Structural Subsystem (LESS) program for acceptance testing of coated RCC. Two platinum rhodium thermocouples are employed to measure furnace temperature.

Test thermocouples were mounted on RCC segments and installed in the furnace as shown schematically on Figure 9-6. Thermocouple leads were insulated to produce a temperature gradient from the thermocouple juncture down the length. The furnace was operated at maximum capacity to produce an RCC temperature of about 2300F. Configurations tested are illustrated on Figure 9-7. Tungsten rhenium thermocouples, insulated with alumina rod, were of primary interest. These were to be compared with chromel alumel and the platinum rhodium furnace thermocouples. For qualitative evaluation Tempilaq temperature indicating paint was also applied to the corners of the RCC segment.

Results of this investigation are summarized on Table 8. The data shows that the tungsten rhenium thermocouples were consistent, with the method of mounting or bonding material making little difference in results. Temperatures compared very favorably with the platinum rhodium thermocouples and the Tempilaq paint. Chromel alunel thermocouples read low for some unknown reason. Even the pyrometer data compared well with the thermocouples except for the test where misfocussing was suspected. A rerun at 2000F brought all measurements into agreement.

It was concluded that the thermocouples like those used in the plasma test will produce accurate, consistent results and the preponderance of data suggests that the thermocouples in plasma tests were reading correctly. The correlary to this is that the pyrometers in plasma test were reading excessively high.

9.2 Plasma Arc Test Anomally - Upon the initial exposure of the plasma arc test model in the NASA-ARC Aerodynamic Heating Tunnel, the temperature soared to 2950F, while the coating on the front face of the graphite holder eroded away. This was surprising, since the calibrator model indicated temperatures should be at the desired 2660F level. Even when the test model was transferred into another holder with sound coating and facility power was reduced, temperature level exceeded expectations. The question posed was why was the temperature significantly higher on the test model than expected from the calibrator data?

THERMOCOUPLE TEST RESULTS

(TEMP, F)

INSTRUMENT	CALIBRATION	SPECIMEN NO. 1 (10 Min.)[1]	SPECIMEN NO. 2 (6 Min.)[1]	SPECIMEN NO. 3 (7 Min.)[1]	PYROM. CHECK 2
MANUAL	-	-	-	-	2057
	-	-	-	-	(1990)
PHOTO II ϵ_λ[2]	2393	2380	2170	2393	2045
ϵ = 1.0 [2]	(2280)	(2270)	(2090)[3]	(2280)	(1980)
IRCON 300 ϵ_λ[2]	2382	2288	2522	2315	2057
ϵ = 1.0 [2]	(2248)	(2177)	(2348)[3]	(2198)	(1990)
P_t/P_t 10 Rh #1	2295	2230	2275	2290	1990
P_t/P_t 10 Rh #2	2300	2290	2300	2290	2010
W/Re ⊥ ASTRO		2260	2260	2270	2000
		2260	2260		
		2255		2270	
W/Re ‖ ASTRO				2280 Failed	
W/Re ⊥ SERM.			2260 Failed		
CHROMEL ALUMEL ⊥ ASTRO		2191	2235		1975
TEMPILAQ 2200F	-	Melt	Melt	Melt	
2300F	-	Melt	Melt	Melt	
2400F	-	No Melt[4]	No Melt	No Melt[4]	
2500F	-	No Melt	No Melt	No Melt	

NOTES:

(1) Time into run when data was taken.

(2) Bracketed values are raw data for an emittance of 1.0. Unbracketed temperatures reflect spectral emittance corrections for the wavelength sensitivity of the specific pyrometer used.

(3) Pyrometers probably misfocussed leading to pyrometer check run data in last column.

(4) No melt but dark spots present.

Several possibilities were investigated analytically using finite element analysis techniques. The postulated contributers to the anomally were:

(1) The presence on the penetration assembly could have altered internal cross-radiation, causing the disc to run hotter.

(2) Loss of coating on the holder produces a catalytic surface with higher operating temperature, thus driving more heat into the disc.

(3) The coated columbiium port could be catalytic thus raising the temperature of the adjacent low catalytic RCC disc.

(4) Local gap heating around the edge of the port could increase the temperature of the disc.

5) A combination of the above could prevail

The catalycity factors were suspected to dominate because the enthalpy of the plasma stream in the NASA-ARC facility was estimated to be at least three times that in the NASA-LaRC test facility. This results in greater dissociation and therefore more pronounced catalytic effects. This would more readily explain why equivalent test models would yield vastly different results.

The approach taken was to analyze the calibrator as a means of establishing (or inferring) the time history and distribution of heat flux that would duplicate the measured temperature response. Next, this heat flux was imposed on the test model geometry, adjusting in accordance with the factor being investigated, to compare analytical predictions against test measured temperature. From these results cnclusions were drawn to determine the most probable explanation for the anomalous behavior. The test model analyzed was the same as that analyzed previously and is shown on Figure 9-1.

The estimated enthalpy level of the test facility was 9000 BTU/LB., but because of the uncertainty of this value, both 7000 and 12000 BTU/LB. enthalpy levels were analyzed to bracket the problem.

It was found that cross-radiation blockage, caused by the penetration assembly, would in fact tend to lower surface temperature. Gap heating was found to be modestly influencial but by no means explained the anomally.

Individual contributions from a catalytic holder front surface or a catalytic port could not replicate the test measured temperatures; but, when these two effects were combined, a reasonable correlation between calculated and measured temperatures was obtained. The results are shown on Figure 9-8. Better correlation could be achieved by slight reshaping of the imposed heat flux, but this was deemed unwarranted, since it would not affect the ability to draw the necessary conclusions.

It was concluded that the temperature surge was probably due to a combination of the catalytic heating on the front face of the graphite holder and a partially catalytic columbium pressure port. Gap heatng provided only a modest contribution. With a partially catalytic pressure port the port temperatures were found to be reasonable, reaching a calculated maximum of 2729F for 7000 BTU/LB. and 2821F for 12000 BTU/LB. enthalpy levels. With the low enthalpy level in the NASA-LaRC facility the catalytic effects would be so small that they would not be observed.

The ramification of having a partially catalytic port installed in the low catalytic nose cap was assessed for the effect upon localized thermal stress in the nose cap and clearances between the port and the hole in the nose cap. Both effects were found to be insignificant.

10.0 FINDINGS

The most significant findings from this program may be summarized as follows:

(1) Holes can be introduced into the nose cap shell without impairing its structural integrity, as determined by analysis.

(2) The introduction of SEADS penetration holes does not reduce the mission life of the nose cap as demonstrated by long term plasma arc test exposure.

(3) Silicide coated columbium will survive the design temperature for multiple missions and will tolerate significant temperature overshoot.

(4) Small diameter, unsupported pressure tubes can be designed to withstand the Shuttle dynamic environment and yet be flexible enough to avoid damaging thermal stress.

(5) With the application of silicon carbide powder, as an anti-sieze compound, self bonding of silicide coated columbium, exposed to high temperature, can be prevented for an acceptable operational period.

(6) Silicide coating of the inside of small diameter columbium tubes can be accomplished.

(7) Siliconized graphite can serve as a viable backup to coated columbium port components, although with a reduced mission life.

(8) Iridium wire provides an effective lockwire approach.

(9) The oxidation rate of unprotected columbium is sufficiently slow, at least in the 2500F region, as to pose no safety of flight concern, when the silicide coating is breached.

(10) Coated columbium is partially catalytic and must be accounted for in high enthalpy environments.

(11) Optical pyrometer and thermocouple temperature measuring techniques can provide widely differing data in plasma arc testing. Controversy persists on which device is the more accurate.

(12) Vibration testing, using two independently controlled shakers, is feasible.

(13) Pressure measurement for this system is practical, even with high temperature, finger tight joints, although response may suffer.

(14) A ball lock device, employing a synthetic sapphire sphere, will provide a satisfactory, high temperature, anti-rotation scheme.

(15) Platinum and cobalt based alloys are chemically incompatible with siliconized RCC when in direct contact.

(16) This development program, involving four entities (NASA/LaRC, NASA/JSC, Rockwell and Vought), with the industrial companies operating under separate contracts was accomplished without conflict only because the personnel assigned worked well together, and were dedicated to producing a satisfactory SEADS system.

11.0 CONCLUSIONS

The SEADS system was developed over a period of years. The design is supported by detailed thermal, static and dynamic analysis, as well as, comprehensive thermal, static and dynamic tests. It is estimated that mission life will be approximately 25-30 missions. At this writing only the insulation subsystem has not been certified for flight, but, a forthcoming system thermo/acoustic test is scheduled to accomplish this task.

As a result of the extensive and satisfactory development activities, the system was judged acceptable to proceed into production design.

12.0 POSTSCRIPT

The SEADS system, which includes the nose cap and support bulkhead, together with the pressure measurement and recording system have been fabricated. It is planned for installation on the OV-102 Orbiter for operations at a convenient refurbishment period.

Photographs of the assembly are provided as Figures 1-1 and 1-2. On Figure 1-2 some of the tubes can be seen, as well as, the insulation on the two manifolds and the pressure transducers mounted on the nose cap support bulkhead.

1. 2-52400/7ACP-2, dated 1/13/77, Final Summary Report, Materials Evaluation For Modification of the RCC Nose Cap for Pressure Analysis Temperature Measurement.

2. 221RP00767, dated 5/1/79, Final Summary Report, Shuttle Entry Air Data System (SEADS) Feasibility Demonstration.

3. 2-53230/7ADP-7, dated 2/9/77, Design Information Release (DIR), Air Data Probe - Phase II Thermal Analysis.

4. 2-53200/7ADP-15, dated 10/17/77, Design Information Release (DIR), Shuttle Orbiter Air Data Probe Support Tube Thermal Analysis.

5. 2-58020/7ADP-11, dated 6/1/77, Design Information Release (DIR), Air Data Probe Dynamic Analysis.

6. 2-30400/8ADP-0037, Rev. "A", dated 9/21/78, Design Information Release (DIR), Structural Analysis of The Shuttle Nose Cap Incorporating Shuttle Air Data System.

7. 2-51210/0DIR-12, dated 12/15/80, Design Information Release (DIR), Stress Analysis of the Presure Ports on Production SEADS Shuttle Nose Cap.

8. 2-30320/8ADP-0035, dated 6/22/78, Design Information Release (DIR), Air Data Probe Predicted Temperatures - Trajectory 14414.1C.

9. 2-30320/9ADP-0013, dated 7/5/79, Design Information Release (DIR), SEADS Cross-Radiation Blockage Thermal Analysis.

10. 2-30400/9ADP-0015, dated 7/20/79, Design Information Release (DIR), SEADS Thermoelastic Stress Analysis, Trajectory 14414.1C.

11. 2-30400/9ADP-0019, dated 9/24/79, Design Information Release (DIR), Strength Determination SEADS Penetration Assembly.

12. 2-30400/9ADP-0014, dated 7/20/79, Design Information Release (DIR), Axial Load Analysis SEADS Penetration Assembly.

13. 221TQ00762, dated 9/10/79, Evaluation of Sticking of Threaded Parts.

14. 2-51600/RCC/8-0045, dated 10/13/78, Design Information Release (DIR), Anti-Rotation Concepts - SEADS System Penetration Assemblies.

15. 2-30400/9ADP-0019, dated 8/28/79, Design Information Release (DIR), Re-Evalution of Anti-Rotation Concepts for SEADS Penetrations.

16. 2-51210/ADP/1-0009, dated 5/20/81, Design Information Release (DIR), Plasma Arc Models Test Summary.

17. 2-30320/RCC/0-0004, dated 1/16/80, Design Information Release (DIR), Thermal Analysis of SEADS Penetration Port Plasma Arc Jet Test.

18. 2-30400/RCC/0-0011, dated 3/12/80, Design Information Release (DIR), Thermocouple Measurement Accuracy Evaluation.

19. 2-53200/ADP/2-001, dated 1/14/82, Design Information Release (DIR), Investigation of SEADS Temperature Anomaly NASA/ARC Plasma Arc Test - DSI 357.

20. TR 80-59940-416, dated 10/30/80, Test Information Report, Thermal Deflection, SEADS Pressure Tube Assemblies.

21. STS-81-0131, dated 1/81, Shuttle Entry Air Data System (SEADS) Static & Dynamic Analysis of Manifold & Pressure Tube Assembly - Final Report (Rockwell).

22. Review Item Disposition (RID) No. 19 Closeout, dated 3/3/81, Frequency Distributions in SEADS Analysis STS-81-0131 (Rockwell).

23. TR-80-59940-415, dated 5/6/80, Test Information Report, Static Load Calibration, Manifold, SEADS Vibration Test.

24. ETL-181, dated 12/17/80, Test Report, Engineering Development Vibration Test of the Shuttle Entry Air Data System (SEADS).

ORIGINAL PAGE
BLACK AND WHITE PHOTOGRAPH

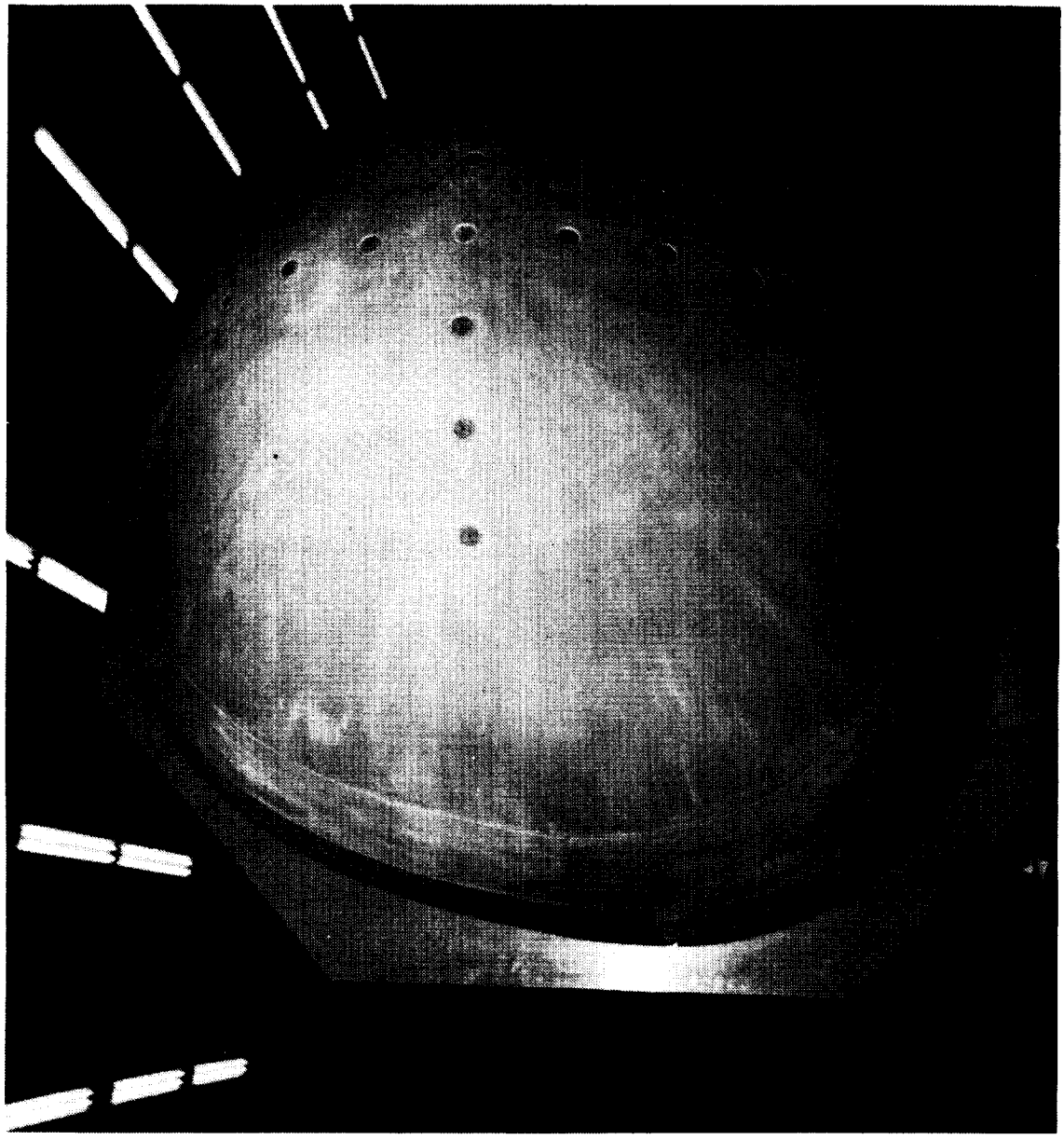

Figure 1–1 Production SEADS Nose Cap Assembly

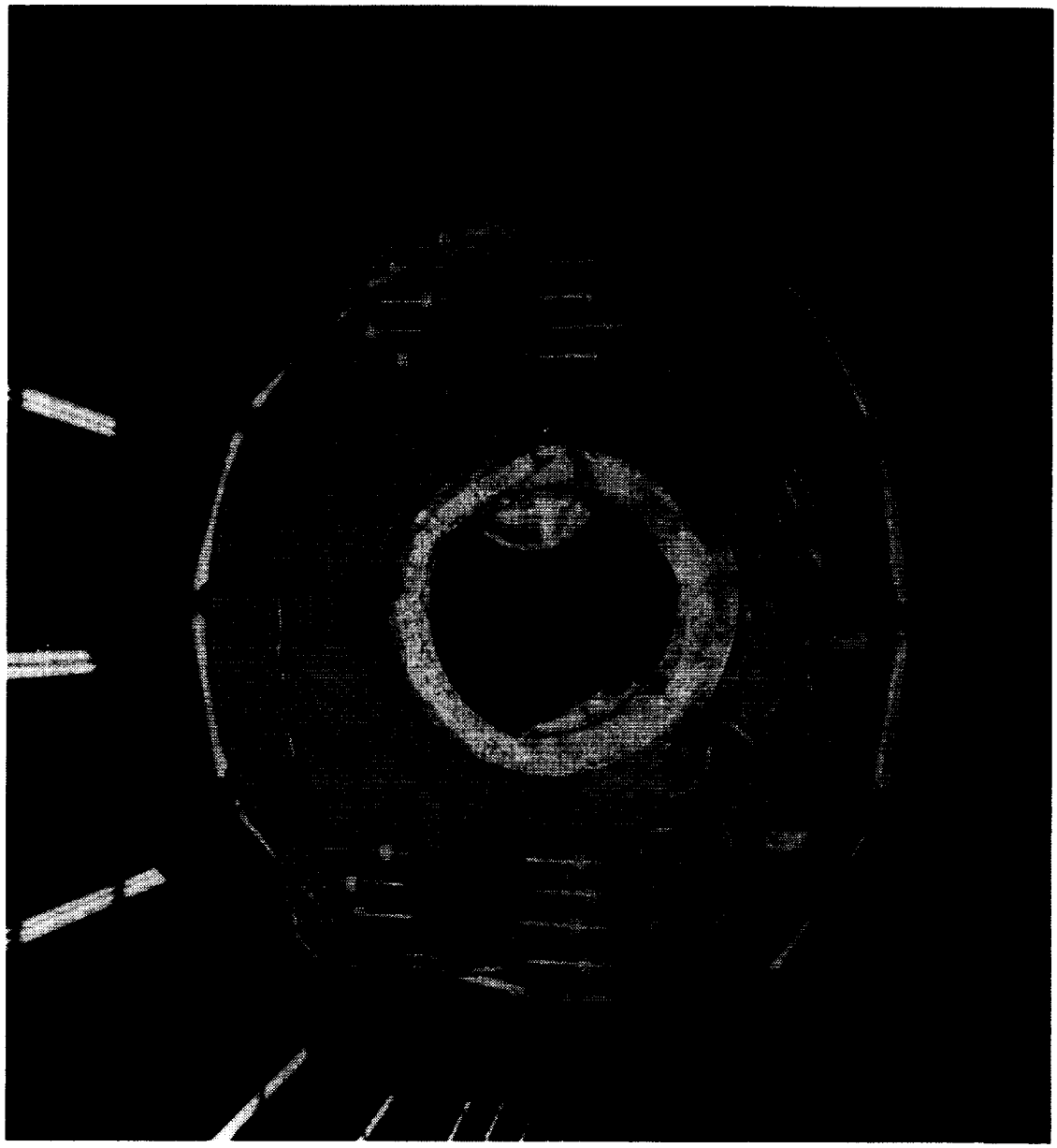

Figure 1–2 Production SEADS Nose Cap Assembly Aft View Showing Location of Pressure Transducers

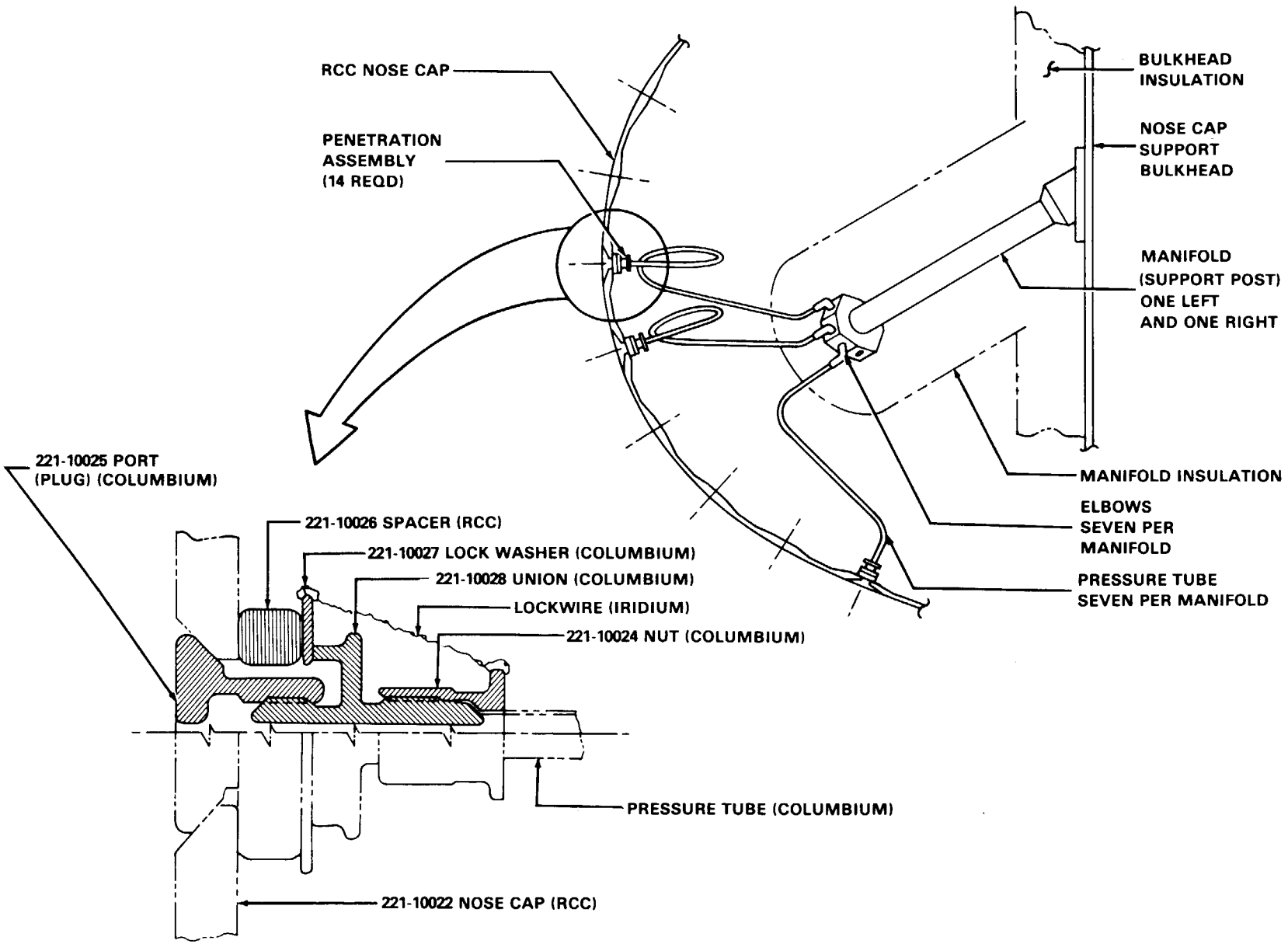

Figure 1-3 SEADS Production Configuration

B2-3592-3

ORIGINAL PAGE
BLACK AND WHITE PHOTOGRAPH

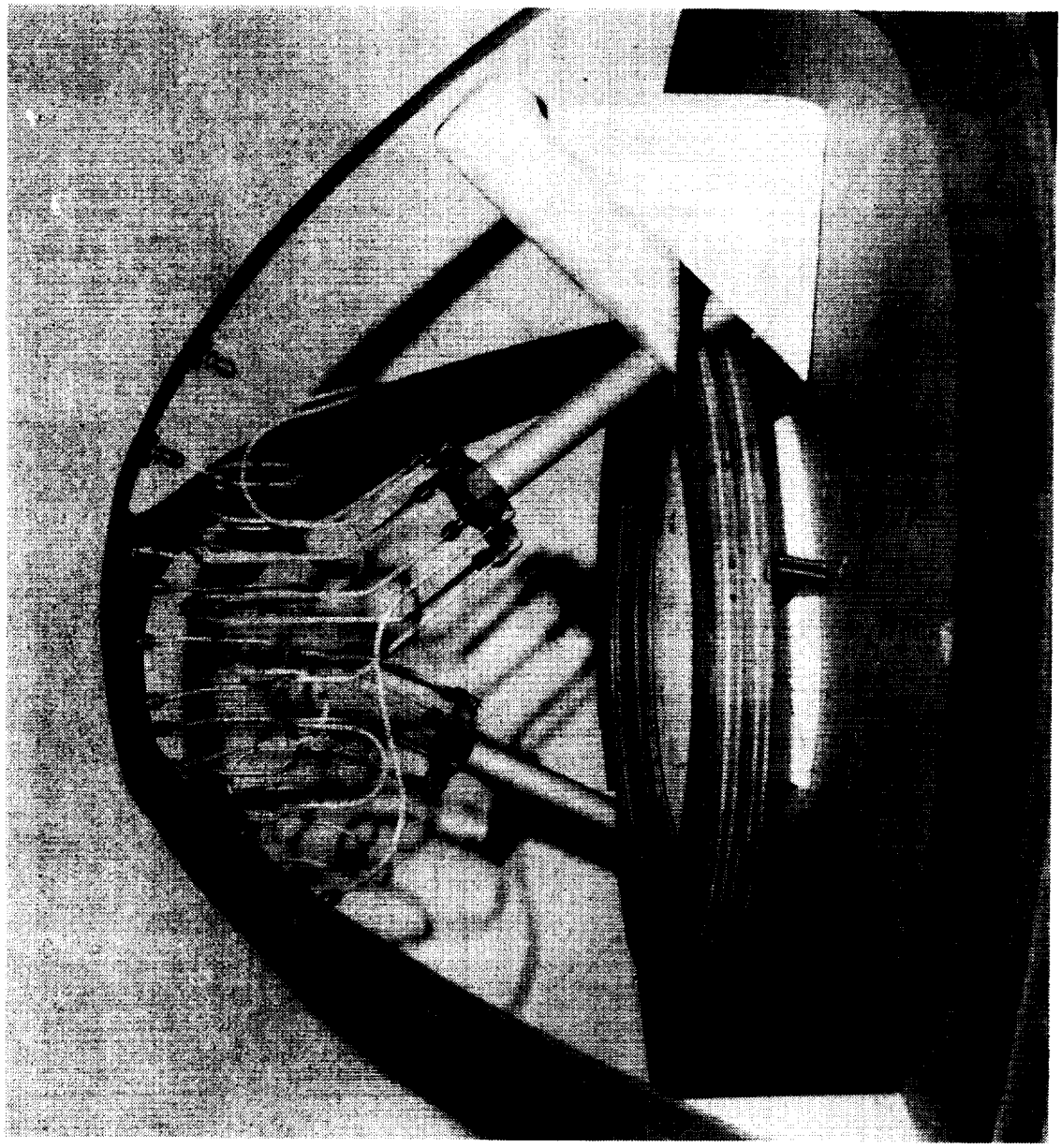

Figure 1–4 Mockup of Pressure Tubes Production Configuration

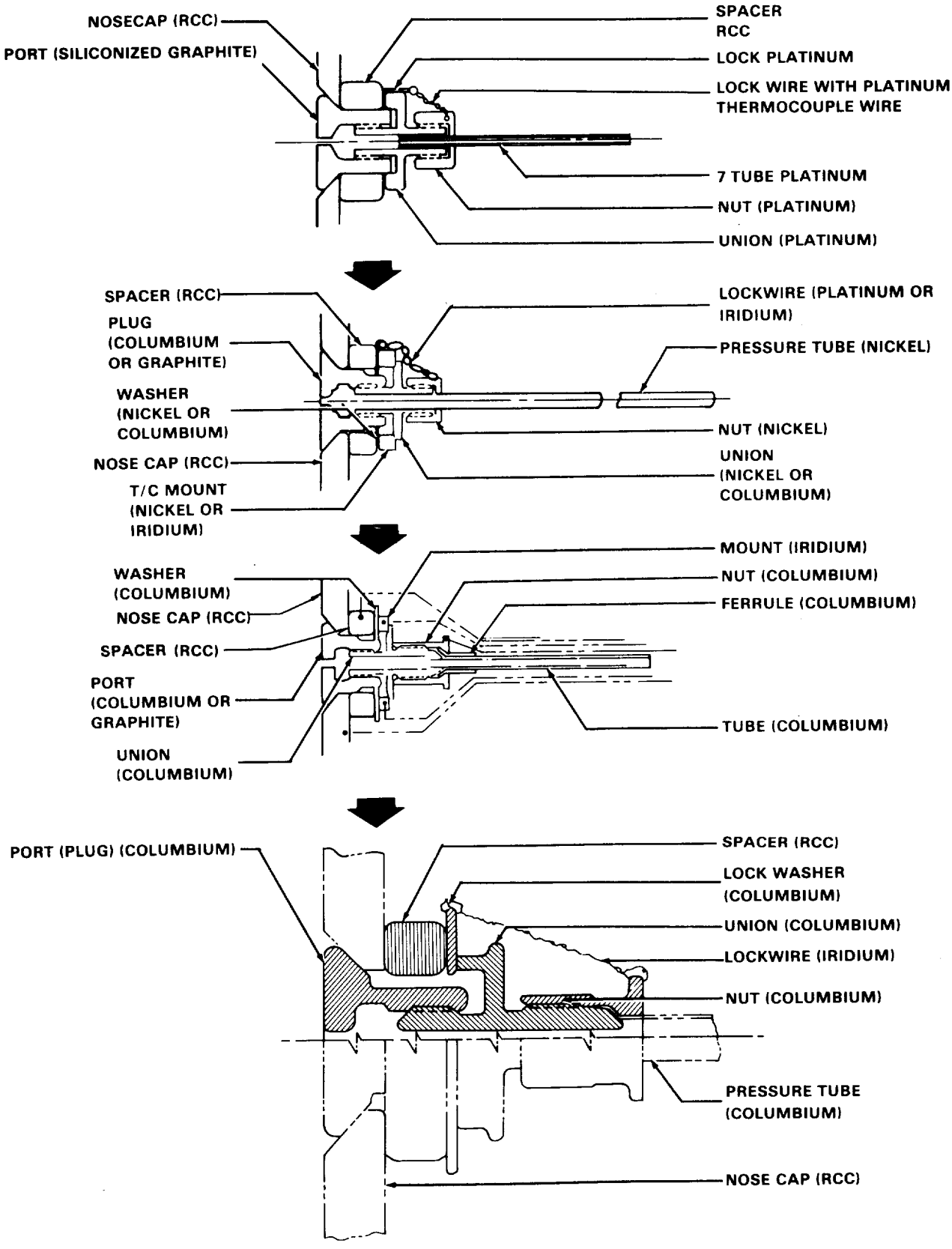

B2-3592-5

Figure 1-5 Evolution of Penetration Assembly Design

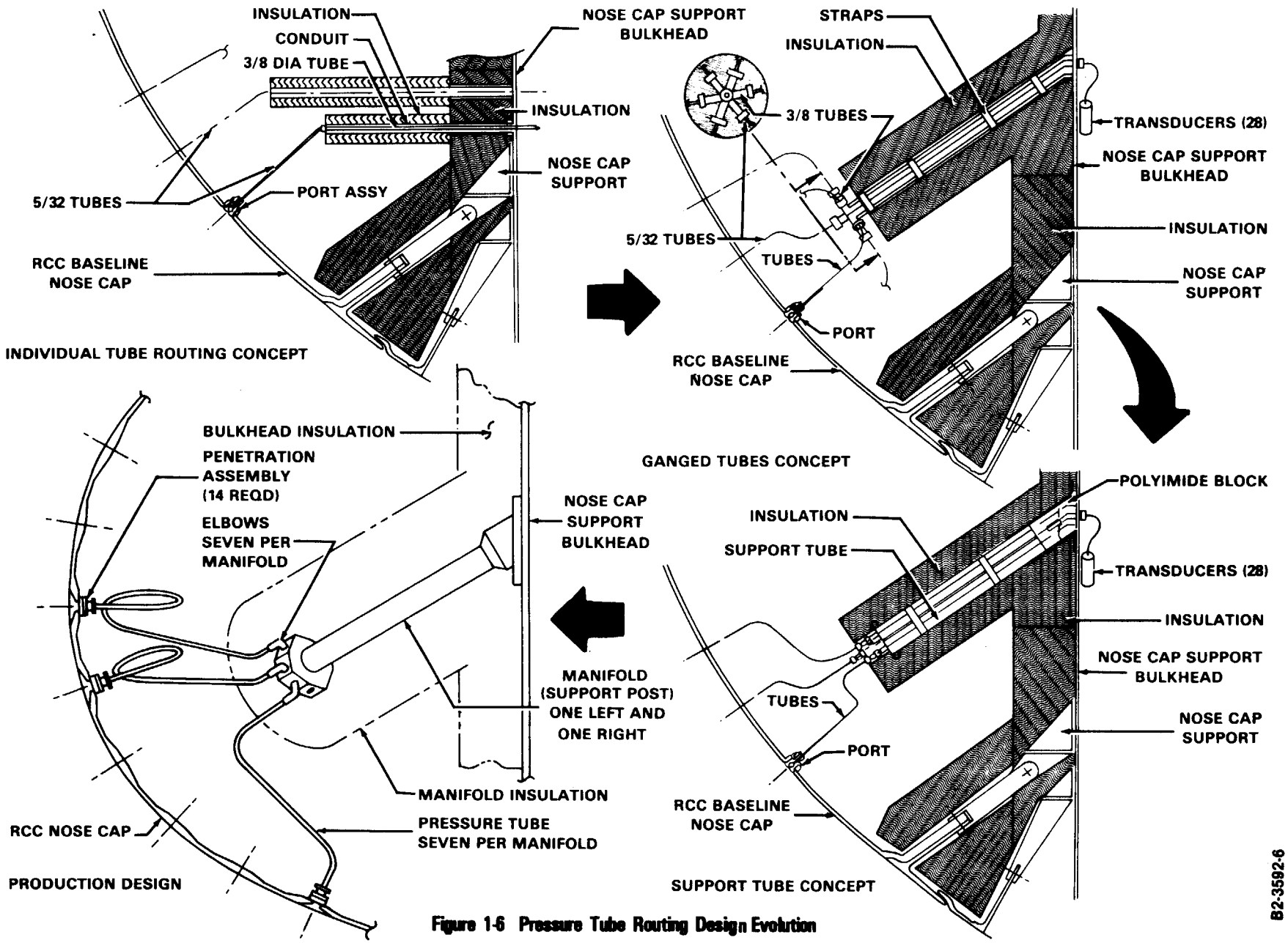

Figure 1-6 Pressure Tube Routing Design Evolution

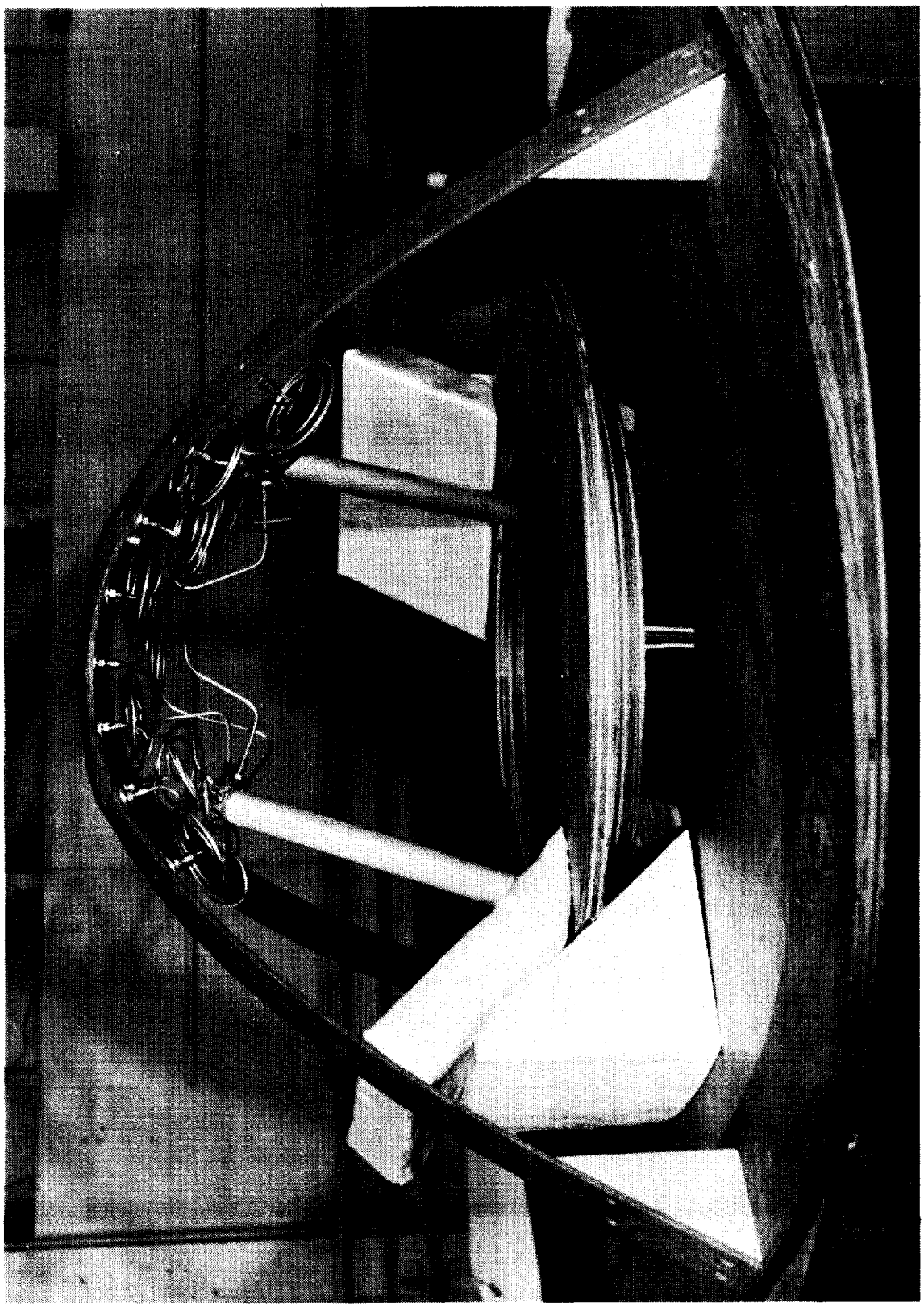

Figure 1–7 Mockup of Early Configuration of Pressure Tubes

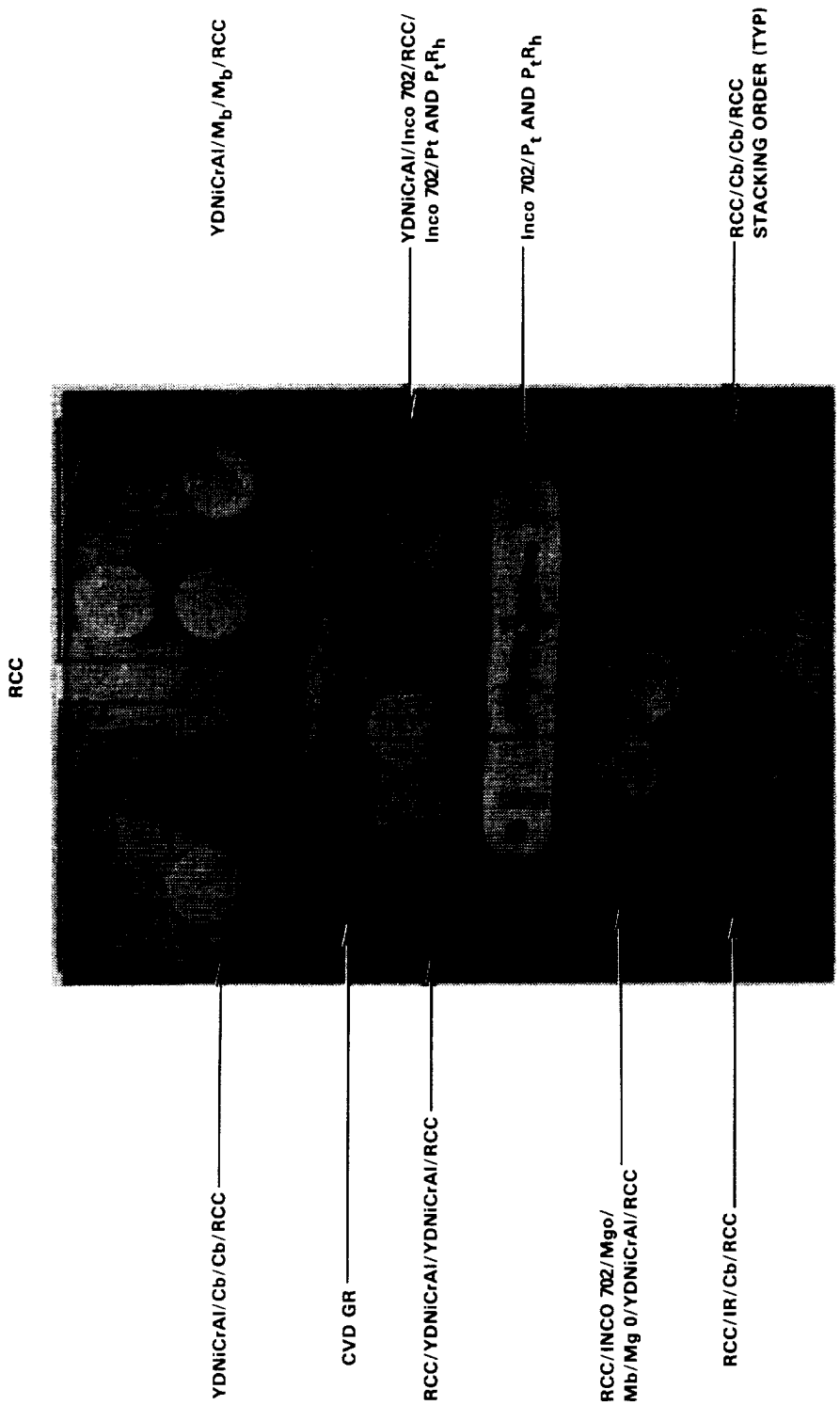

Figure 4–1 Typical Chemical Compatibility Test Arrangement

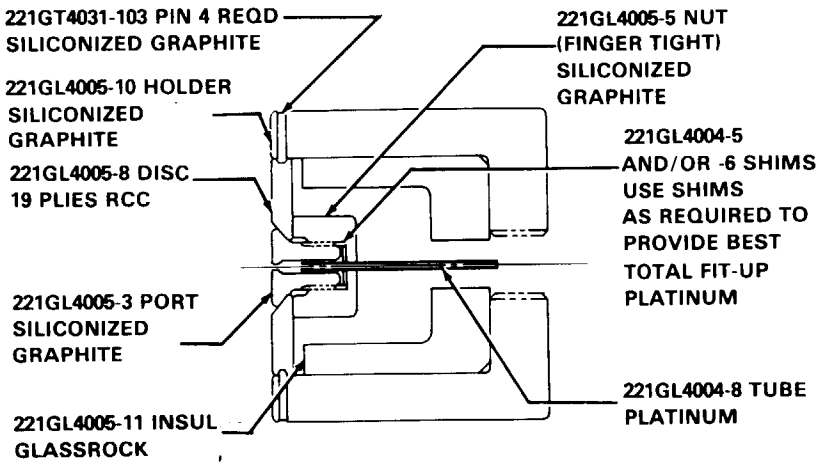

CONCEPT 1A ASSEMBLY

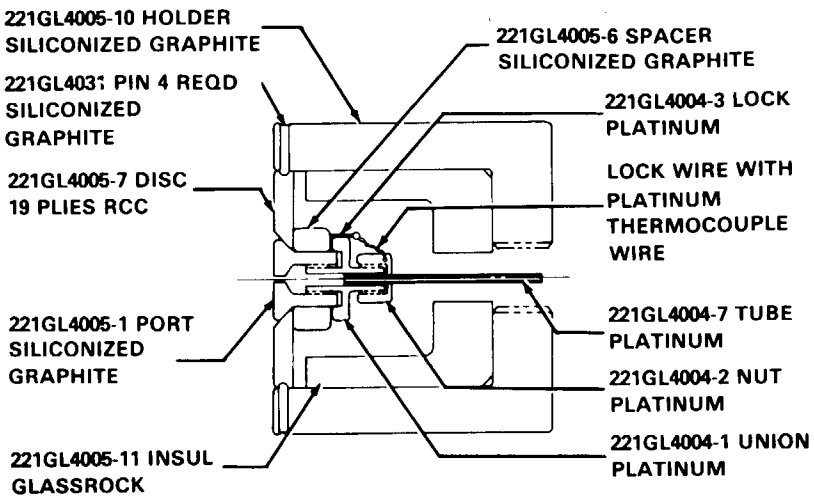

CONCEPT 6 ASSEMBLY

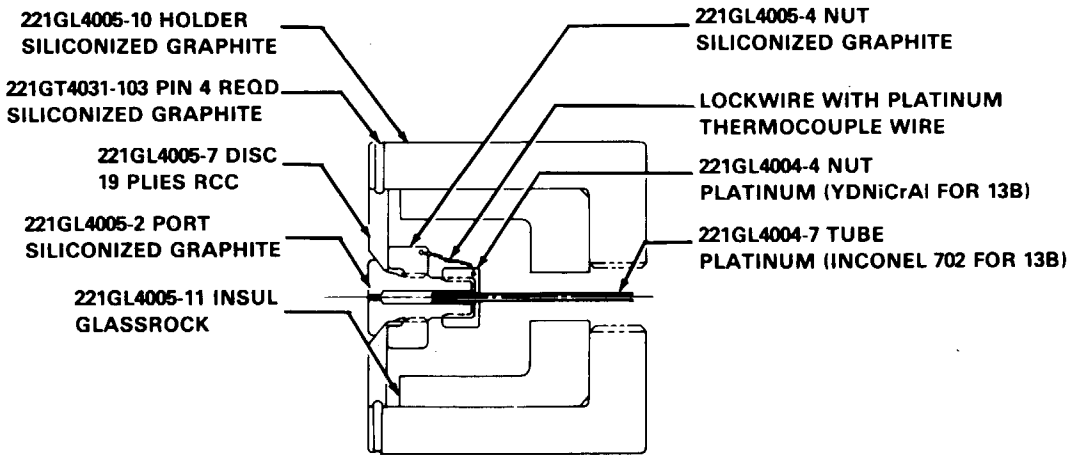

CONCEPT 13 ASSEMBLY

Figure 5-1 Initial Plasma Arc Test Models

B2-3592-9

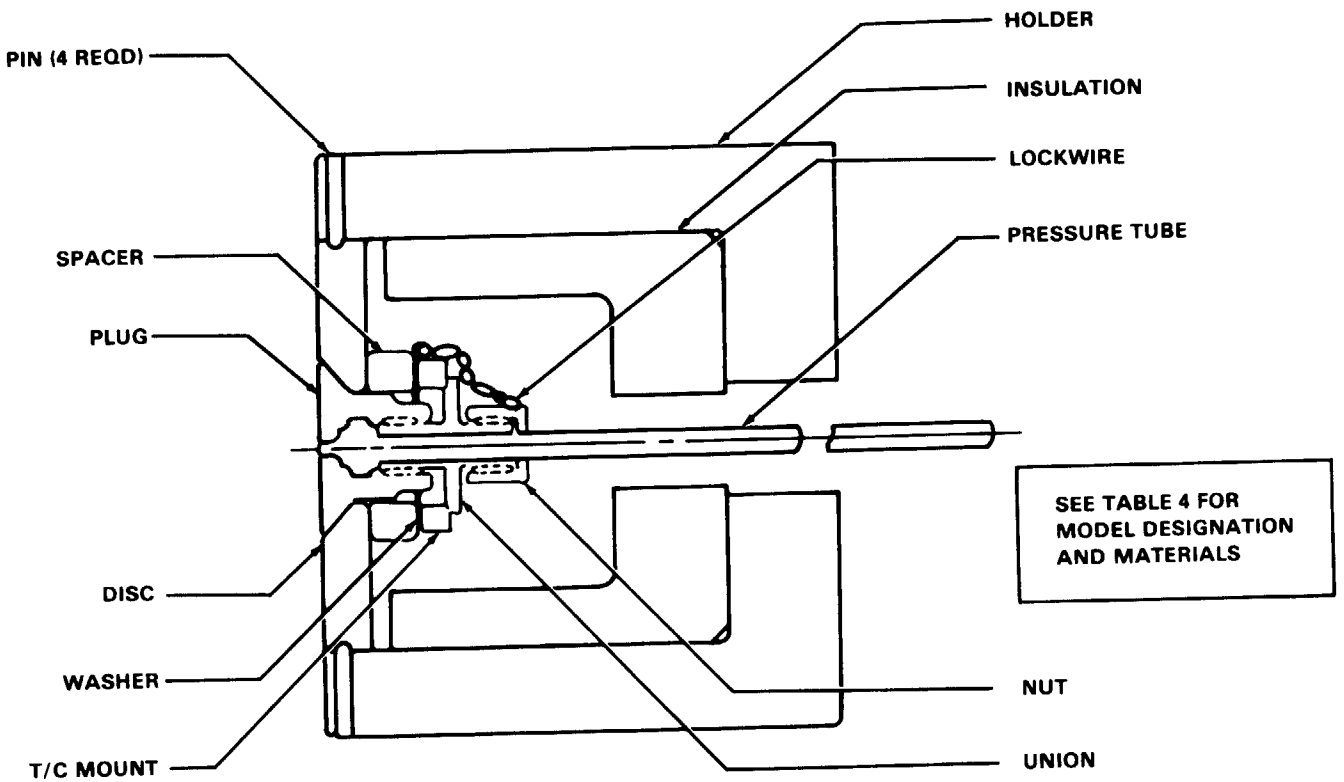

B2-3592-10

Figure 5-2 Configuration of Penetration Assembly for Second Series Plasma Arc Tests

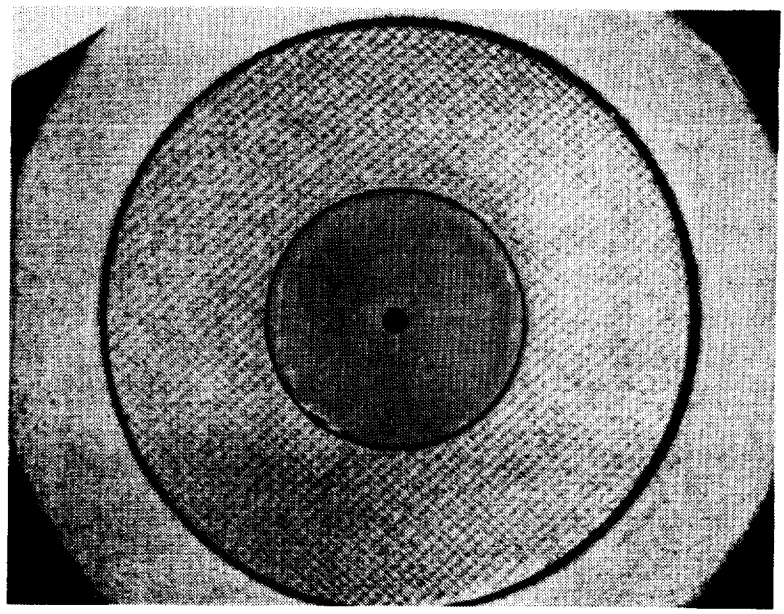

Figure 5–3 –10 Model After 3-Hours of Test

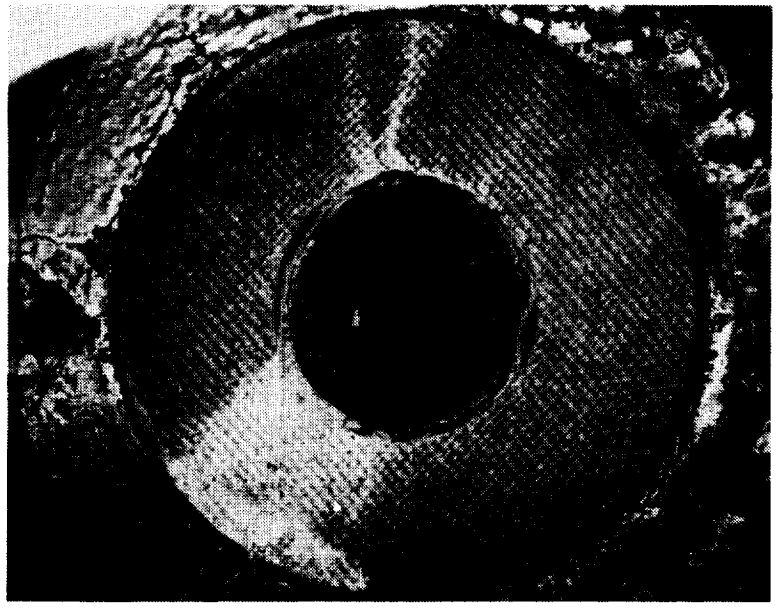

Figure 5–4 –10 Model at Conclusion of 5-Hour Test

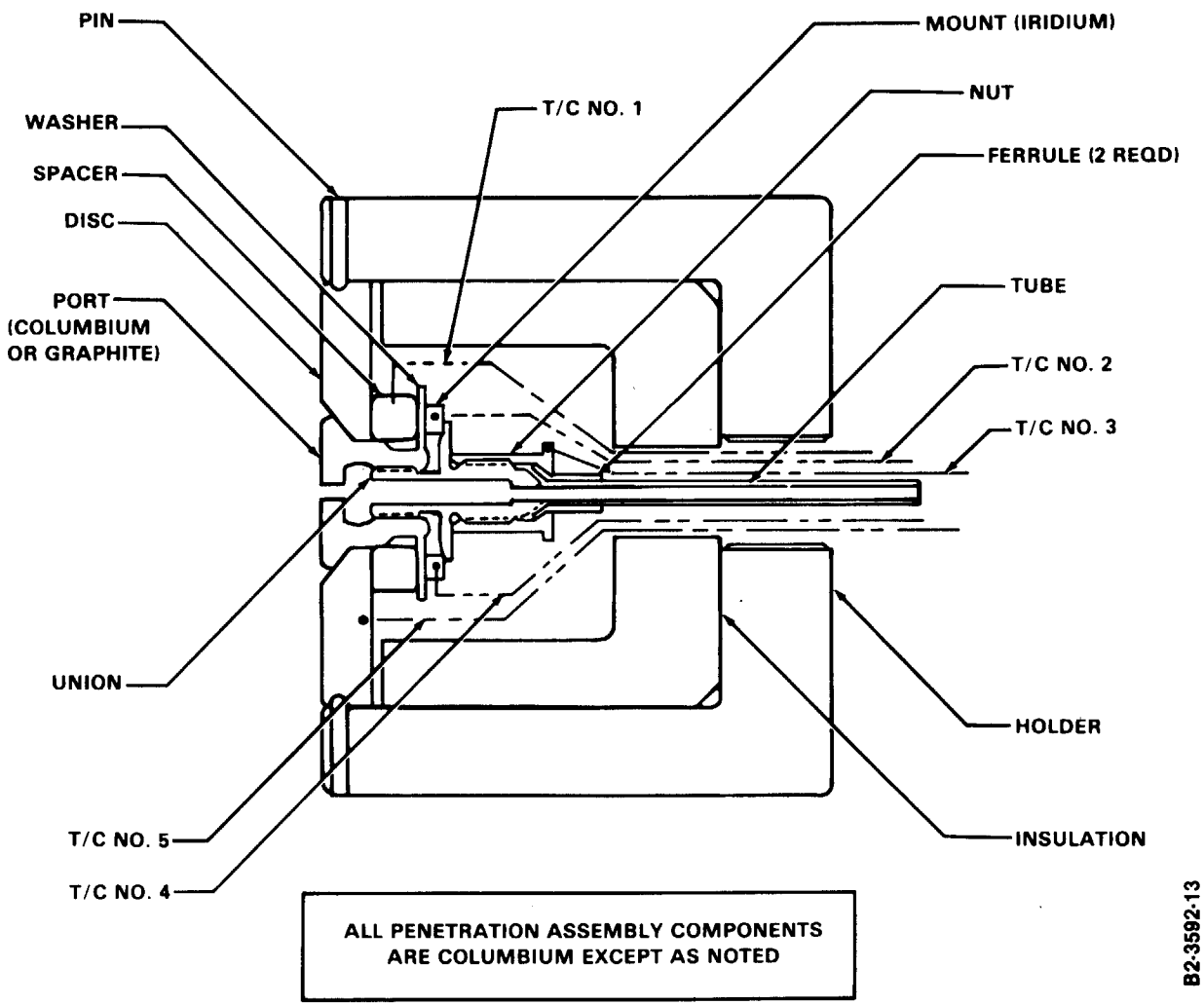

Figure 5-5 Test Model Configuration for 2,660°F Temperature Requirement

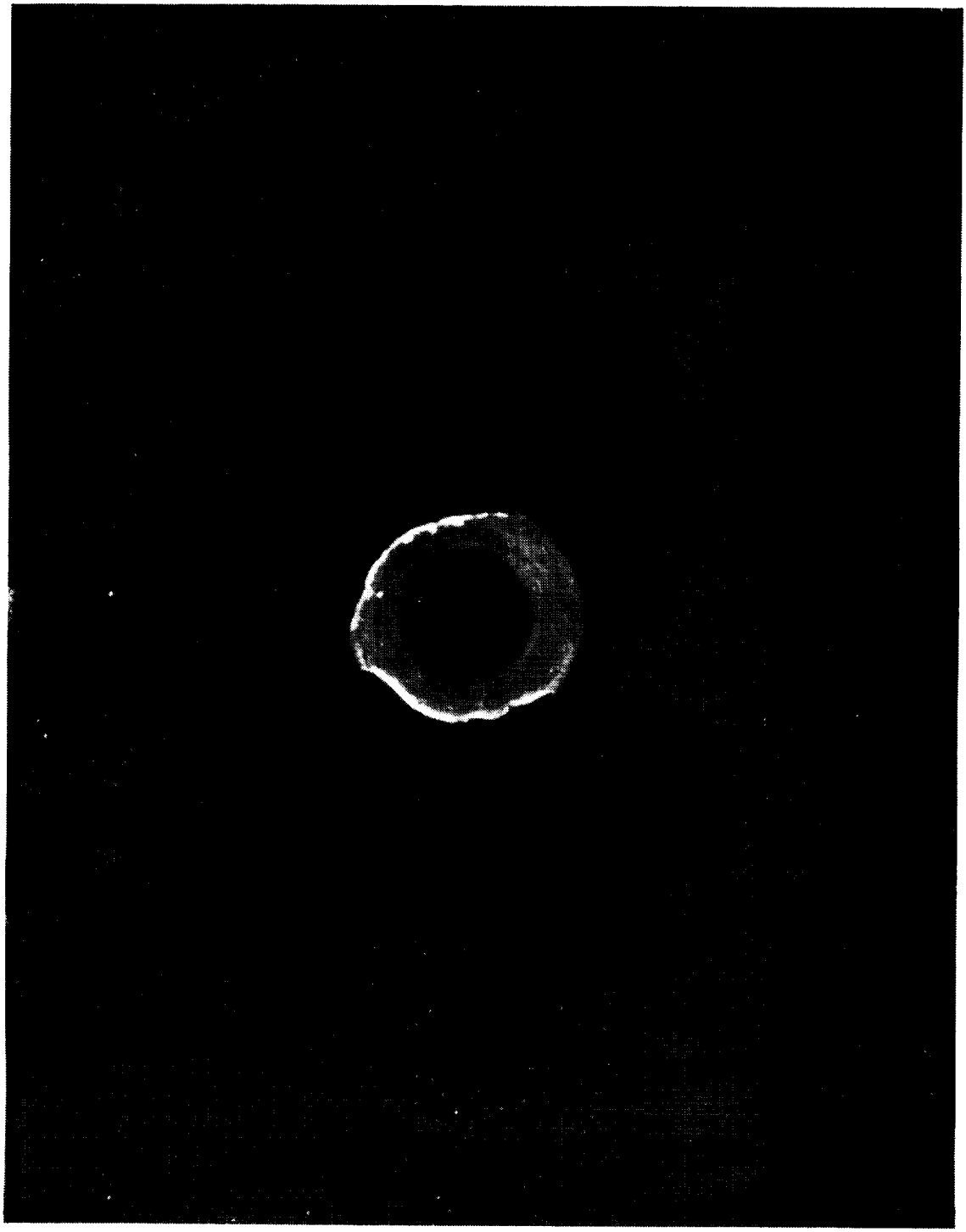

Figure 5–6 –2 Model Pressure Tube, 5 Hours Exposure

ORIGINAL PAGE
BLACK AND WHITE PHOTOGRAPH

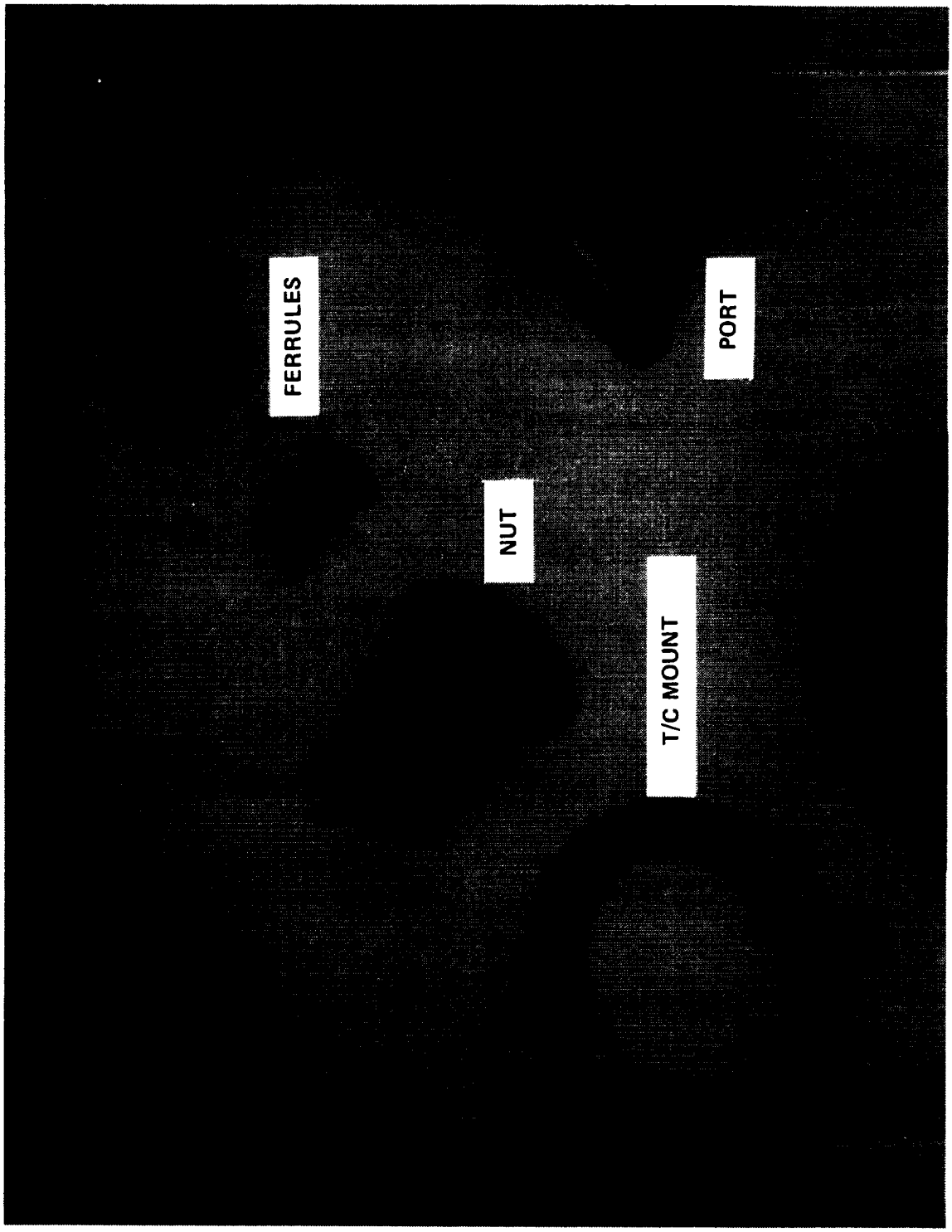

Figure 5–7 –2 Model Components, 5 Hours Exposure

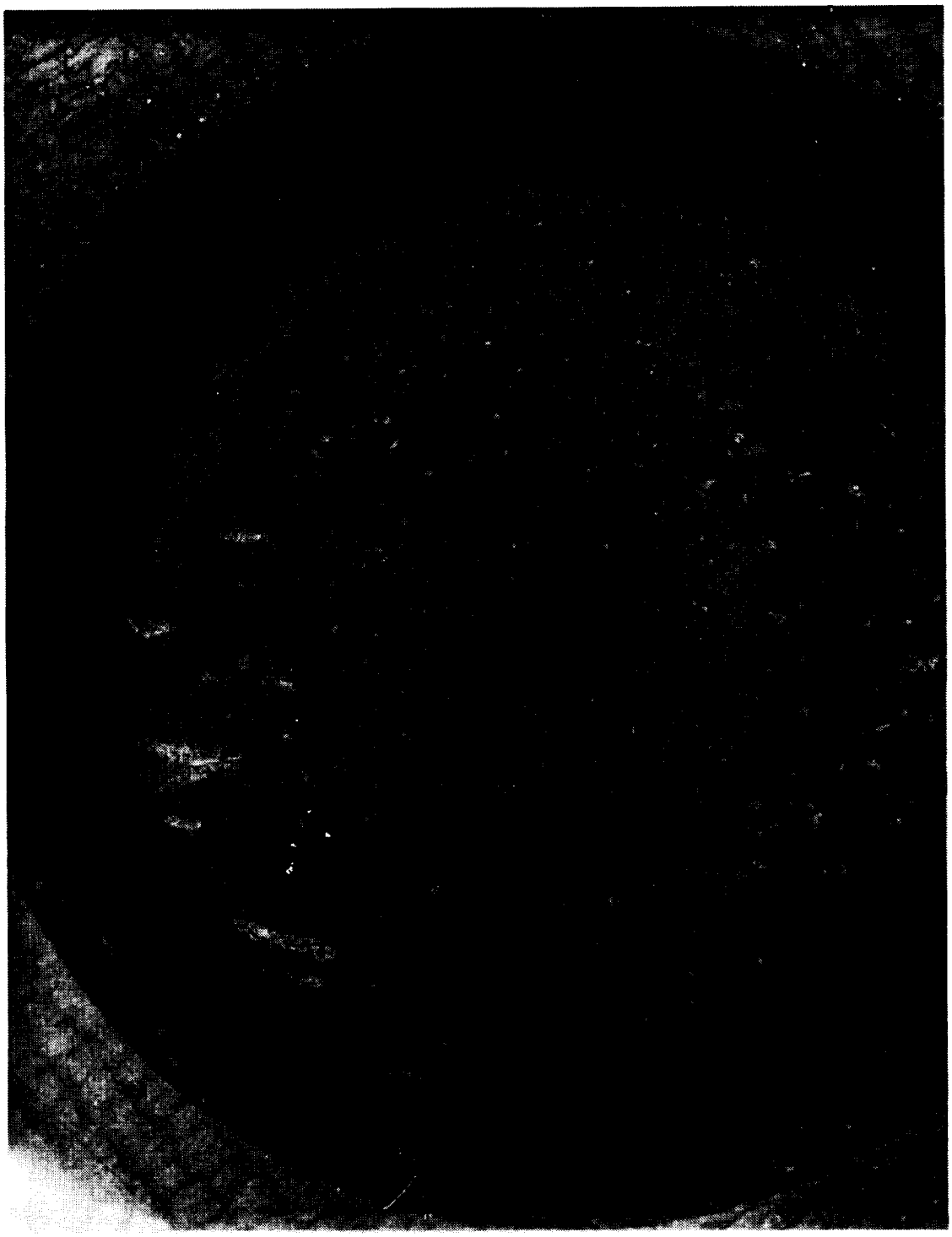

Figure 5–8 –2 Model Columbium Port Front Face, 5 Hours Exposure

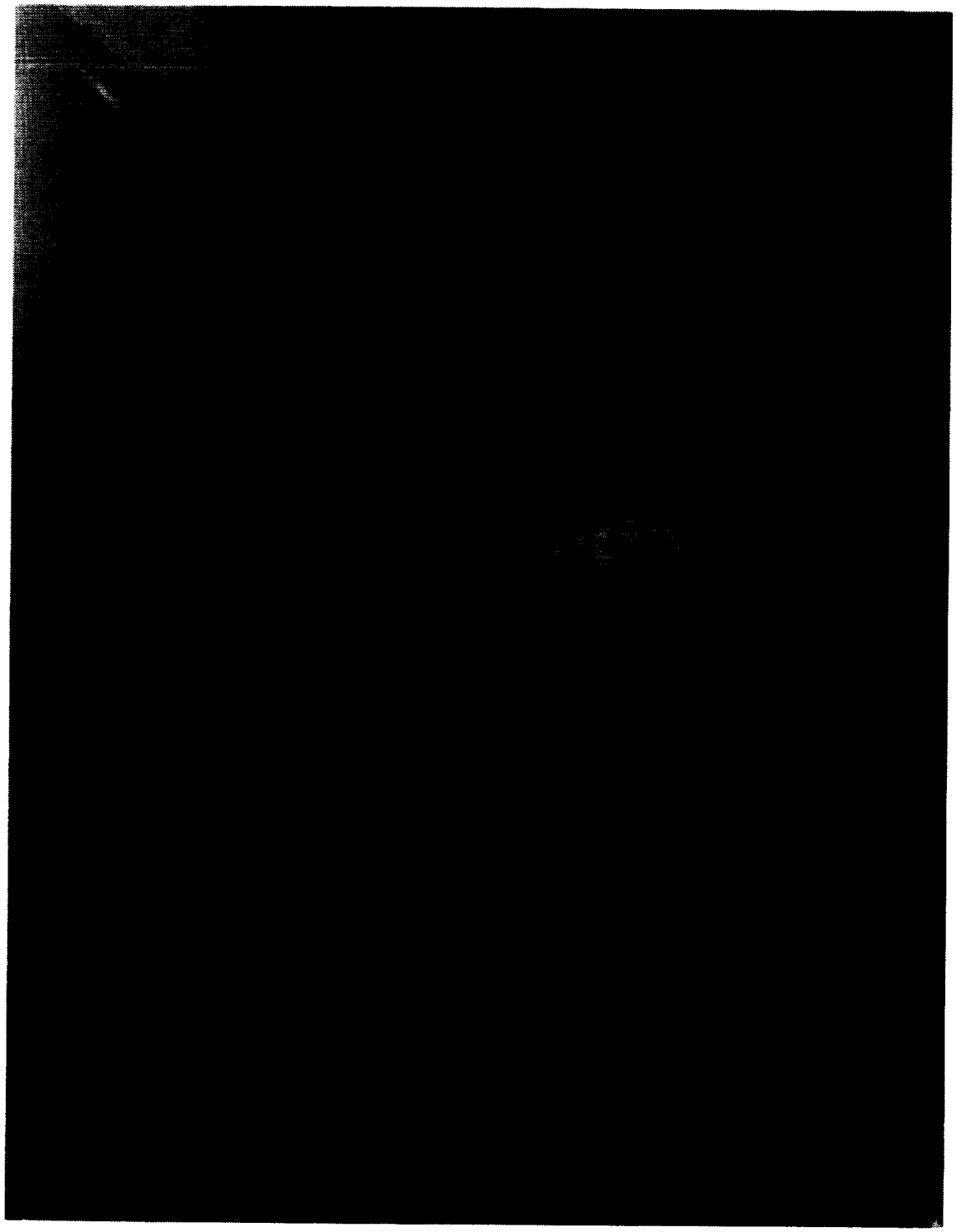

Figure 5–9 –1 Model Pressure Tube Showing Local Scalloping Due to Oxidation, 5 Hours Exposure

ORIGINAL PAGE
BLACK AND WHITE PHOTOGRAPH

Figure 5-10 — 1 Model Components after 5-Hour Test Exposure

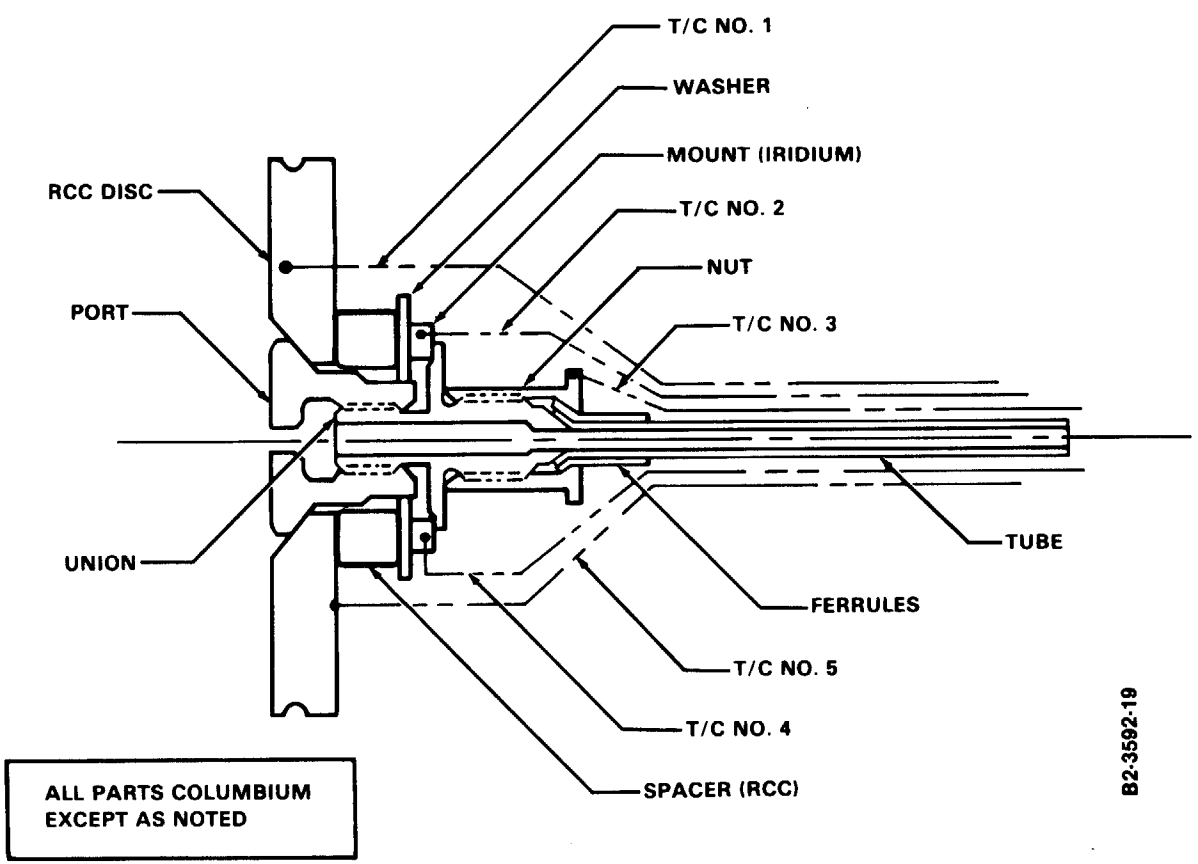

Figure 5-11 SEADS Penetration Assembly for NASA-ARC Test

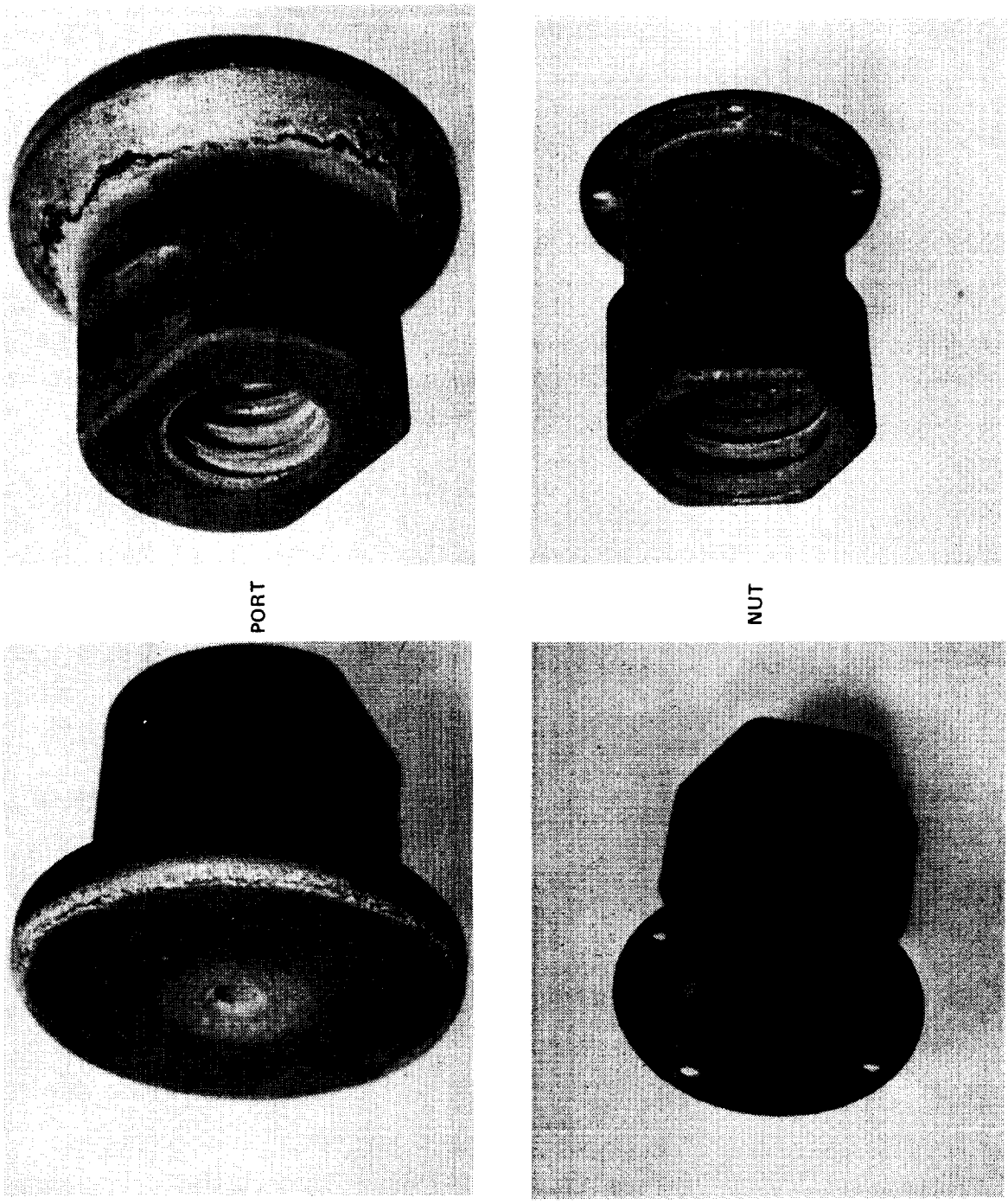

Figure 5–12 Port and Nut at Conclusion of NASA-ARC Test

Figure 5–13 Union and Ferrules at Conclusion of Test

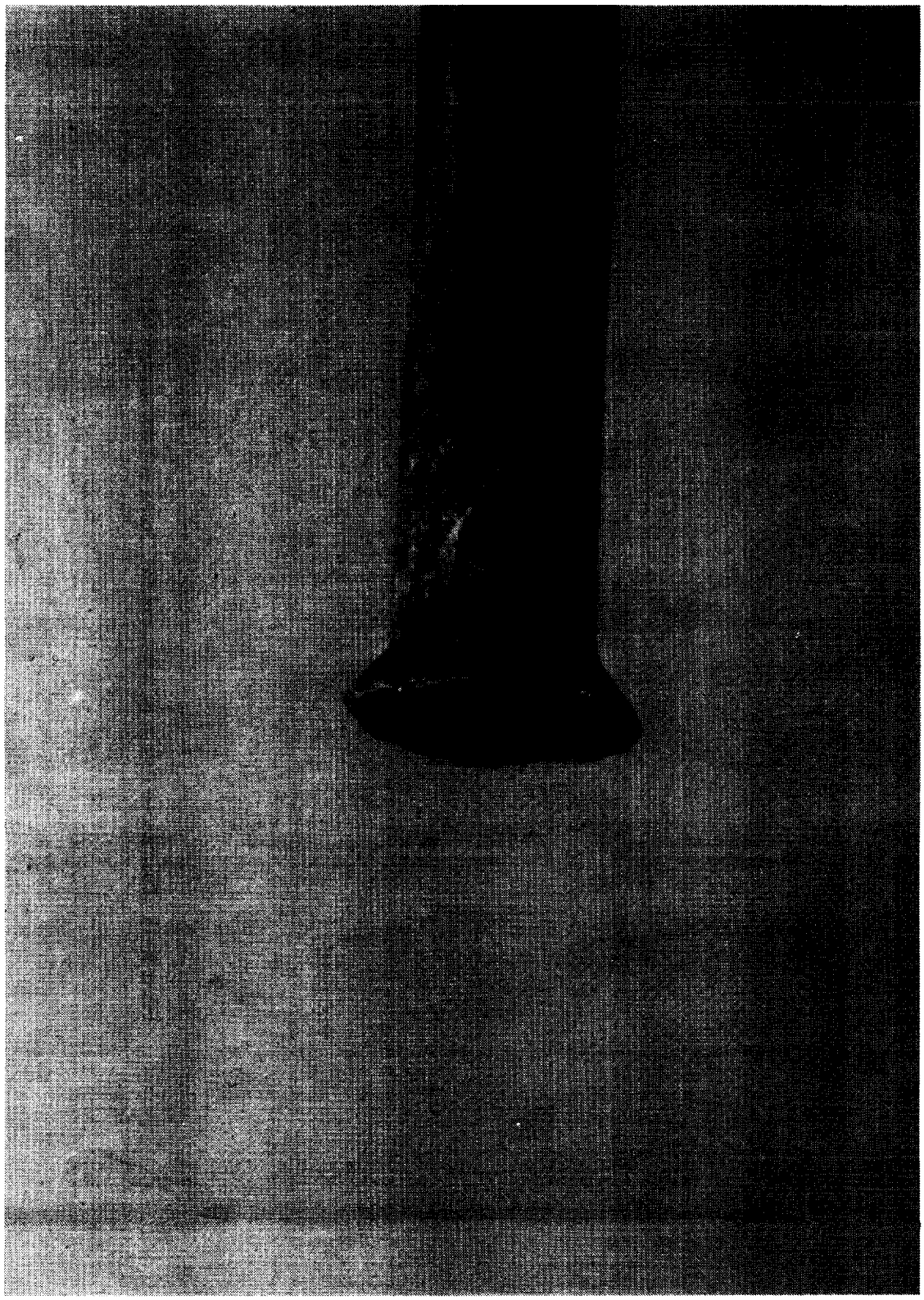

Figure 5–14 Pressure Tube at Conclusion of Test

Figure 5–15 Countersunk Hole in RCC Disc and RCC Spacer at Conclusion of Test

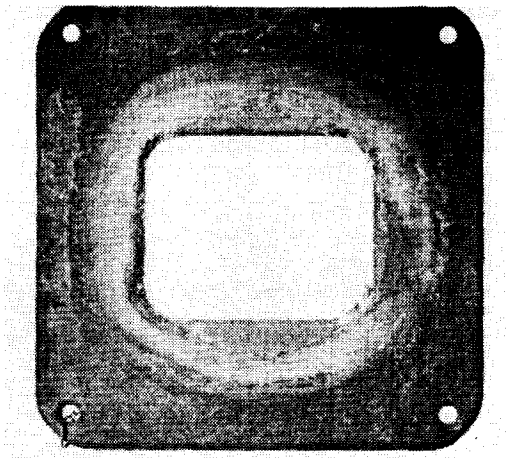

LOCKWASHER

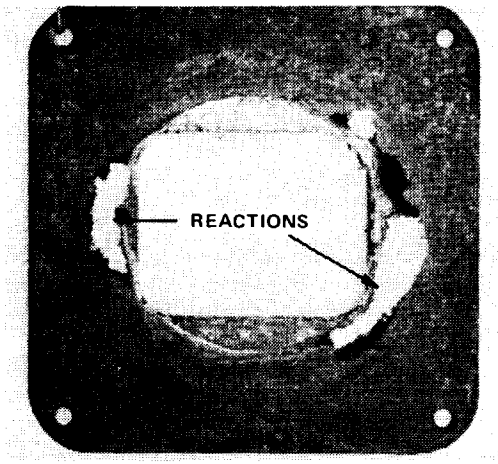

LOCKWASHER

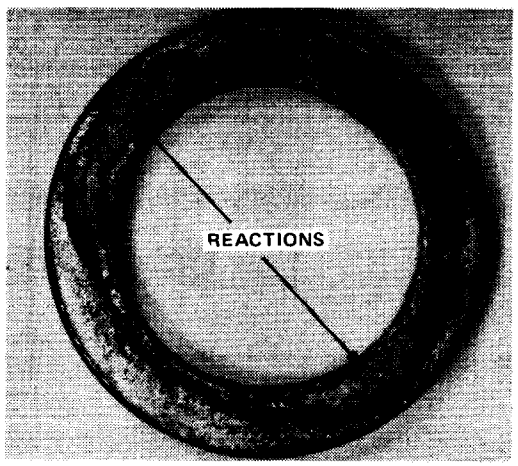

IRIDIUM T/C MOUNT

Figure 5–16 Lockwasher and Iridium T/C Mount at Conclusion of Test

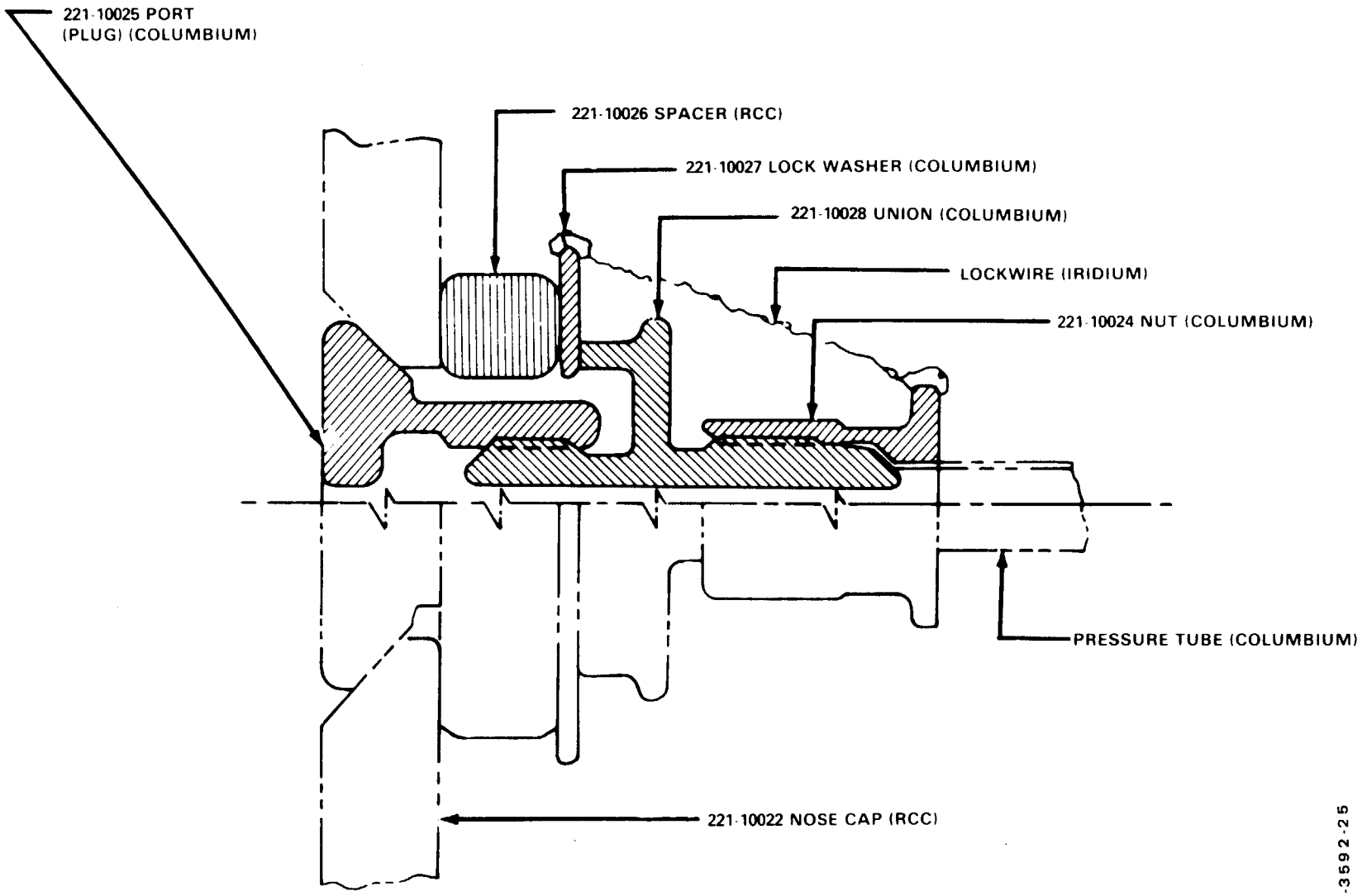

Figure 5-17 Penetration Assembly Production Design

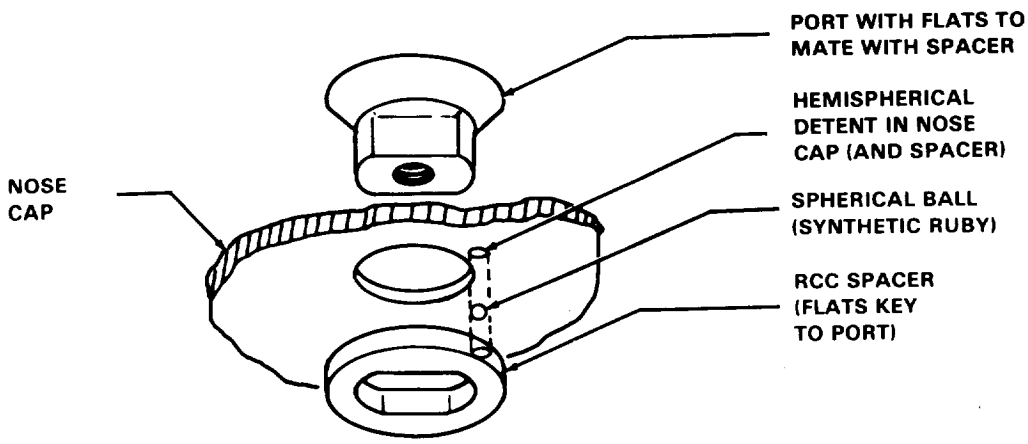

BALL LOCK CONCEPT

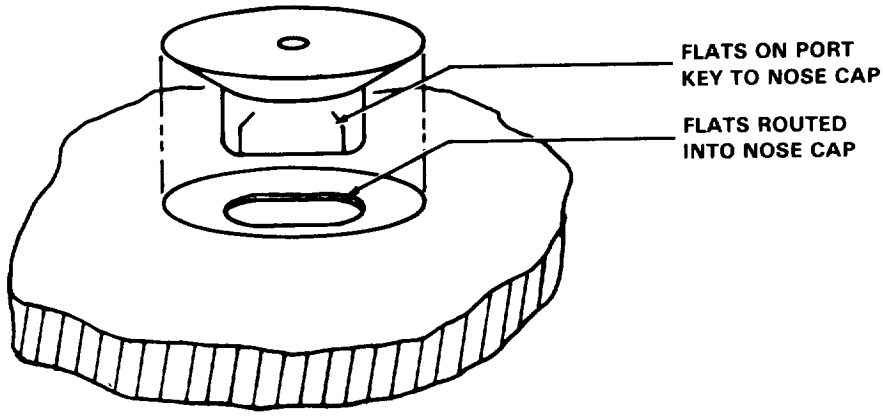

FLAT-SIDED HOLE CONCEPT

Figure 5-18 Best Antirotation Concepts

B2-3592-26

COMPONENT	ZONE 2 NODE NO.	ZONE 1 NODE NO.	(TEMP)	ZONE 3 NODE NO.	(TEMP)
UNION	6	37	(2594)F	45	(2593)F
T/C MOUNT	16	36	(2599)	44	(2598)
T/C MOUNT	17	38	(2599)	46	(2599)
SPACER	19	39	(2607)	47	(2606)
SPACER	21	40	(2618)	48	(2617)
NOSECAP	23	41	(2636)	49	(2636)
BHD INSUL	51	50	(2567)	52	(2551)

NODE 51 NOSE CAP INSIDE SURFACE 2551F

NODE 53 BULKHEAD INSULATION 2528F

ZONE 1 LEE SIDE QUADRANT

ZONE 2 SIDE QUADRANTS

ZONE 3 WINDWARD QUADRANT

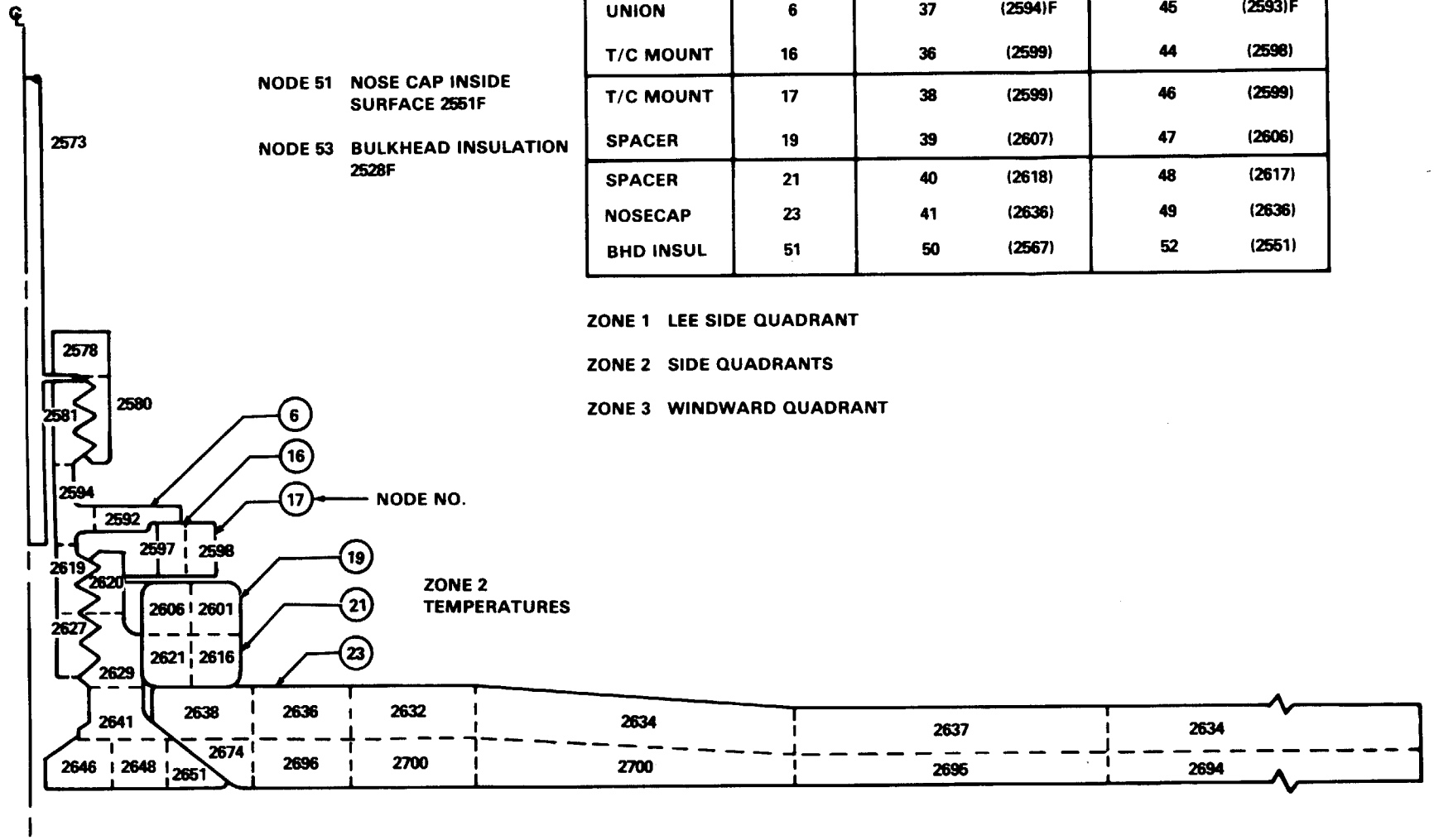

Figure 5-19 Temperature Distribution (F) at 700 Seconds Penetration Plug Location No. 7 Windward Side

B2-3592-27

COMPONENT	ZONE 2 NODE NO.	ZONE 1 NODE NO.	(TEMP)	ZONE 3 NODE NO.	(TEMP)	ΔT, F
UNION	6	37	(2270)F	45	(2299)	29
T/C MOUNT	16	36	(2269)	44	(2287)	18
T/C MOUNT	17	38	(2268)	46	(2287)	19
SPACER	19	39	(2257)	47	(2293)	36
SPACER	21	40	(2247)	48	(2274)	27
NOSECAP	23	41	(2244)	49	(2246)	2
BHD INSUL	51	50	(2119)	52	(2567)	NA

NODE 51 NOSE CAP INSIDE SURFACE 2344F

NODE 53 BULKHEAD INSULATION 2346F

ZONE 1 LEE SIDE QUADRANT

ZONE 2 SIDE QUADRANTS

ZONE 3 WINDWARD QUADRANT

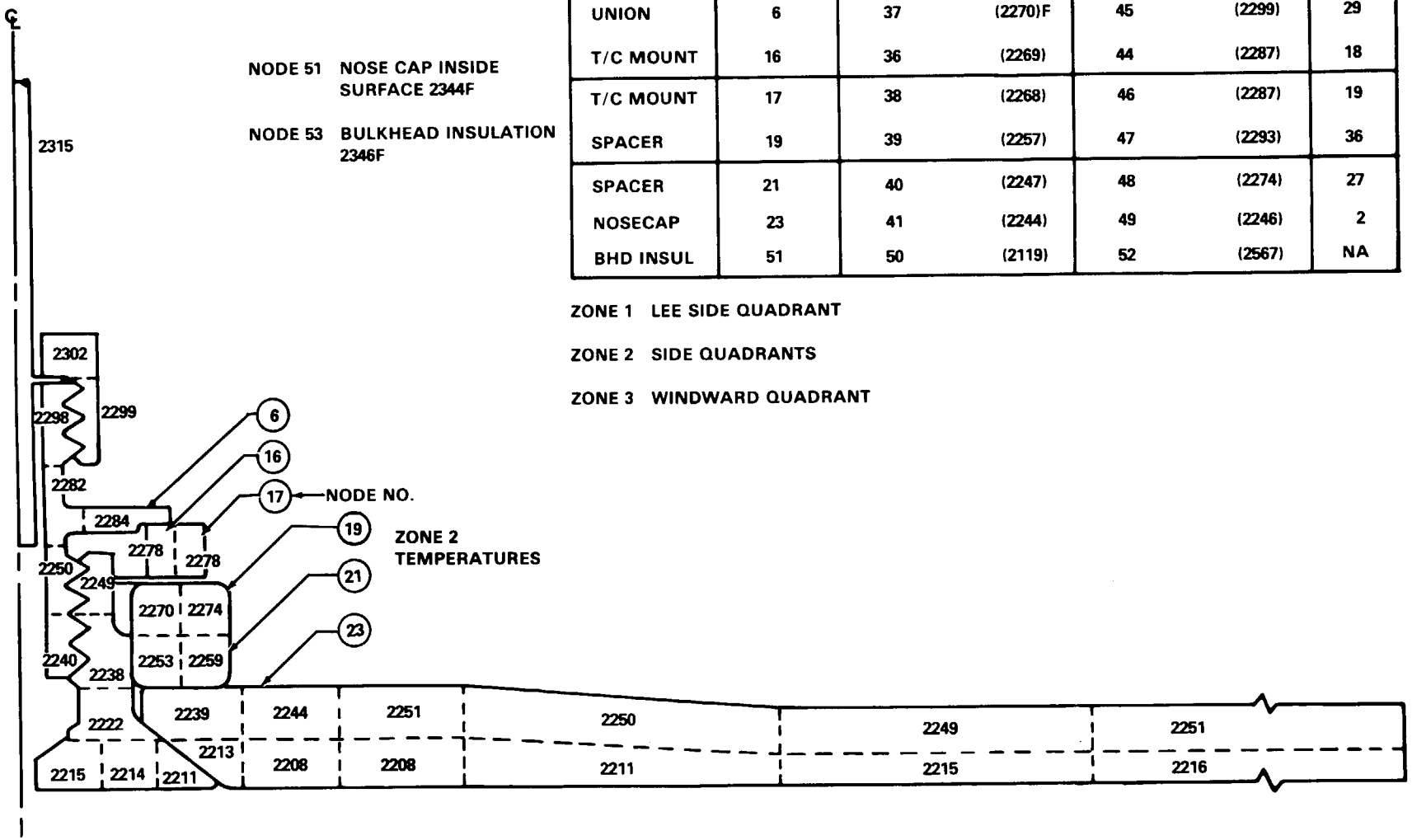

Figure 5-20 Temperature Distribution (F) at 700 Seconds Penetration Plug Location No. 1 Leeward Side

B2-3592-28

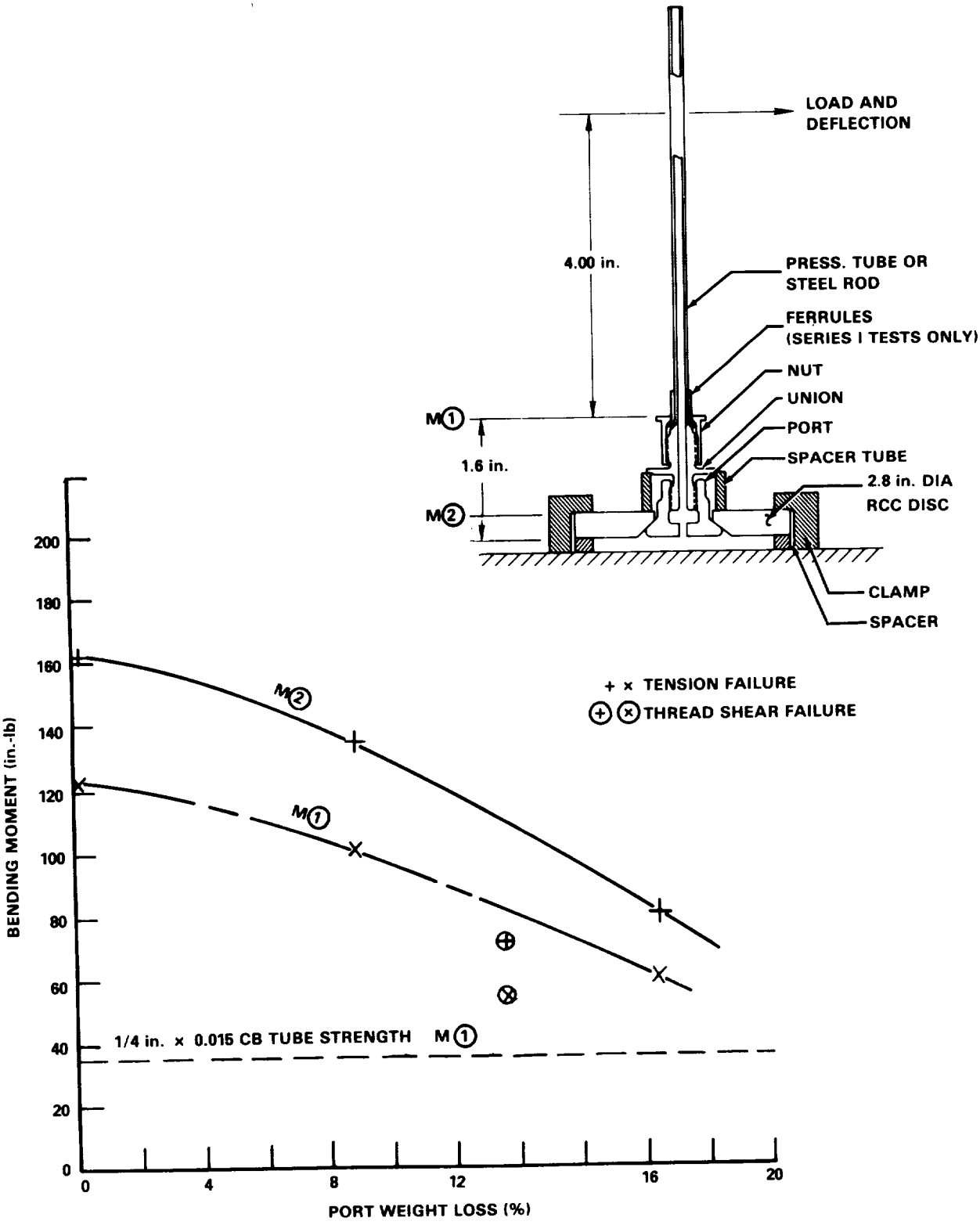

Figure 5-21 Graphite Port Bending Failing Load Test

B2-3592-29

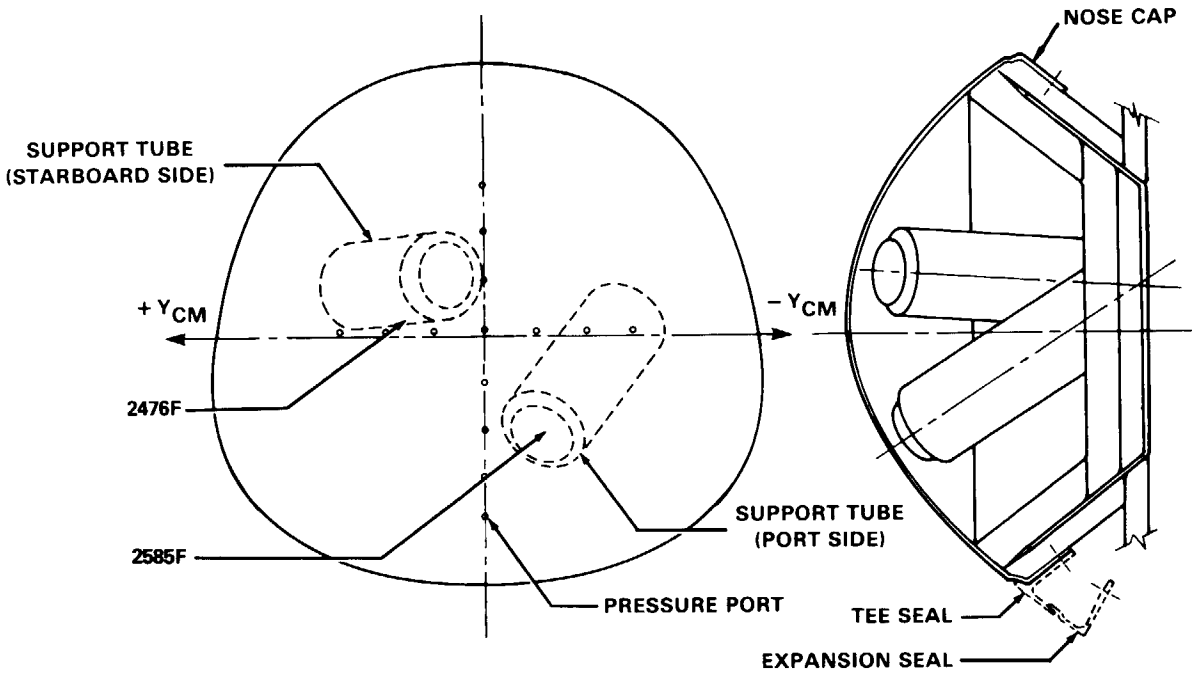

SEADS SUPPORT TUBE ARRANGEMENT

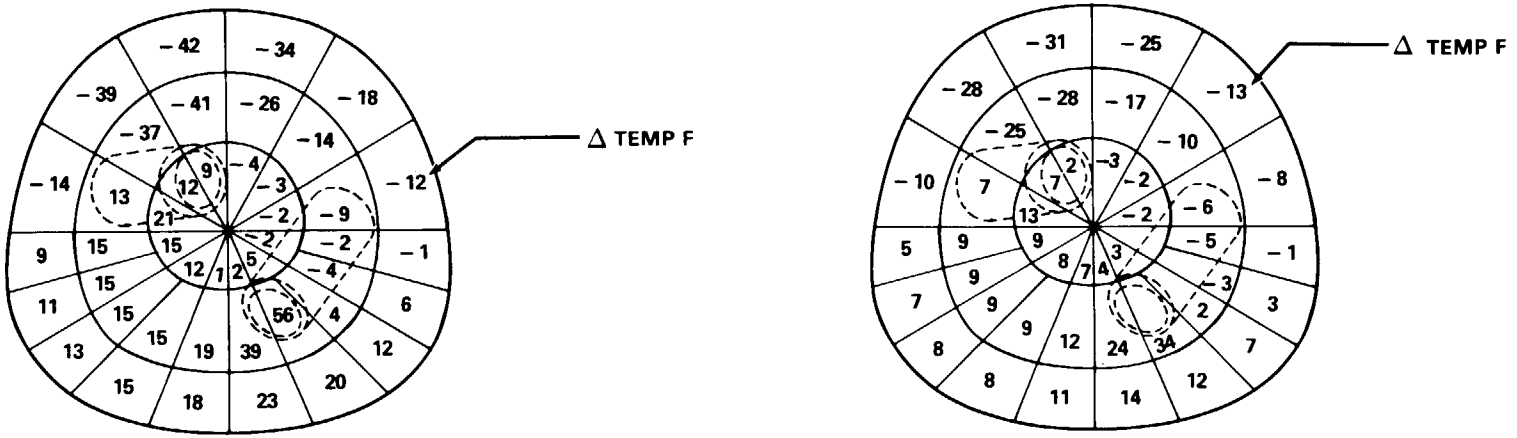

INTERNAL SURFACE NODES

EXTERNAL SURFACE NODES

CHANGE IN PEAK TEMPERATURES CAUSED BY SUPPORT TUBES

Figure 6-1 Heat Blockage Analysis

B2-3592-30

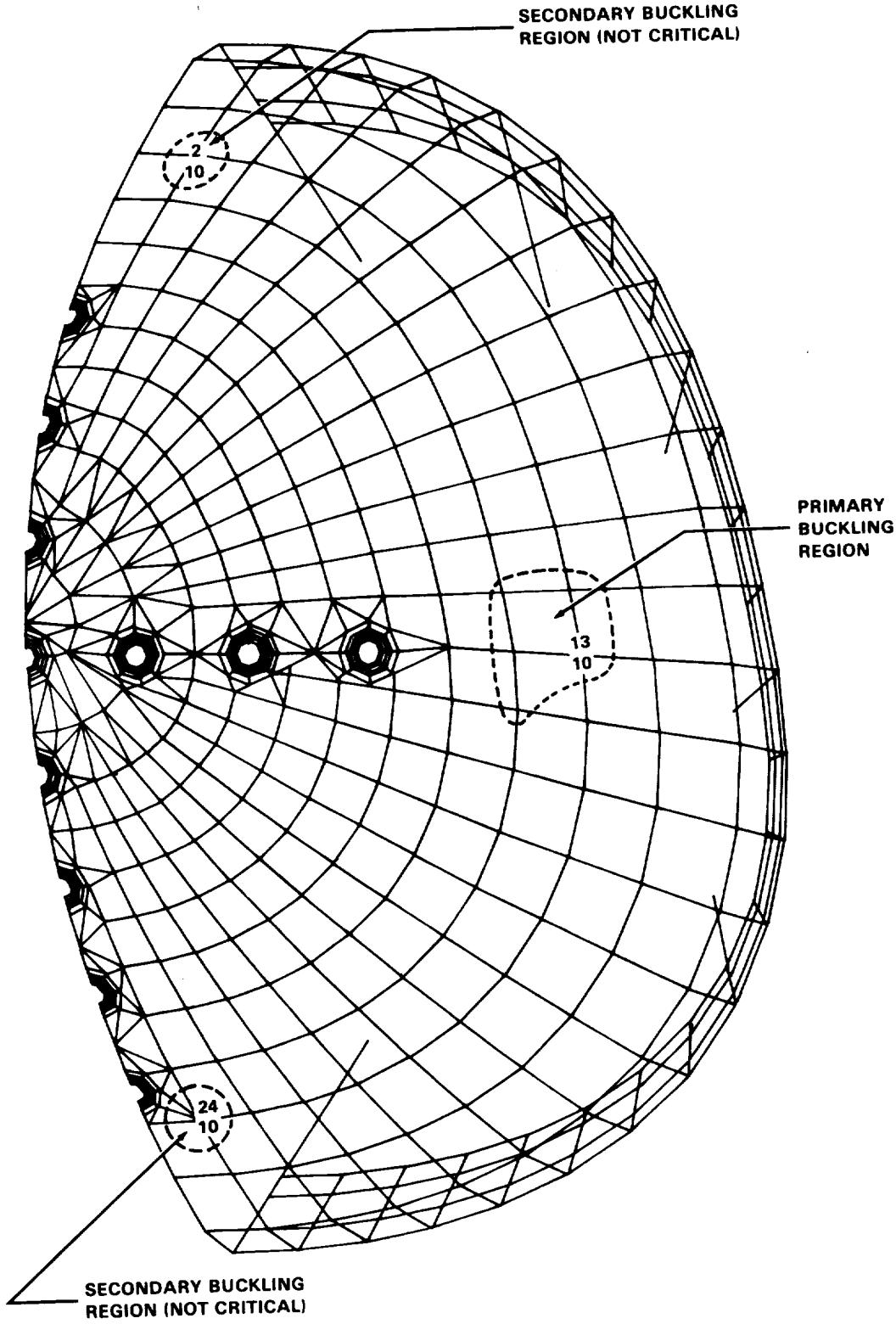

Figure 6-2 SEADS Nose Cap, Regions of Instability

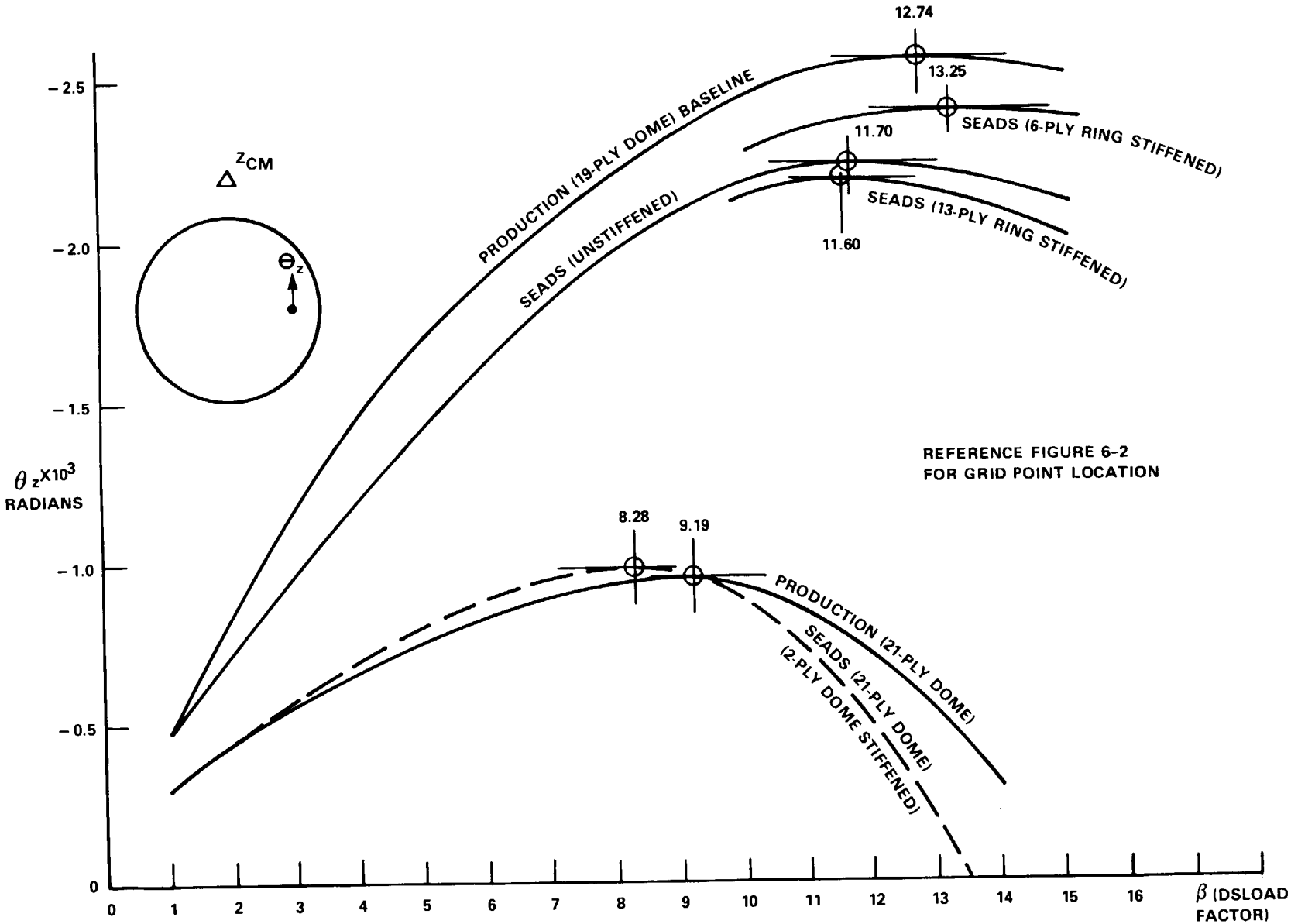

Figure 6-3 Grid Point 1310, Rotational Tracking, Production and SEADS Nose Caps

B2-3592-32

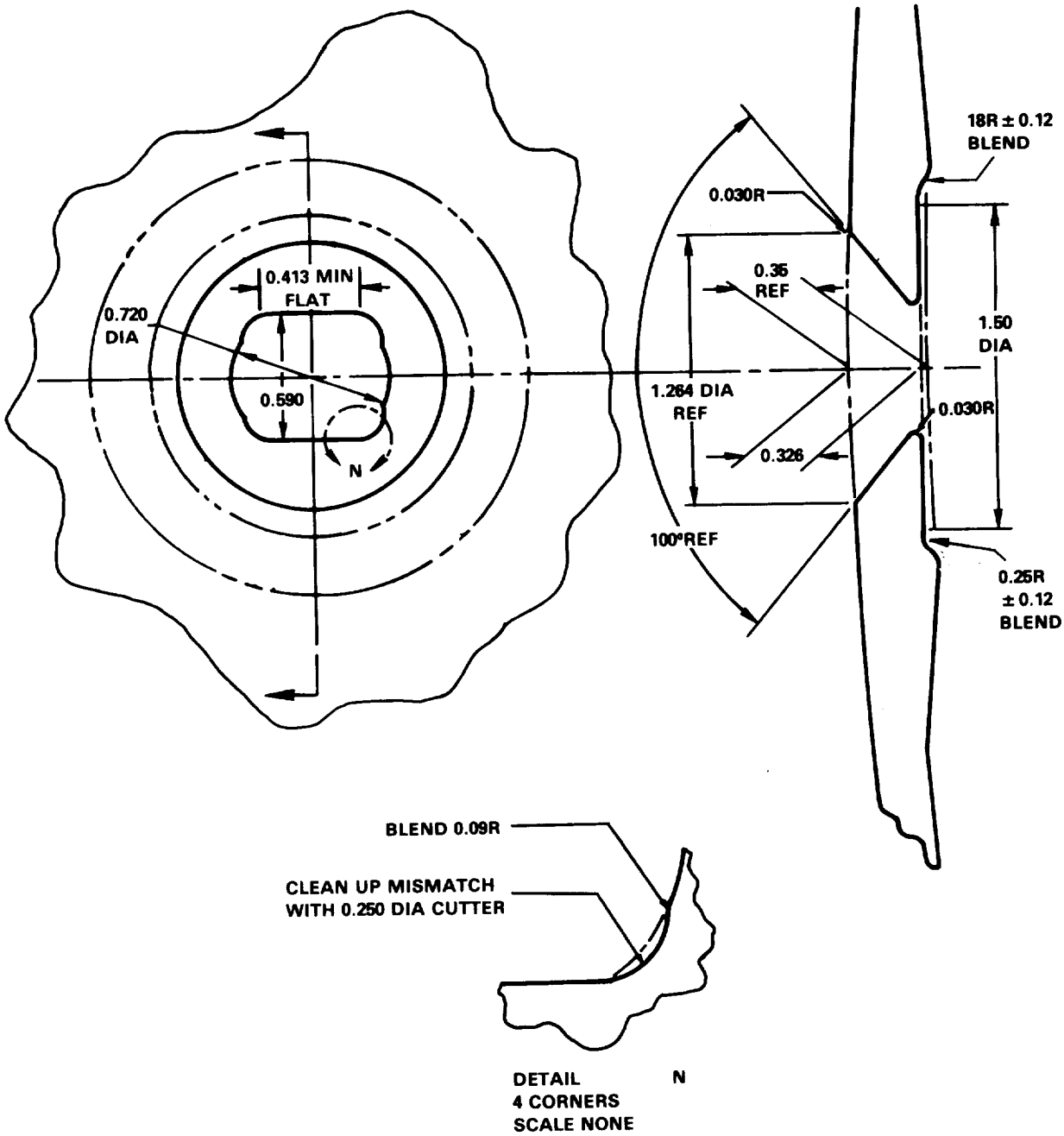

Figure 6-4 SEADS Flat-Sided Hole

B2-3582-33

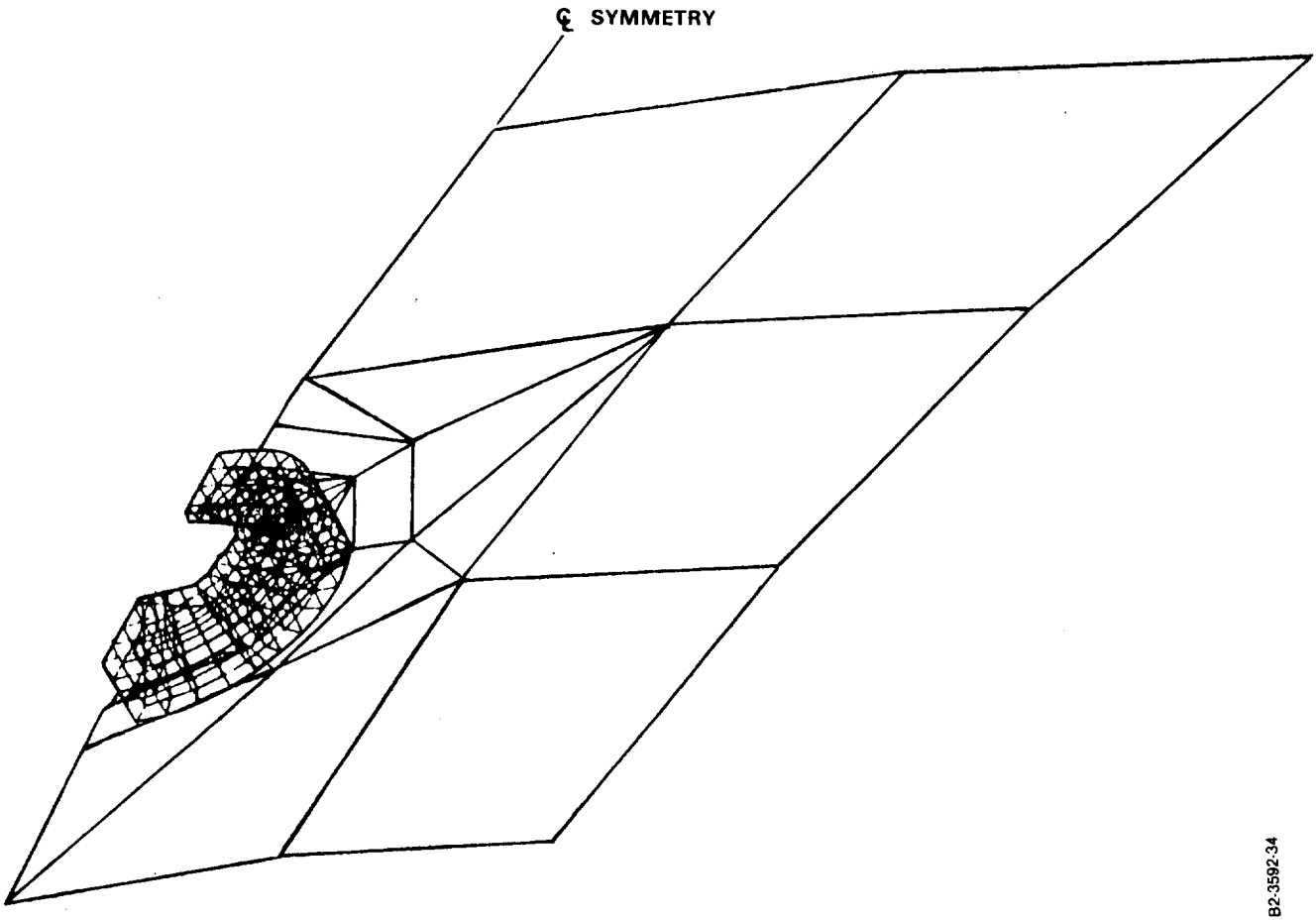

Figure 6-5 Detail SEADS No. 1 Hole – NASTRAN Model, 2D and 3D Elements

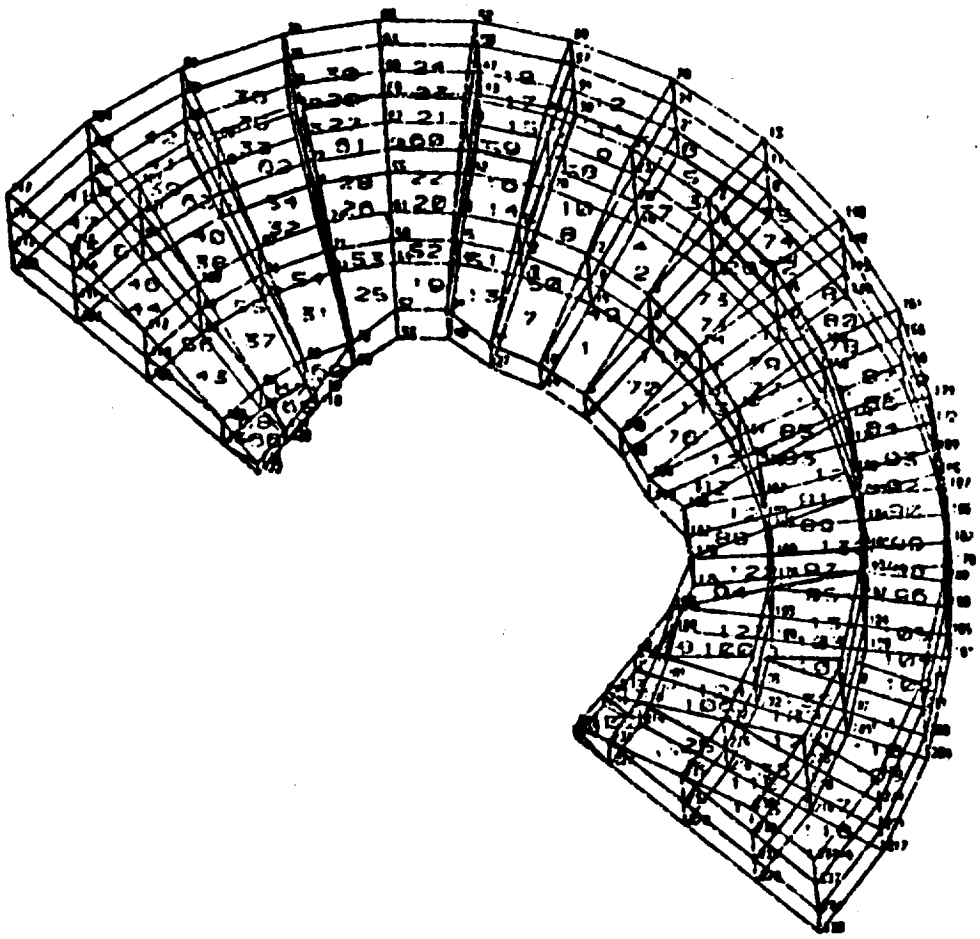

Figure 6-6 Detail - SEADS No. 1 Hole - NASTRAN Model - 3 D Elements

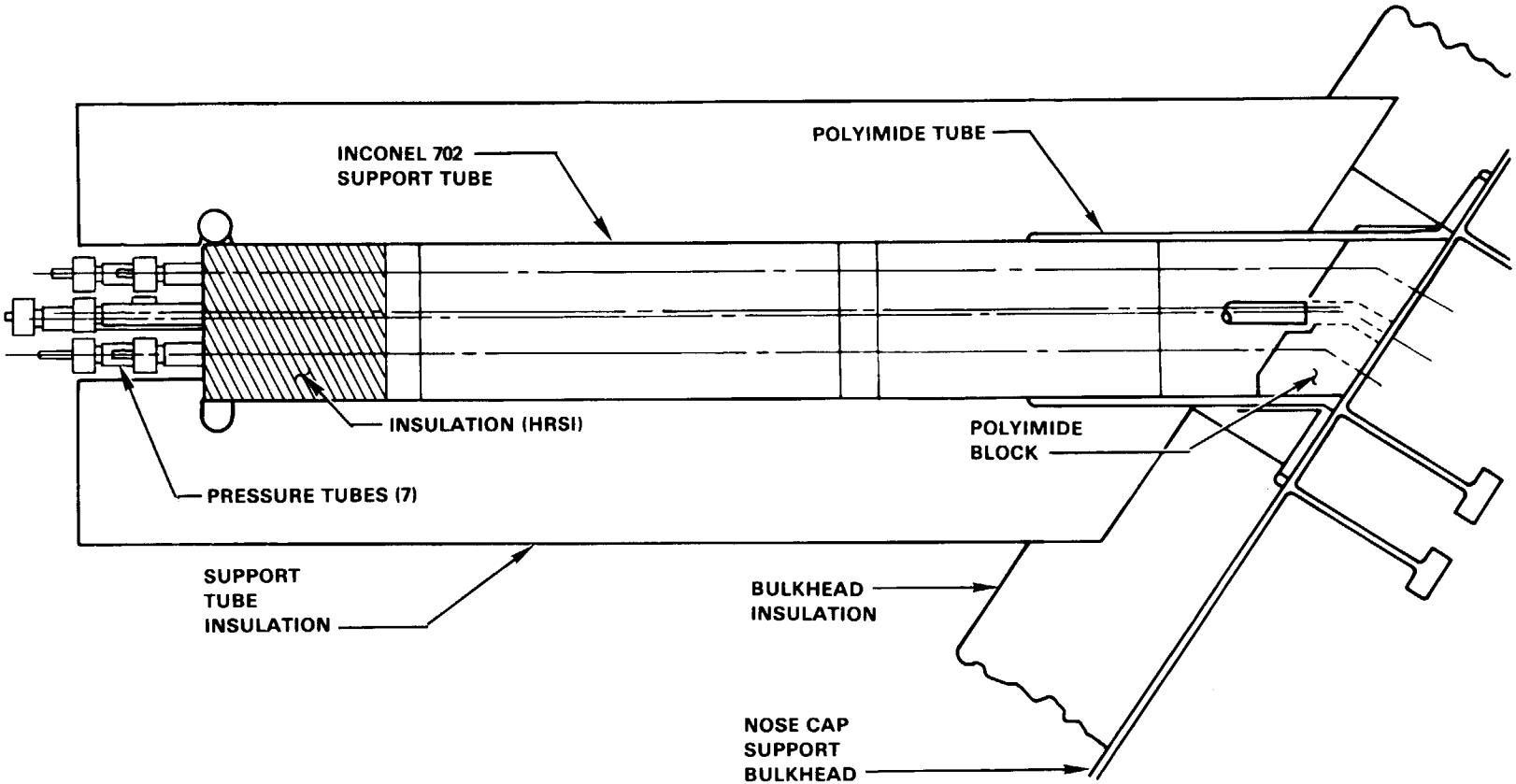

B2-3592-36

Figure 7-1 Initial Support Tube Design for Feasibility Evaluation

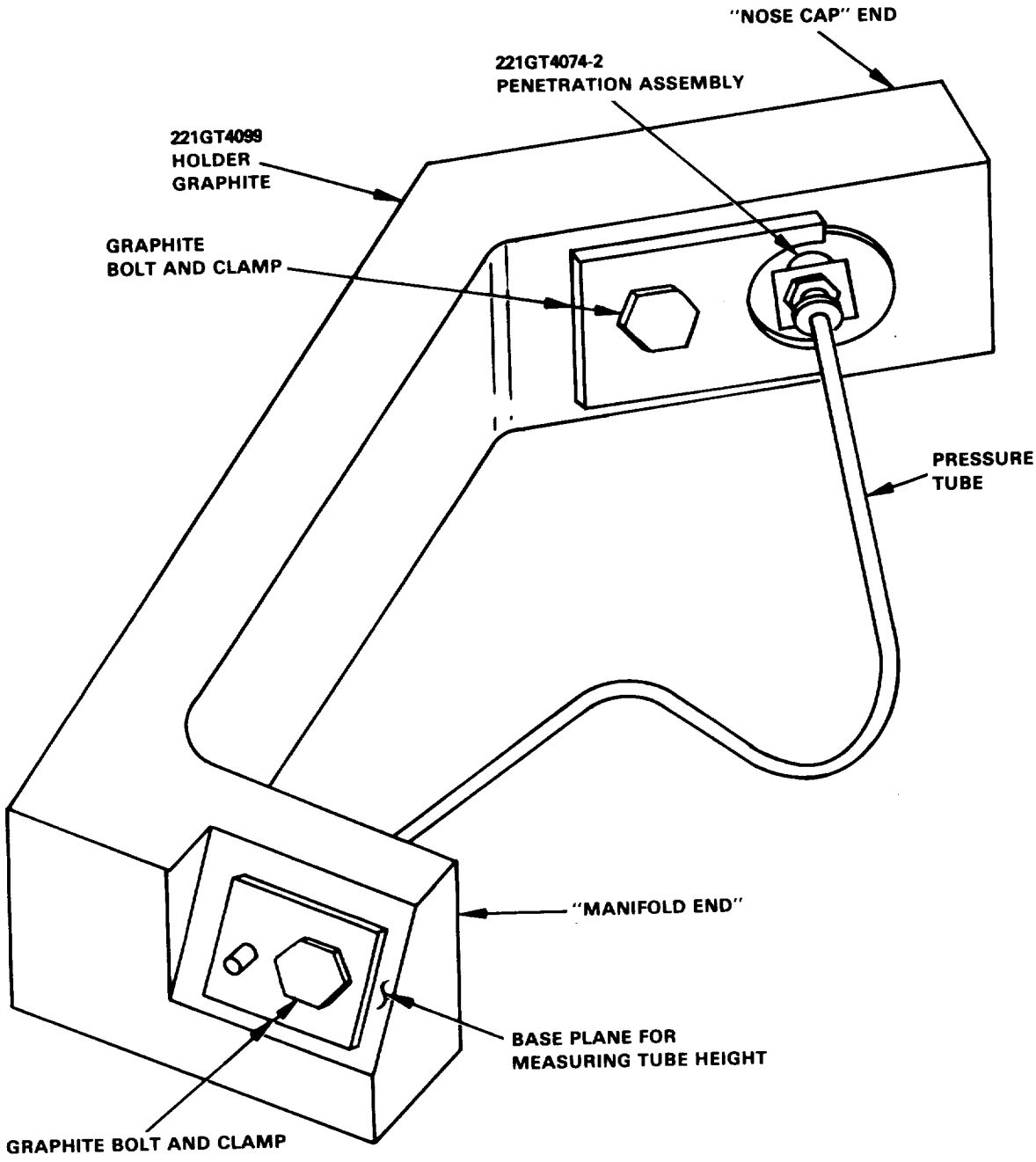

B2-3592-37

Figure 8-1 Test Configuration — Thermal Deflection Test

ORIGINAL PAGE
BLACK AND WHITE PHOTOGRAPH

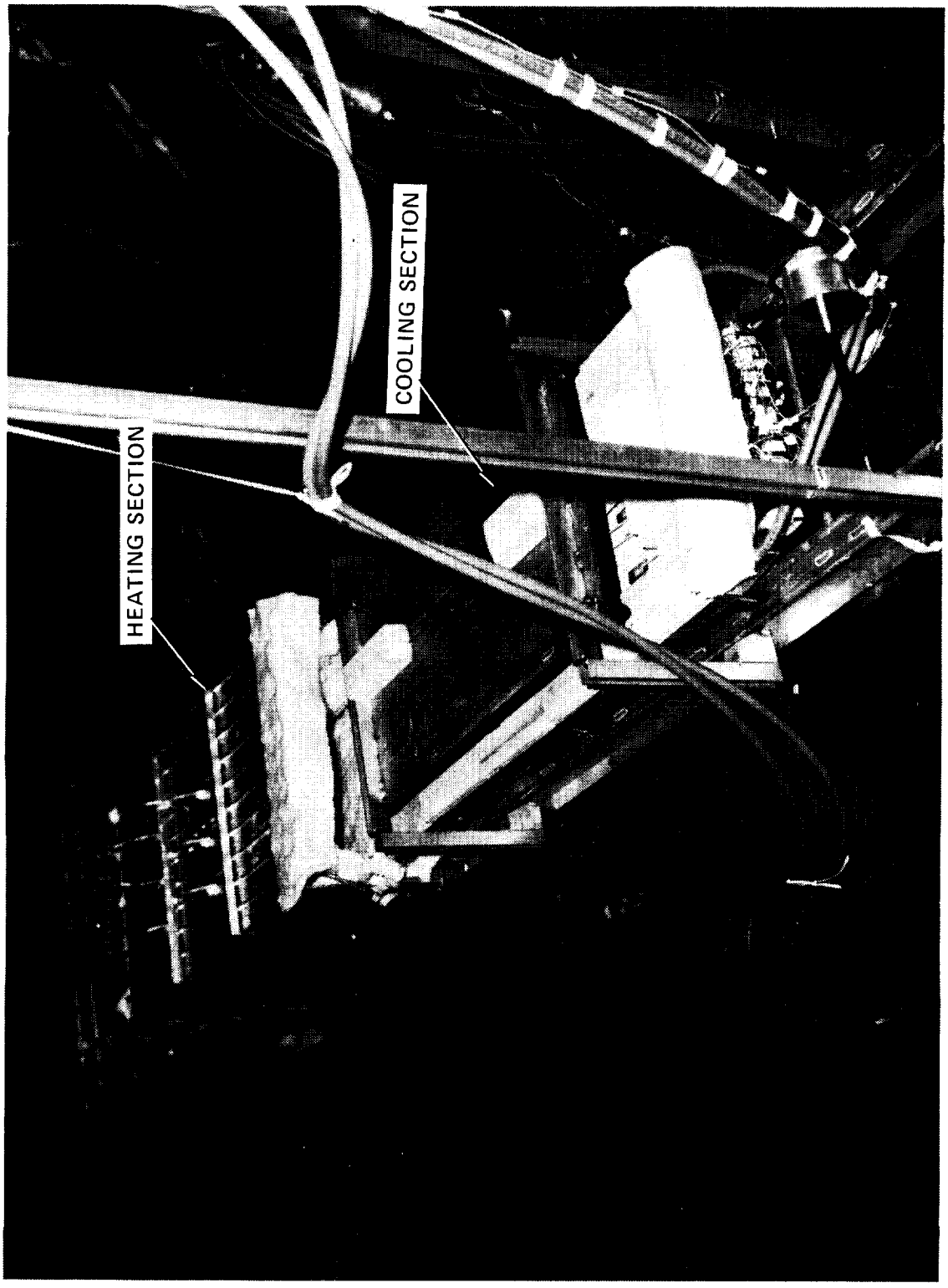

Figure 8–2 Thermal Deflection Test Facility

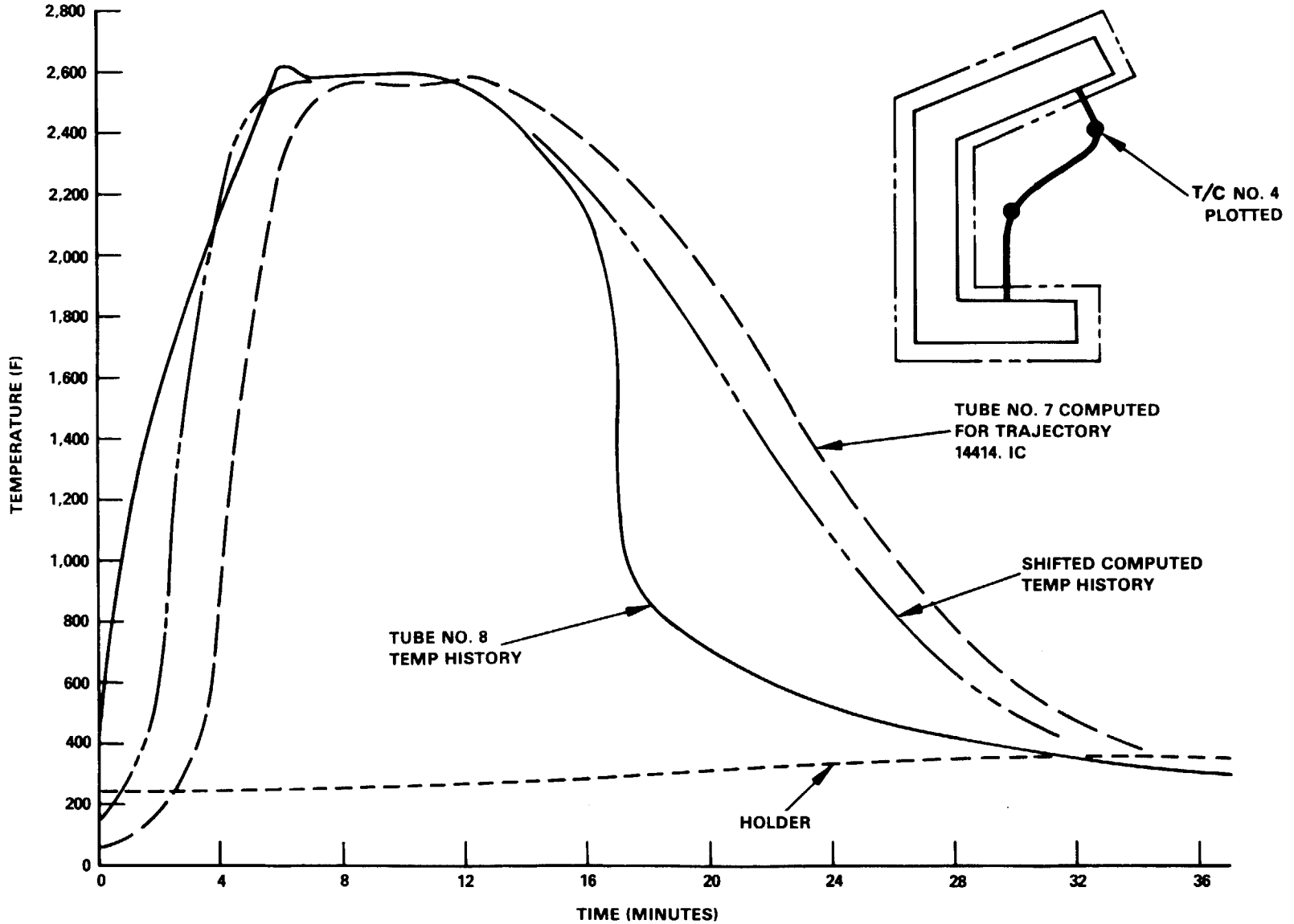

Figure 8-3 Typical Thermal Test Temperature History

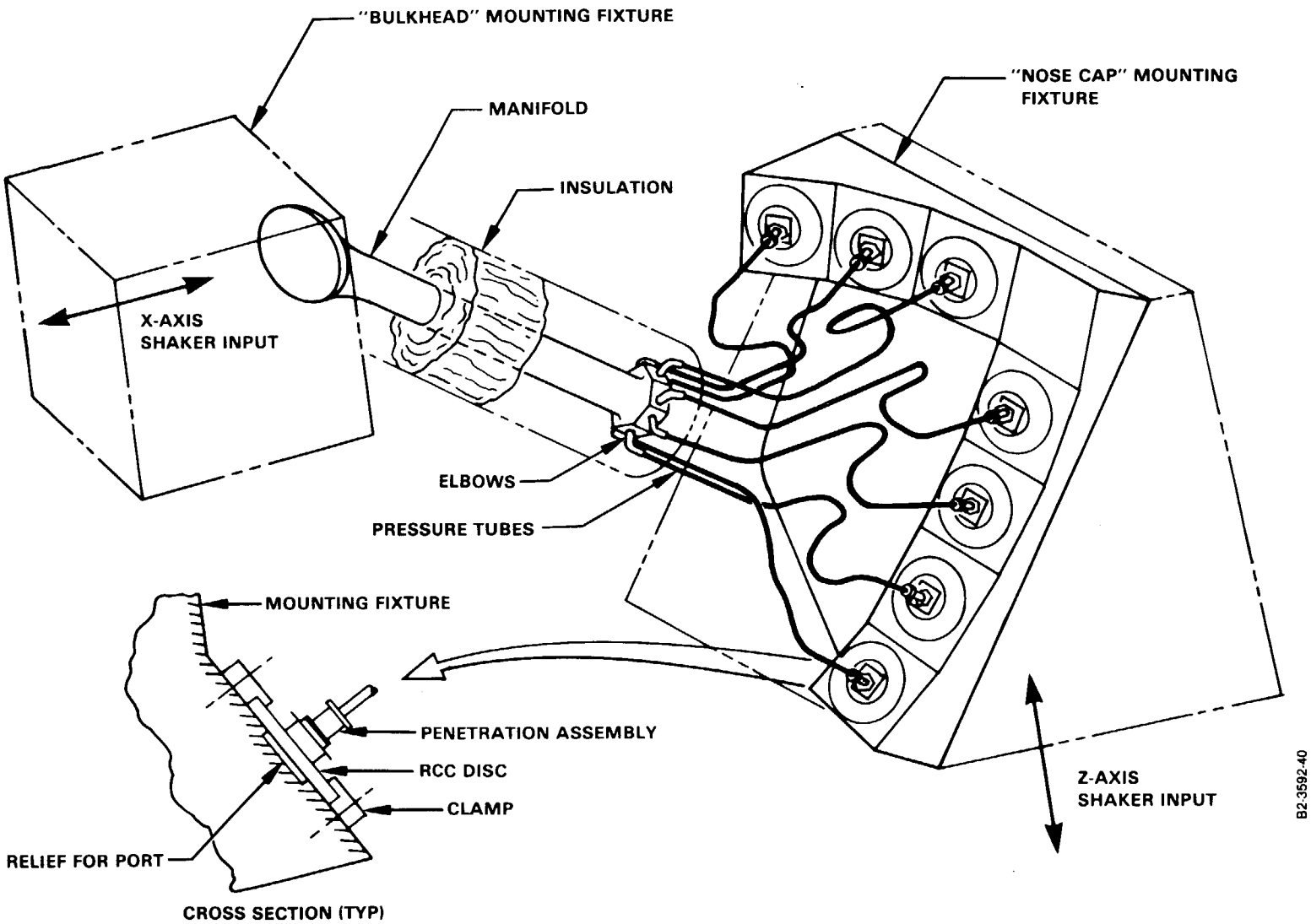

Figure 8-4 Vibration Test Concept

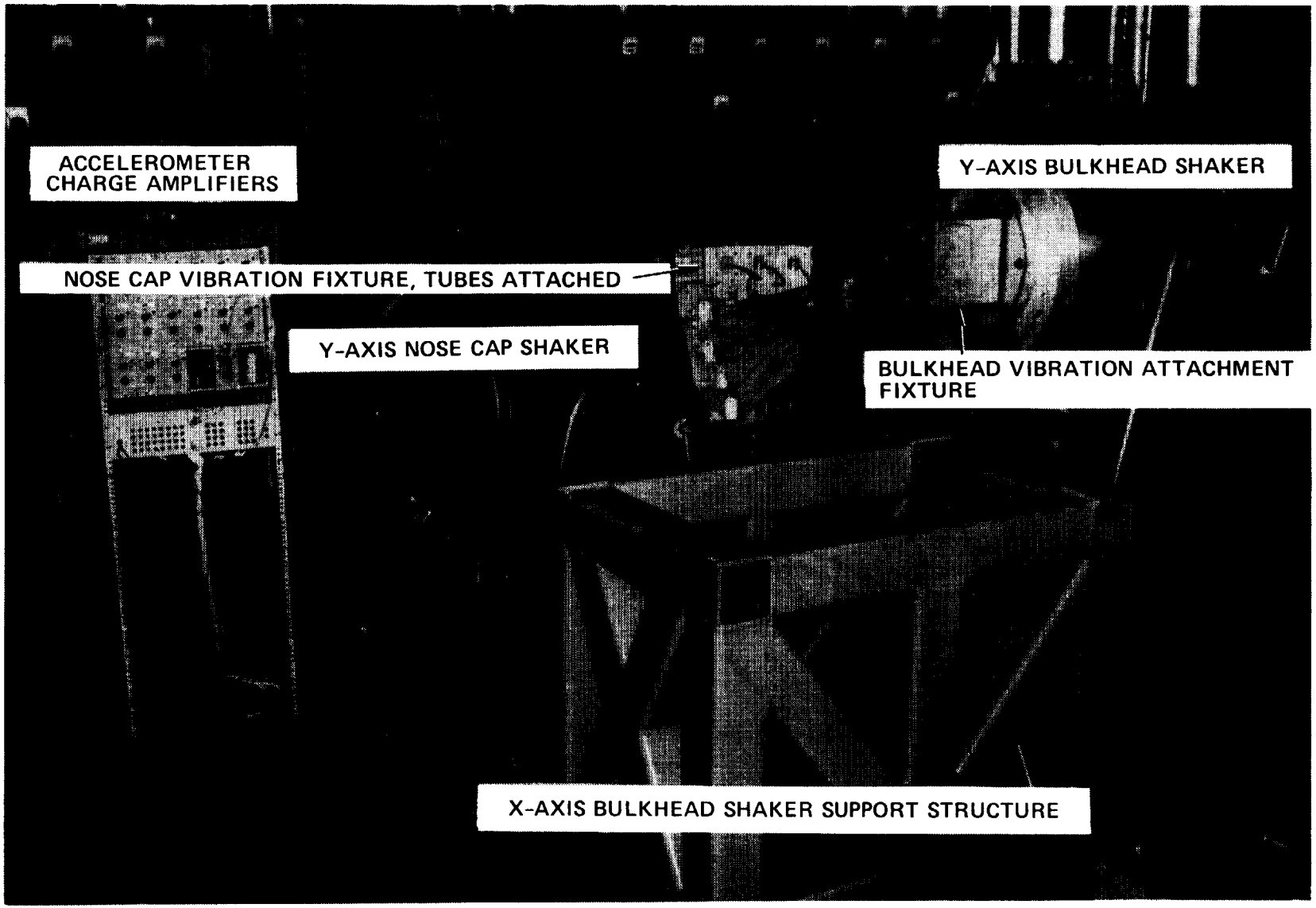

Figure 8–5 Vibration Test Setup, Y–Y Axis Configuration

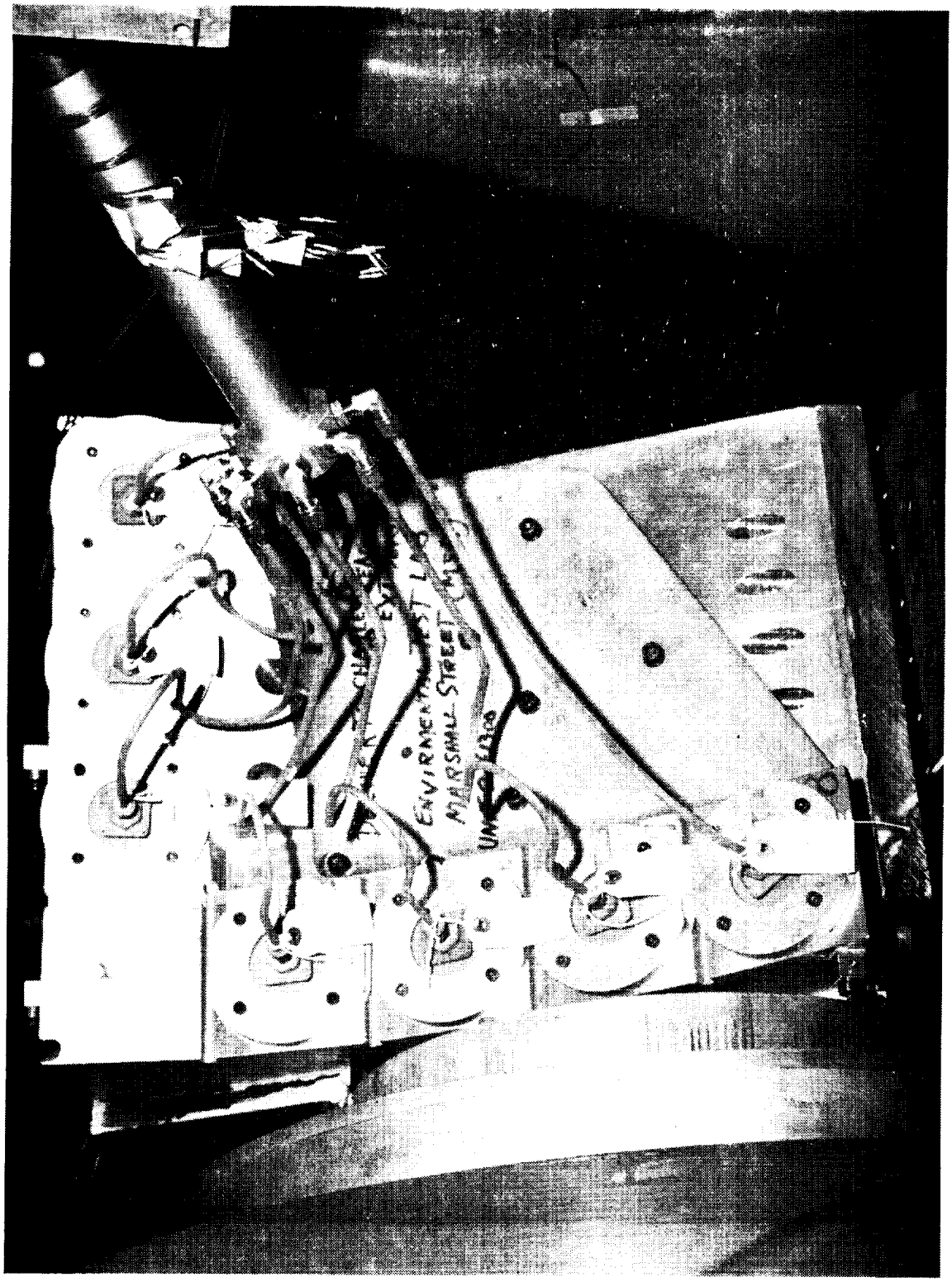

Figure 8–6 Components Installation for Vibration Test

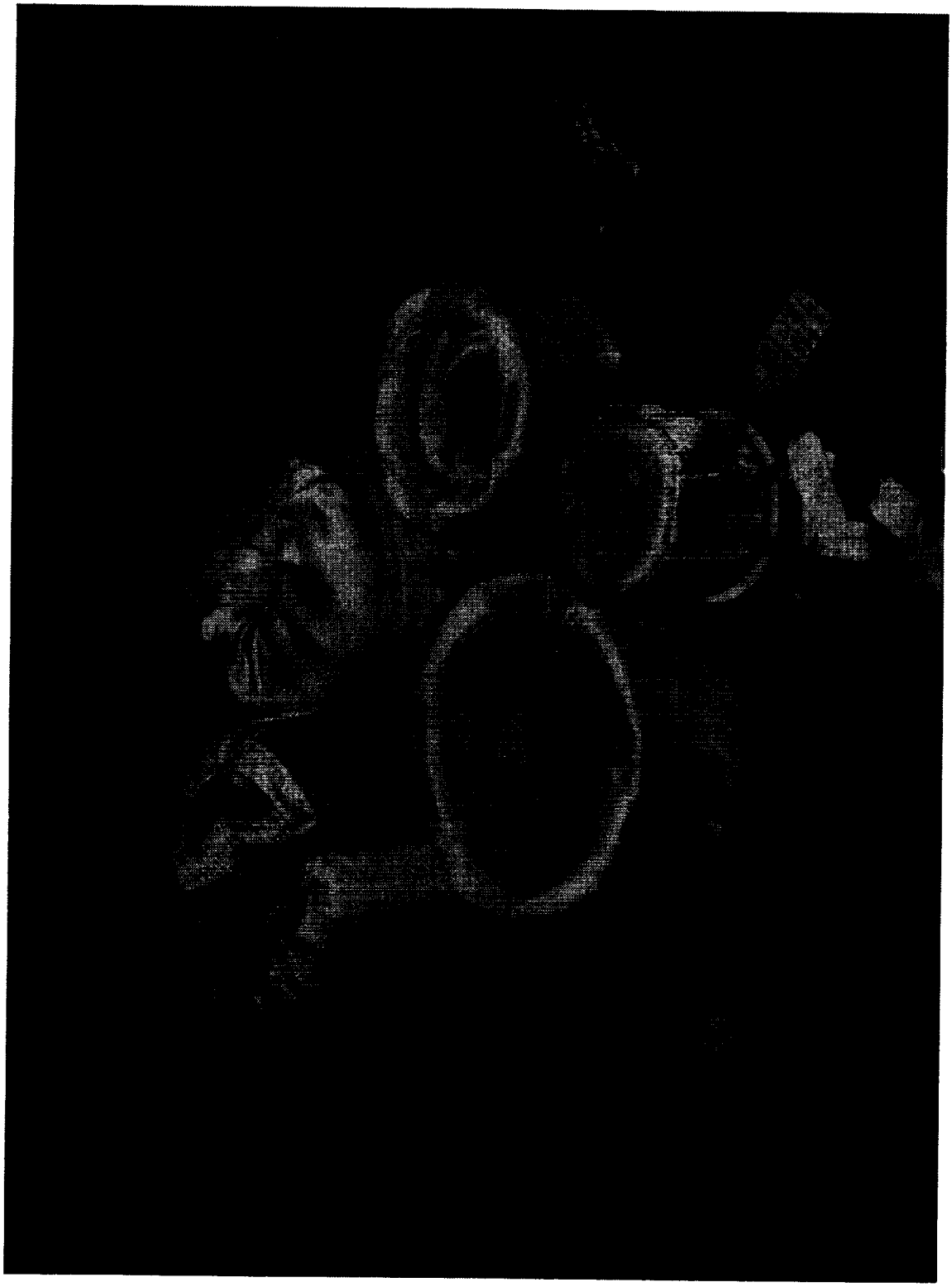

Figure 8–7 Insulation Components

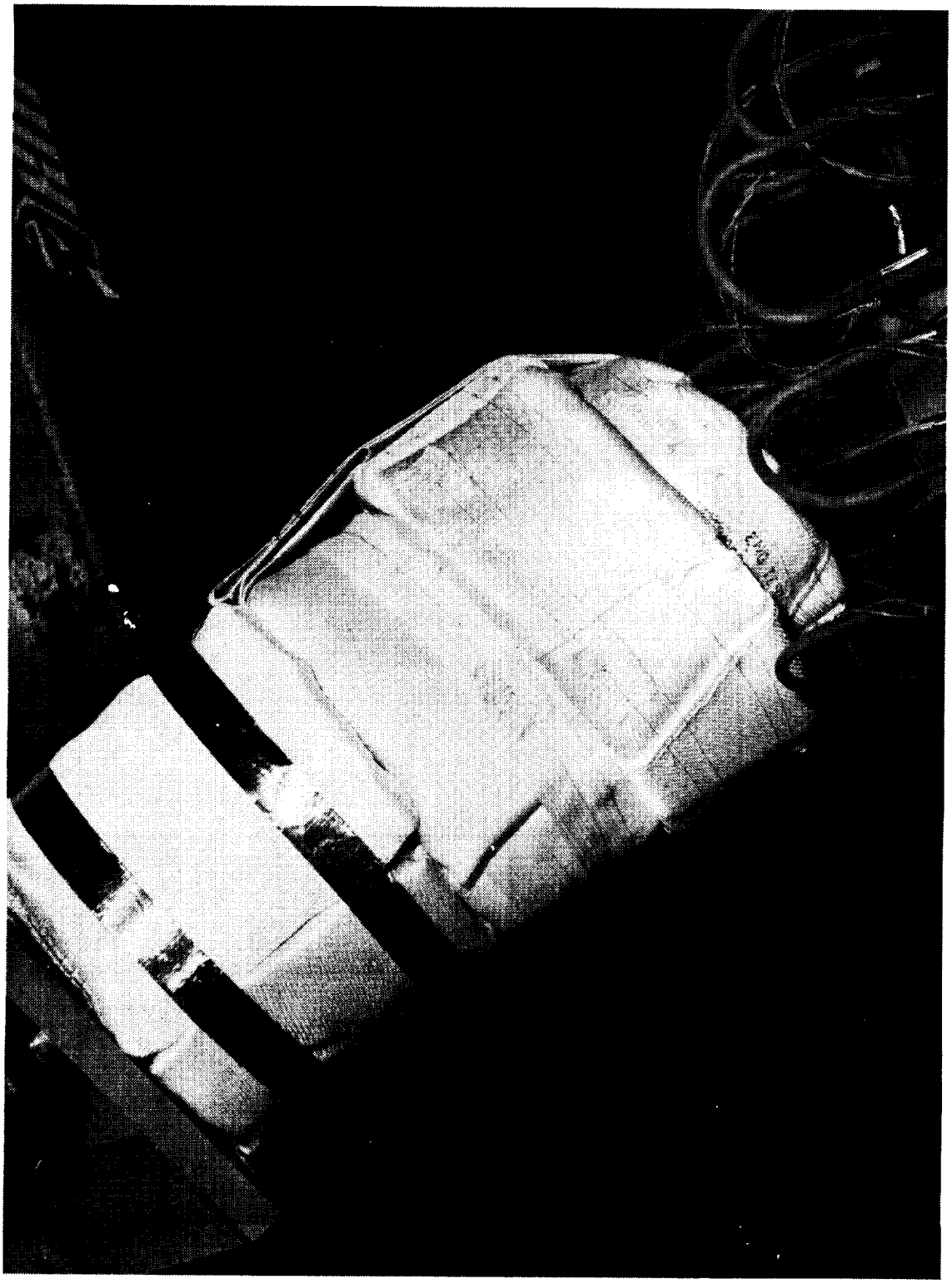

Figure 8–8 Insulation Installed on Manifold

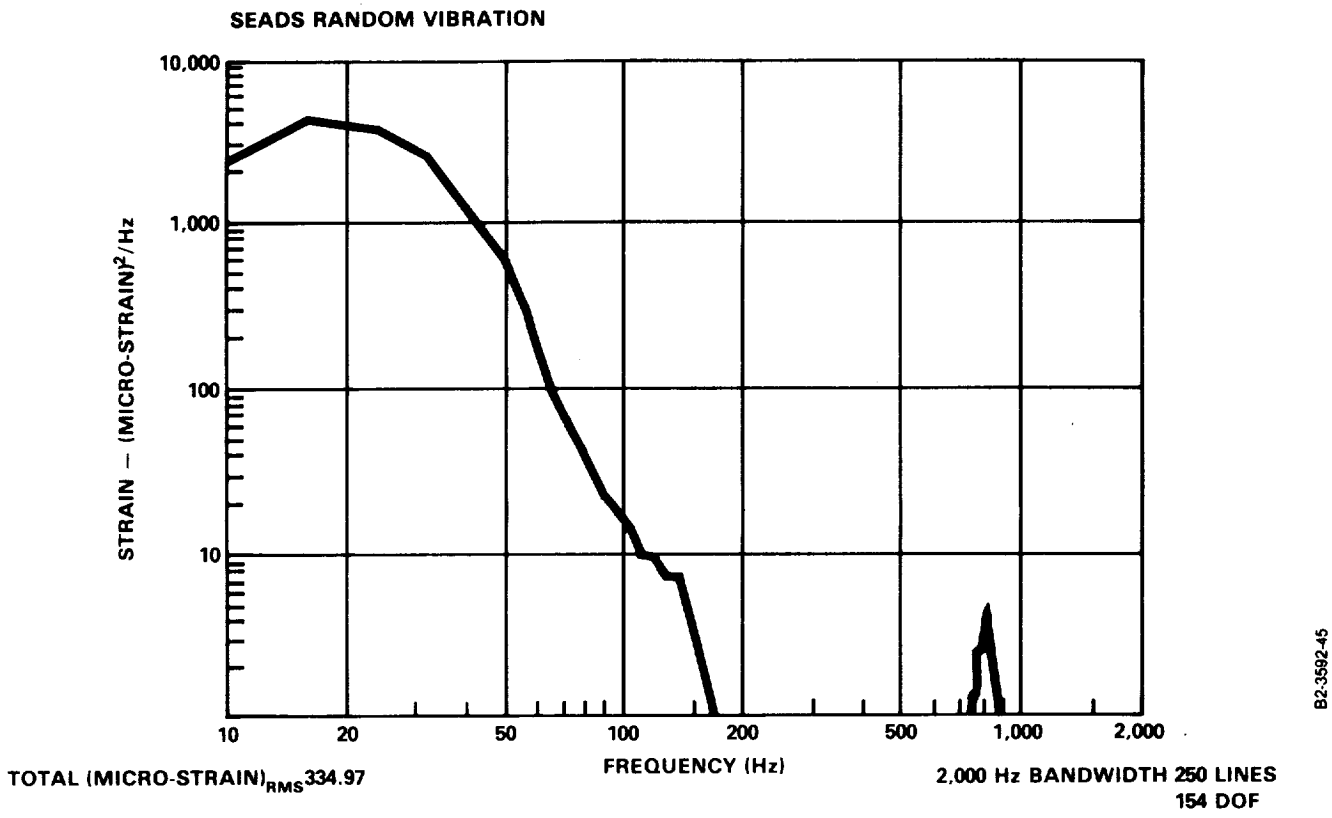

Figure 8-9 Strain Response Plot Y-Y Axis Strain Gage 800m

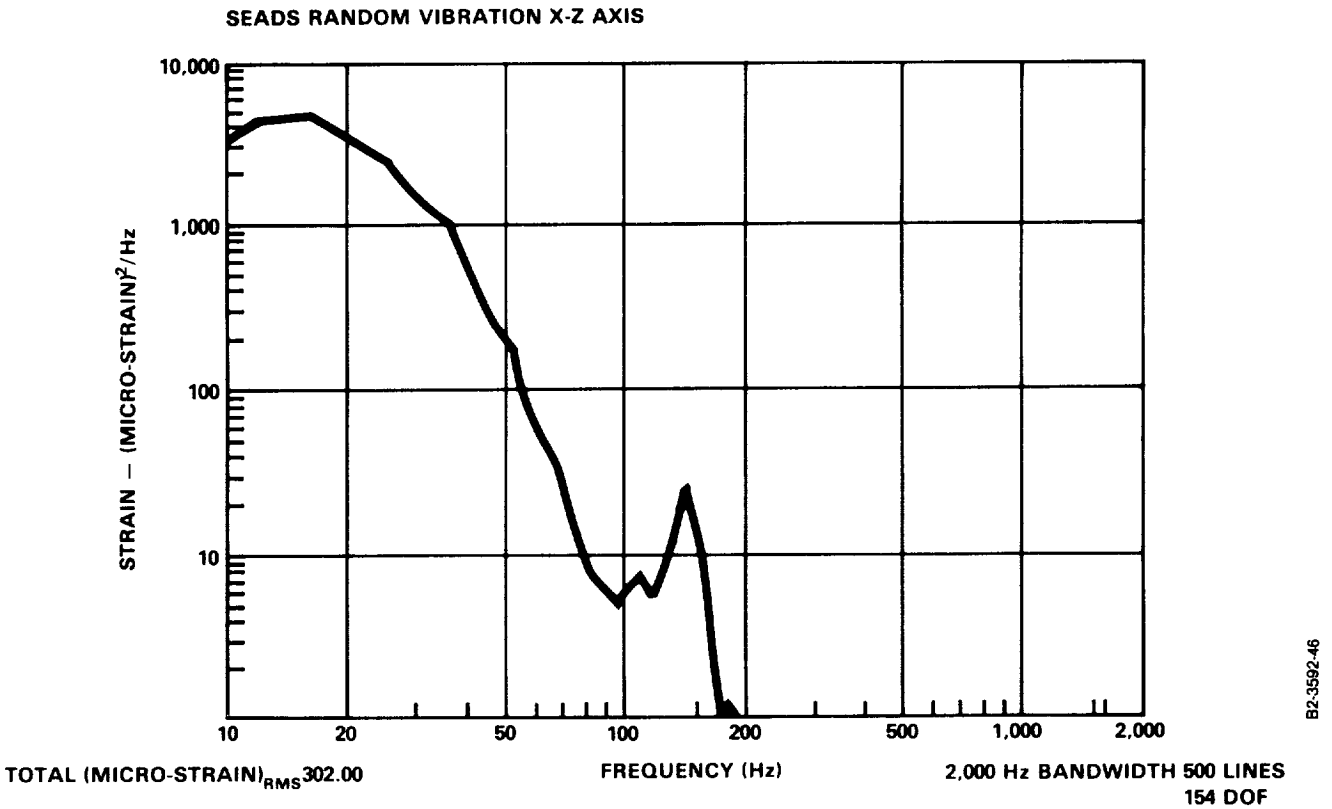

Figure 8-10 Strain Response Plot X-Z Axis Strain Gage 800m

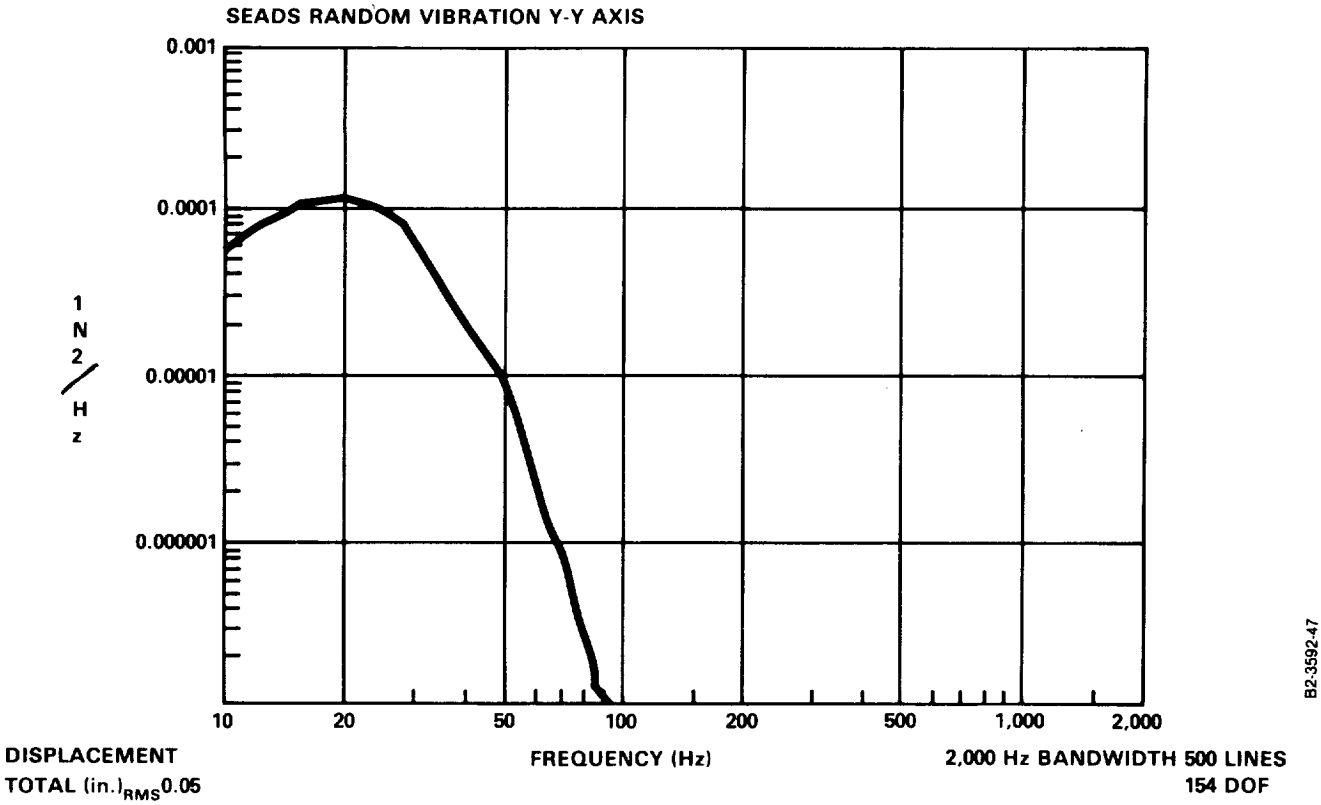

Figure 8-11 Displacement Plot of Nose Cap Input Spectrum Y-Axis

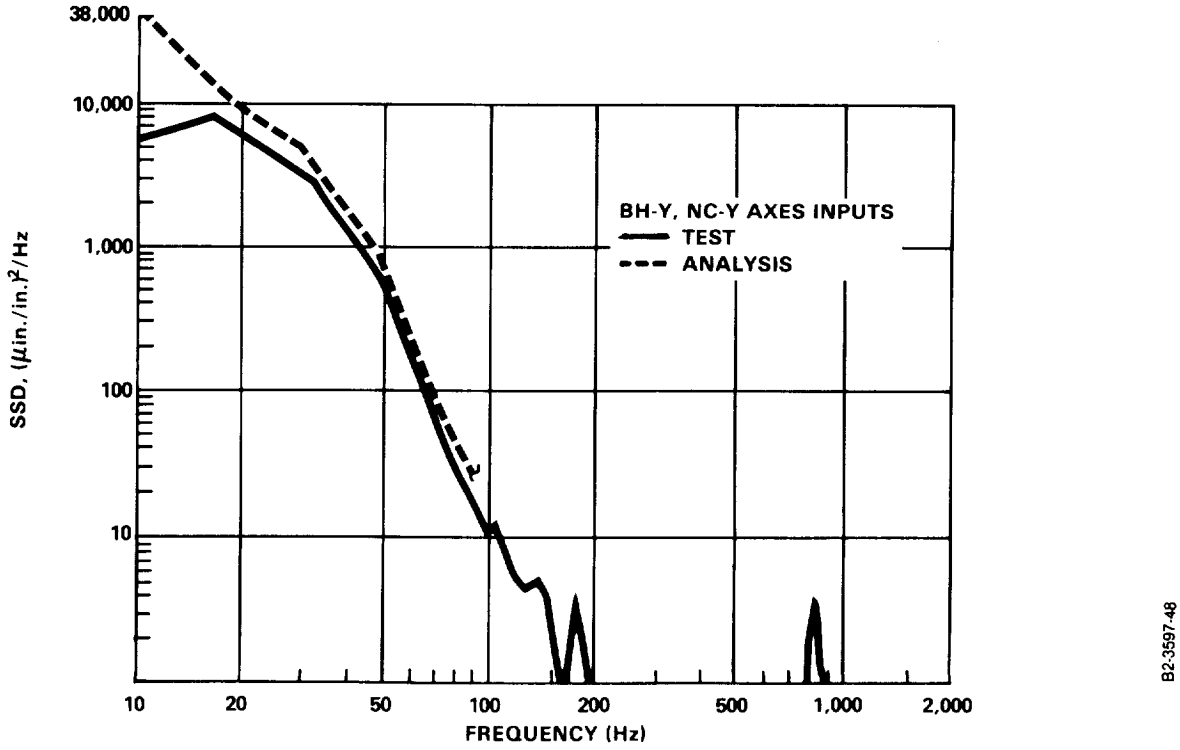

Figure 8-12 Strain Spectral Density Comparisons — Tube 8/Manifold End

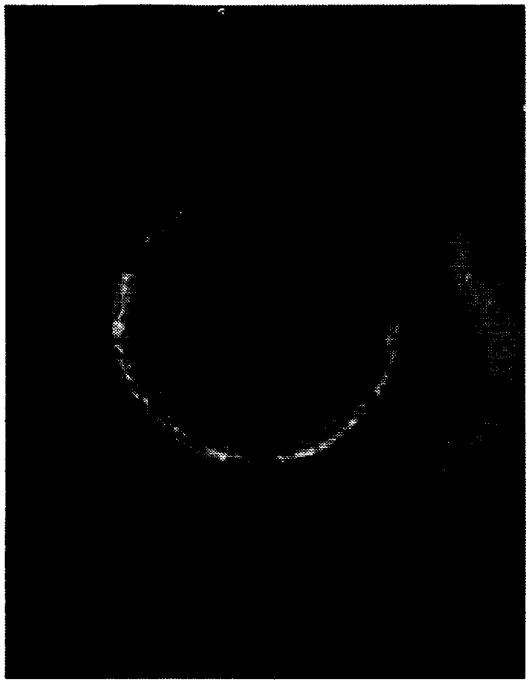

TUBE NO. 11

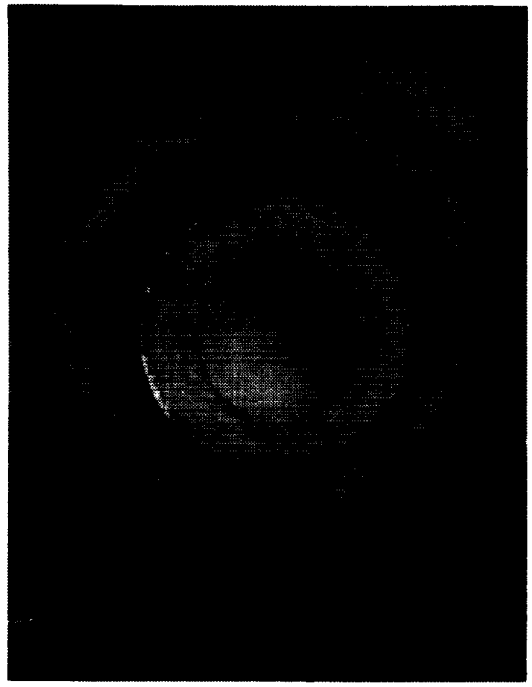

TUBE NO. 5

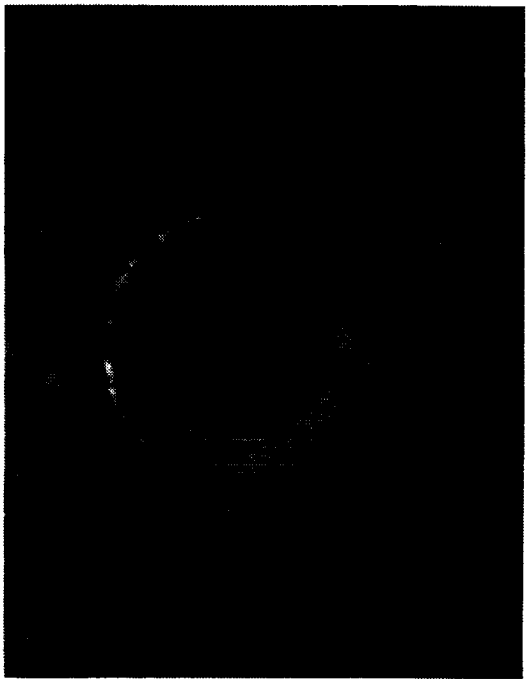

TUBE NO. 8

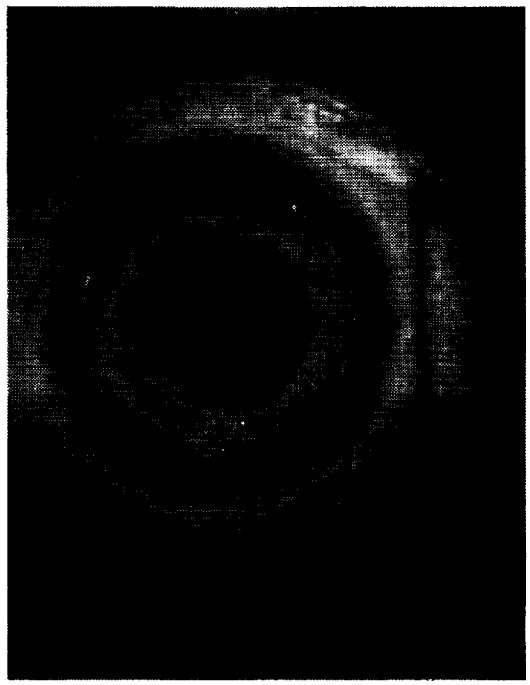

TUBE NO. 6

Figure 8–13 Tube Ends After Vibration Test

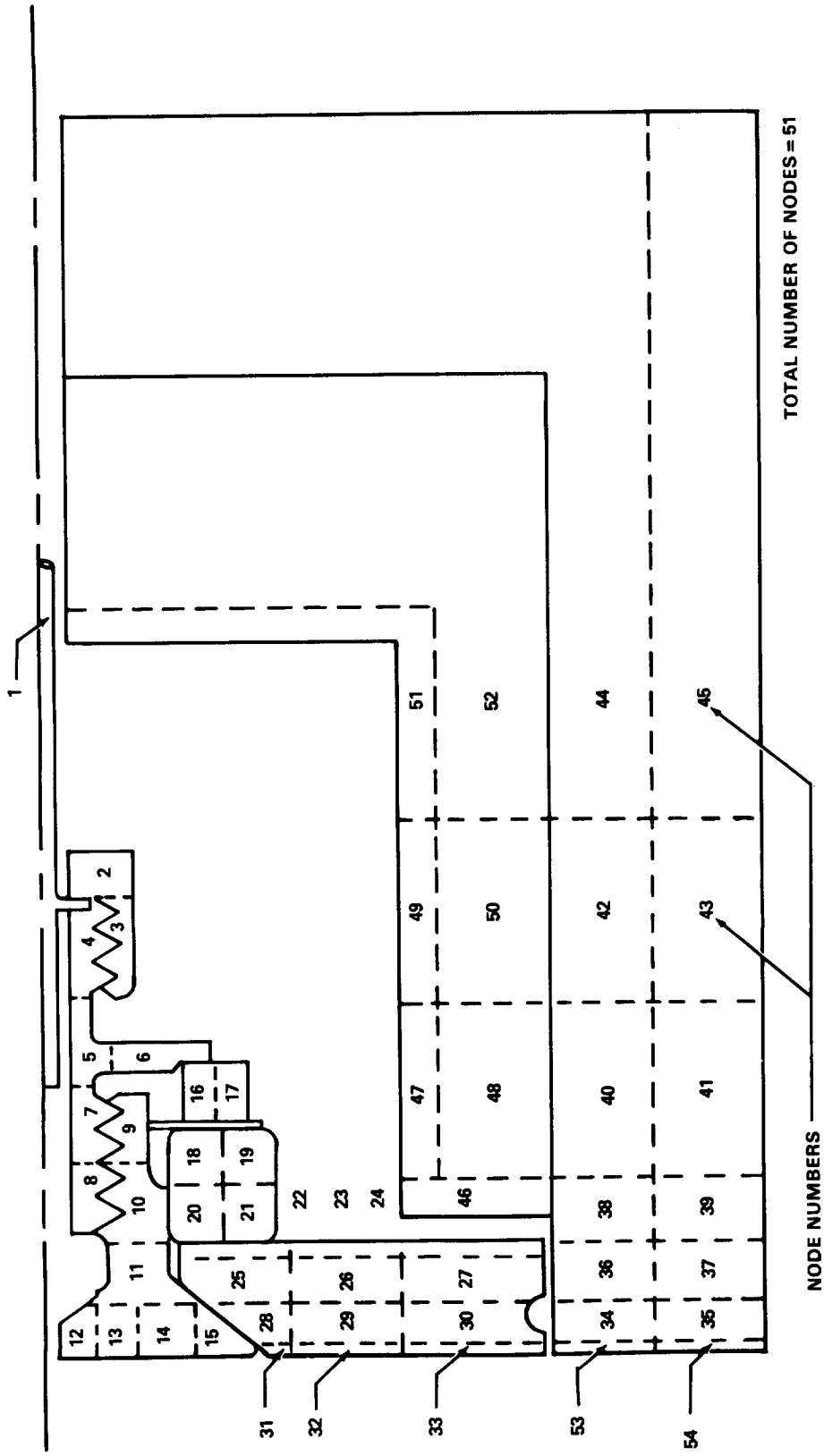

Figure 9-1 SEADS Test Specimen Thermal Model

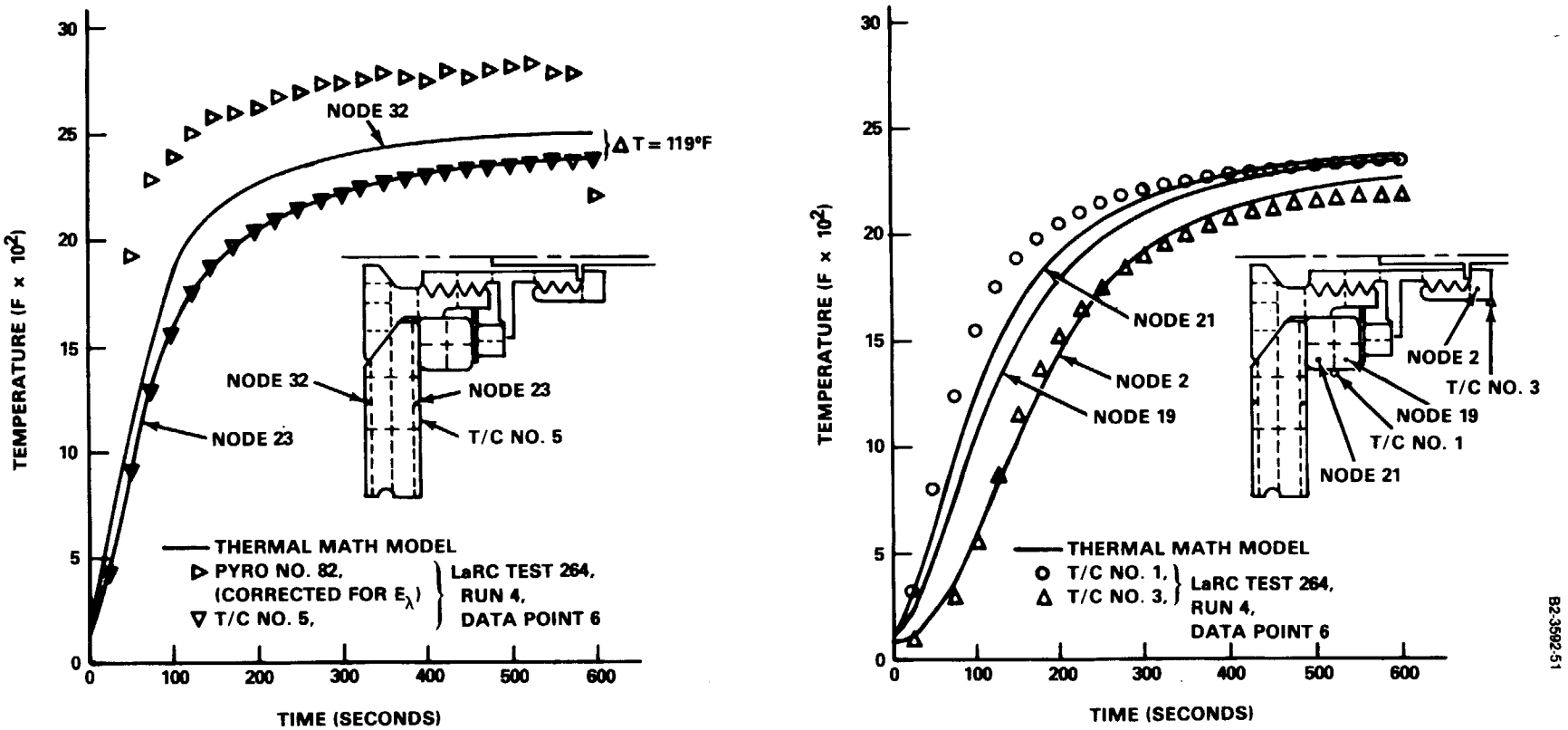

Figure 9-2 Temperature History Comparison Analysis Controlled to Thermocouple No. 5 Heat Up

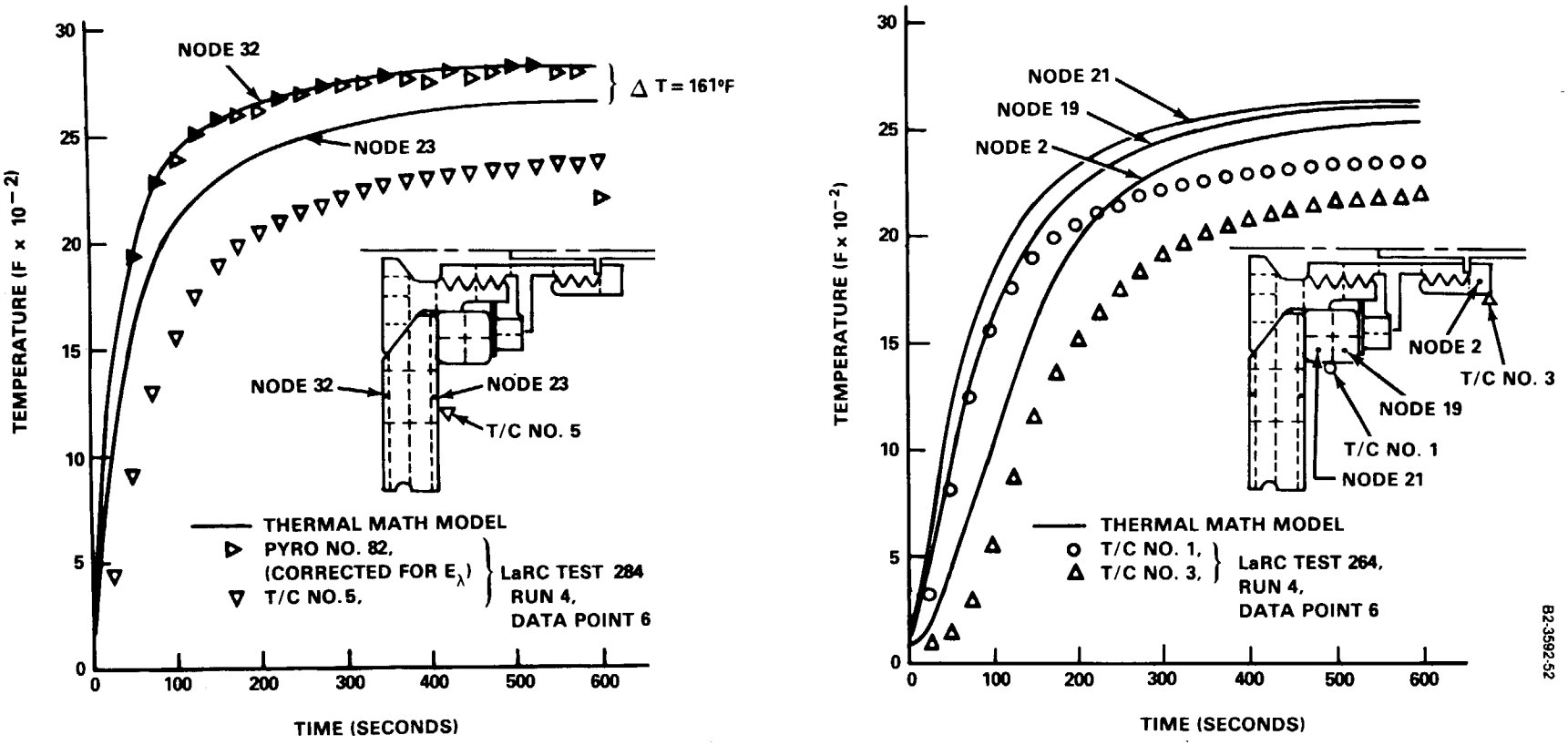

Figure 9-3 Temperature History Comparison Analysis Controlled to Pyrometer No. 82 Cool Down

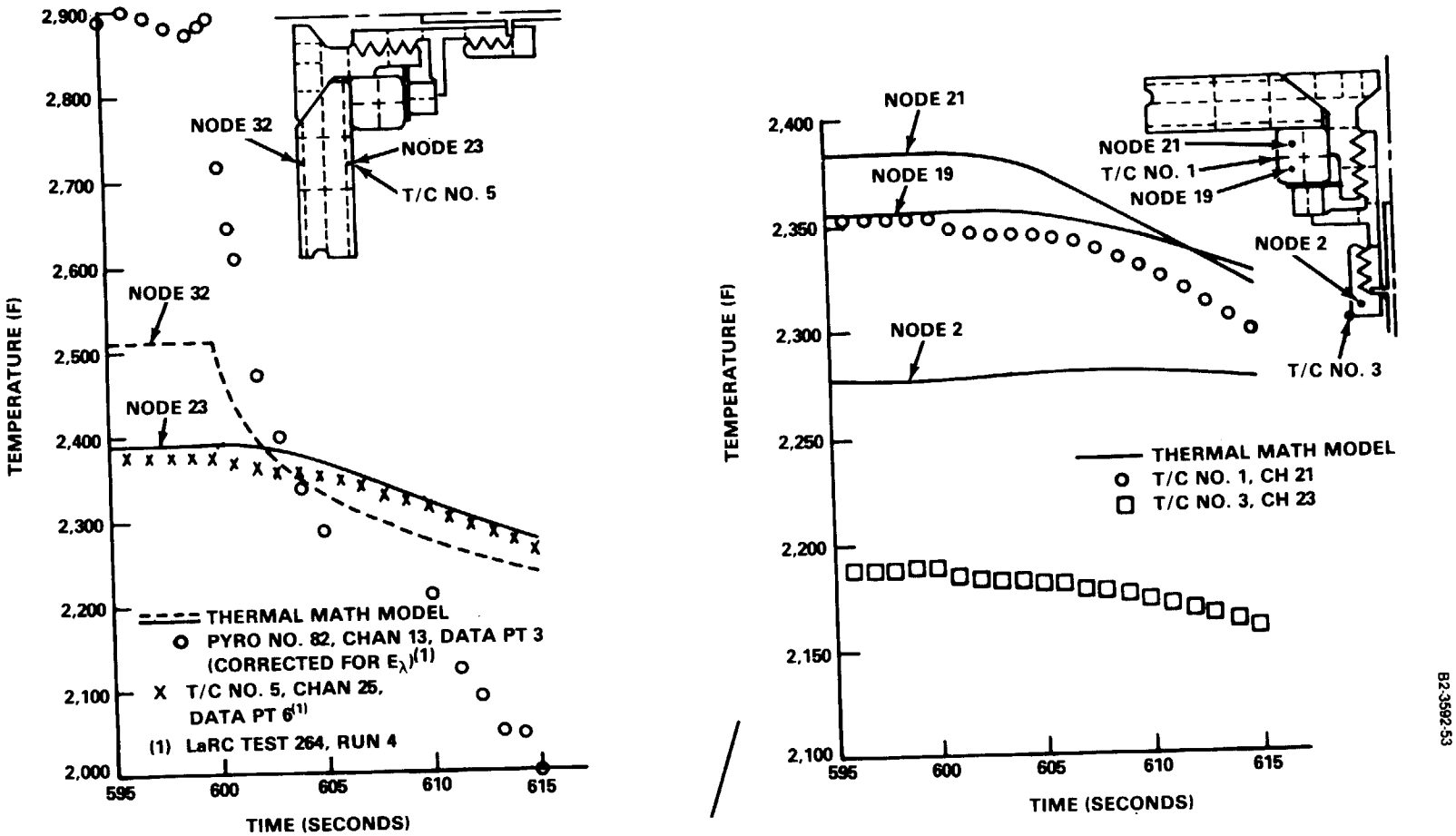

Figure 9-4 Temperature History Comparison Analysis Controlled to Thermocouple No. 5 Cooldown

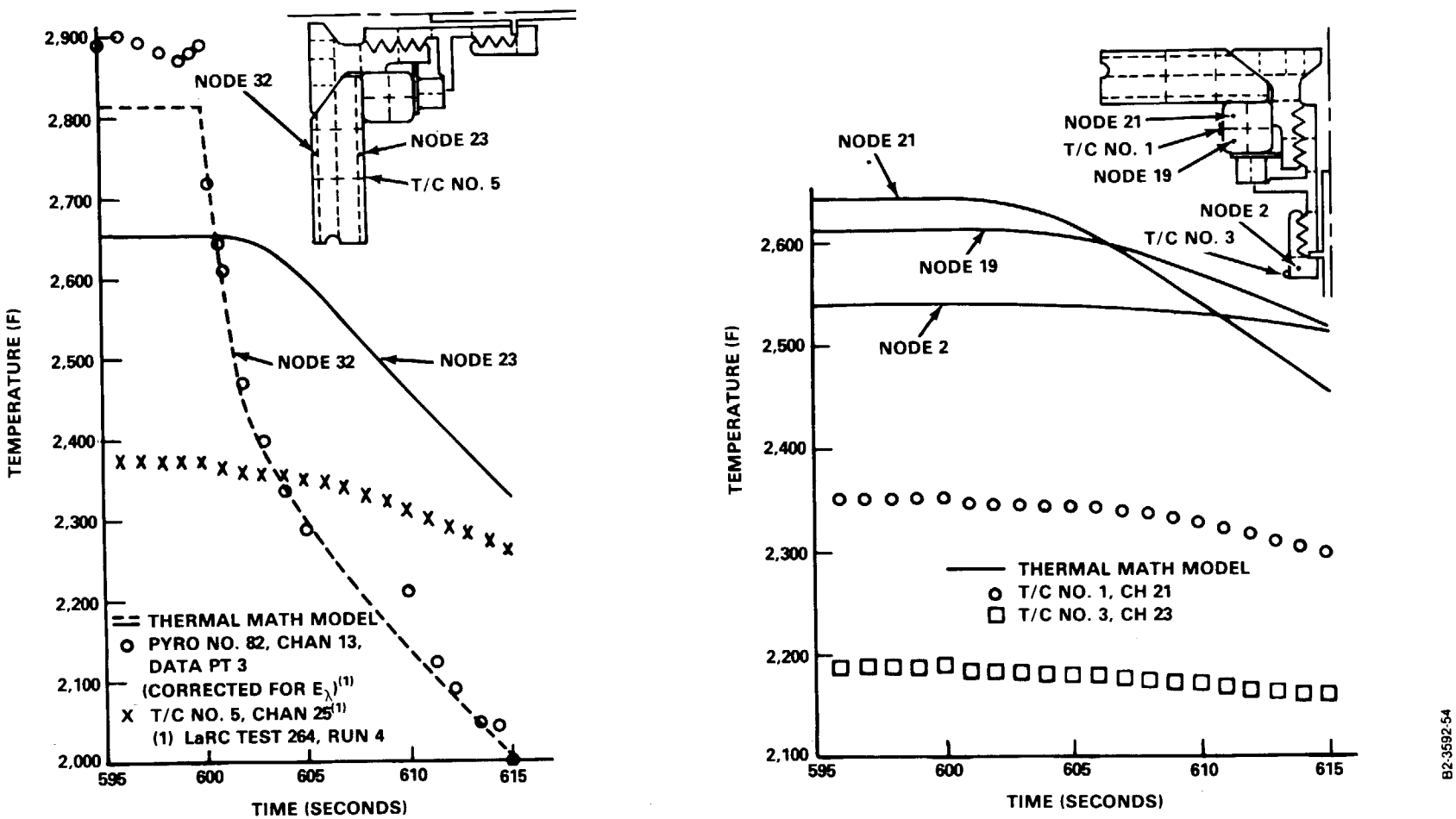

Figure 9-5 Temperature History Comparison Analysis Controlled to Pyrometer No. 82 Cooldown

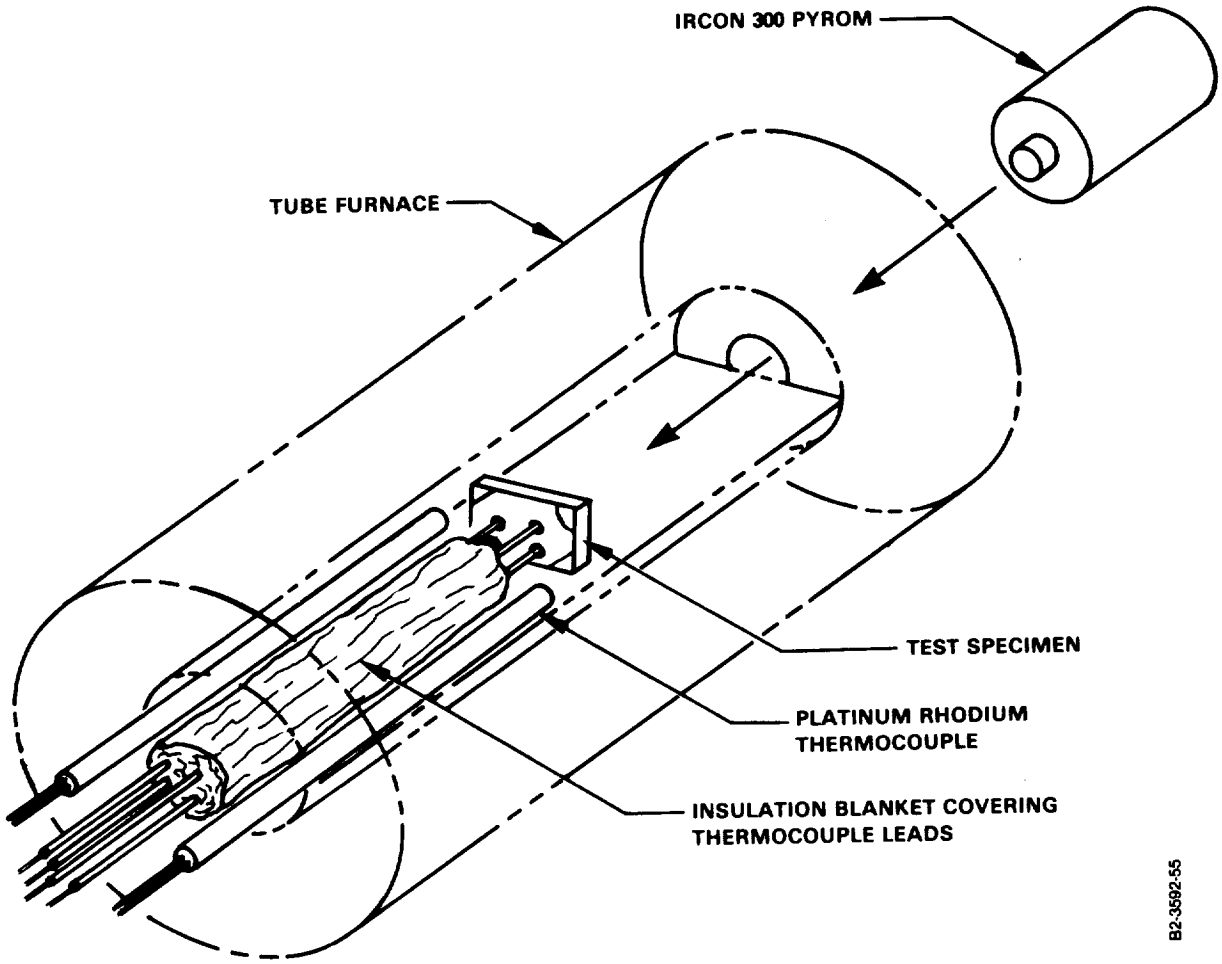

Figure 9-6 Testing Approach for Thermocouple Evaluation

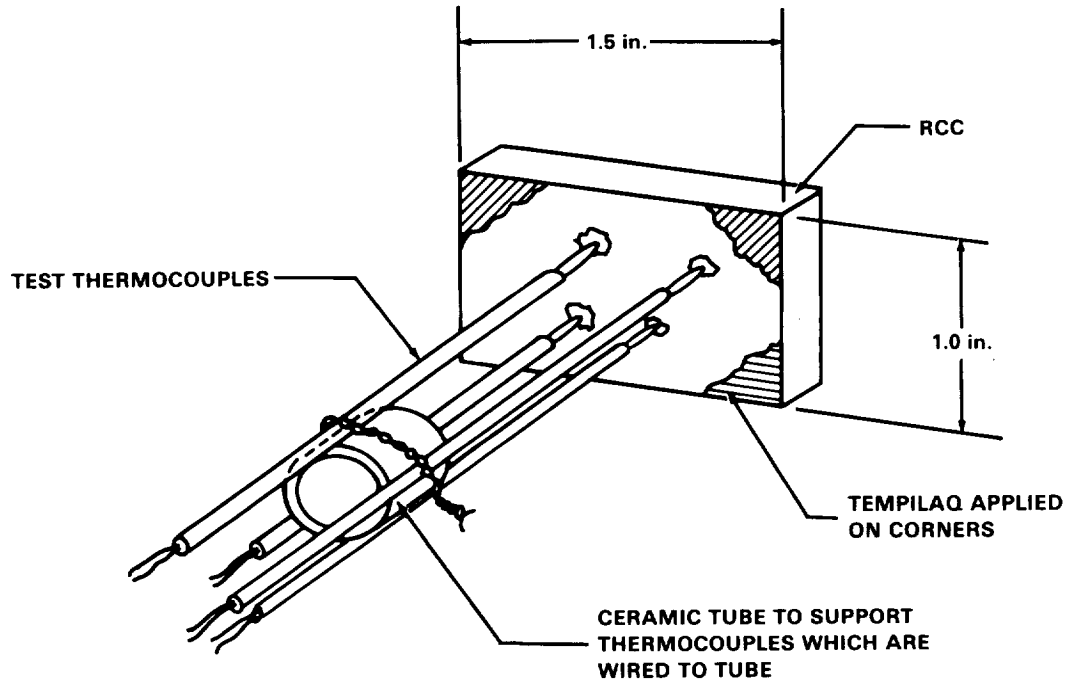

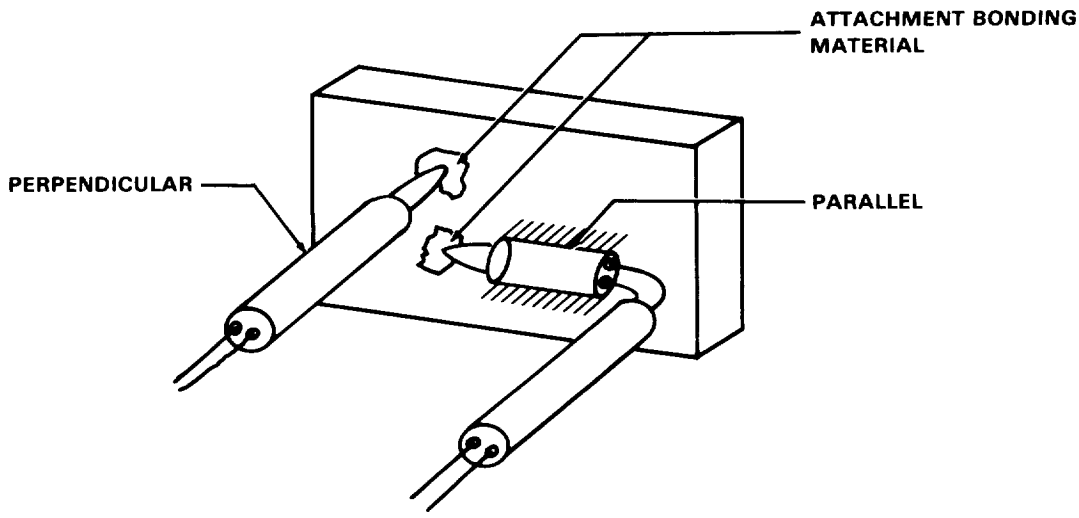

Figure 9-7 Typical Test Specimen and Attachment Types

B2-3592-56

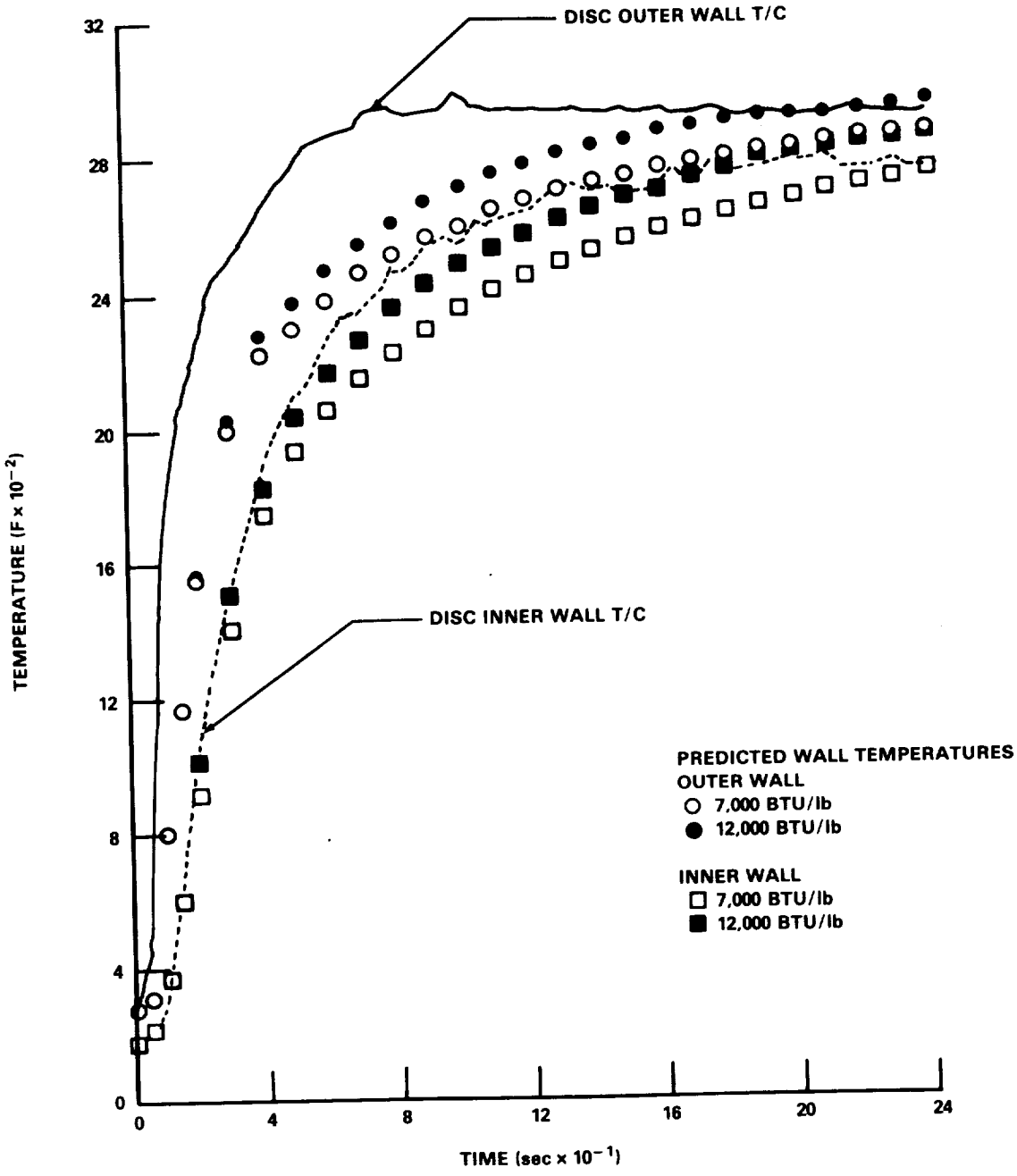

Figure 9-8 Comparison Predicted Temperatures with Test Run No. 6, SEADS Test Specimen with Holder Face Fully Catalytic and Penetration Port Partially Catalytic

B2-3592-57

1. Report No.	2. Government Accession No.	3. Recipient's Catalog No.
NASA CR-166044 (Vol I)		

4. Title and Subtitle	5. Report Date
Shuttle Entry Air Data System (SEADS) Hardware Development Volume I, Summary	January, 1983
	6. Performing Organization Code
7. Author(s)	8. Performing Organization Report No.
D. M. While	
	10. Work Unit No.
9. Performing Organization Name and Address	
Vought Corporation P. O. Box 225907 Dallas, Texas 75265	11. Contract or Grant No. NAS1-16000
	13. Type of Report and Period Covered
12. Sponsoring Agency Name and Address	Summary, 11-75 to 1-82
NASA Langley Research Center Hampton, Virginia 23665	14. Sponsoring Agency Code

15. Supplementary Notes

Mr. Paul M. Siemers, III was the NASA technical monitor.

16. Abstract

Hardware development of the Shuttle Entry Air Data System (SEADS) is described. The system consists of an array of fourteen pressure ports, installed in an Orbiter nose cap, which, when coupled with existing fuselage mounted static pressure ports permits computation of entry flight parameters. Elements of the system described herein include: penetration assemblies to place pressure port openings at the surface of the nose cap; pressure tubes to transmit the surface pressure to transducers; support posts or manifolds to provide support for, and reduce the length of, the individual pressure tubes; insulation for the manifolds; and a SEADS nose cap. Design, analyses, and tests to develop and certify design for flight are described. Specific tests include plasma arc exposure, radiant thermal, vibration, and structural.

The successful accomplishment of these tasks led to the fabrication of SEADS for early installation on Orbiter OV-102.

Volume I summarizes highlights of the program, particularly as they relate to the final design of SEADS. Volume II summarizes all of the Vought responsible activities in essentially a chronological order.

17. Key Words (Suggested by Author(s))	18. Distribution Statement
Space Shuttle Air Data System Carbon-Carbon Columbium	Distribution made by NASA

19. Security Classif. (of this report)	20. Security Classif. (of this page)	21. No. of Pages	22. Price
Unclassified	Unclassified		

For sale by the National Technical Information Service, Springfield, Virginia 22161